THESIS

THE RADIATIVE AND HYDROLOGIC EFFECTS OF A LOCAL SWITCH FROM MAIZE TO MISCANTHUS

Submitted by

Gavin R. Roy

Department of Atmospheric Science

In partial fulfillment of the requirements

For the Degree of Master of Science

Colorado State University

Fort Collins, Colorado

Spring 2013

Master's Committee:

Advisor: Dr. Thomas Vonder Haar

A. Scott Denning
Jeffrey Niemann
Christa Peters-Lidard

ABSTRACT

THE RADIATIVE AND HYDROLOGIC EFFECTS OF A LOCAL SWITCH FROM MAIZE TO MISCANTHUS

Miscanthus (*Miscanthus giganteus)*, a lush, dense grass that grows to be 3-4 meters tall, has been proven to be a substantially more productive biofuel crop than maize (*Zea mays*) due to its higher biomass output per unit area for conversion into ethanol. Moreover, Miscanthus is a perennial, biogeochemically sustainable crop, returning most of its nutrients to the soil each fall and needing less year-to-year maintenance than maize after its initial planting. Due to these potential benefits, a switch to Miscanthus as a viable biofuel alternative to maize has been suggested as a way to meet the current US energy goal of 30% displacement of domestic petroleum use by ethanol in the transportation sector by 2030, a goal that the existing US maize crop alone cannot achieve. Because maize and Miscanthus have significantly different vegetation characteristics, however, it is hypothesized that such a switch will lead to changes in the local surface radiation budget and hydrology. This study seeks to evaluate these changes.

Perennial agriculture such as Miscanthus contributes to a greener surface earlier in the spring and later in the fall than maize (annual agriculture), subsequently leading to higher year-round albedo and water usage. Due to the denser growth of Miscanthus, evapotranspiration and thus absolute water usage are also higher than maize, especially during the summer. However, Miscanthus exhibits a deeper rooting depth than maize and therefore has access to deeper soil water. In this study, representative shifts in year-round albedo, green vegetation fraction, rooting depth, and leaf area index are parameterized and their combined radiative and hydrologic effects evaluated through uncoupled retrospective runs of a well-tested land surface model over an existing area of maize in the US Corn Belt. Sensitivity experiments are undertaken that likewise evaluate the individual contributions of each shifted parameterization scheme.

It is found that the combination of these shifts leads to a yearlong average increase in latent heating of 12.16 W/m^2 and a nearly commensurate decrease in average sensible heating of 12.67 W/m^2 at the surface. It is also found that soil moisture availability plays a large role in the temporal persistence of these radiative effects, as modeled Miscanthus depletes the soil moisture in its rooting zone much more quickly, ending the growing season with an 11% decrease in volumetric soil moisture from maize. It is hypothesized that if soil moisture availability remains at a sustainable level, these effects will directly contribute to local cooling and moistening of the near-surface atmosphere.

ACKNOWLEDGEMENTS

This research was made possible by numerous individuals. I would like to give my appreciation to Dr. Tom Vonder Haar, whose offer brought me to Colorado State University and who has provided wisdom and encouragement throughout this study. I would also like to extend my sincere gratitude to Dr. Christa Peters-Lidard, Dr. Jeffrey Niemann, and Dr. Scott Denning for their invaluable guidance and constructive criticism during the various phases of development and culmination of this research. Their insight and advice was paramount to my navigation of the scientific process in addition to the science itself. I would like to thank Steve Finley, Sarah Ringerud, John Forsythe, Andy Jones, Karll Renken, and Michael Hyatt for their local hardware and programming support. I would like to acknowledge the support and creative influence of my peers at Colorado State, specifically my officemates Lance VandenBoogart, Kim Erickson, and Eric Guillot, as well as Rob Seigel, James Ruppert, Ghassan Alaka, and Walter Hannah. Finally, I would like to express my deepest appreciation to my family and specifically to my wife Lauren, whose strong will and reassurance proved to be a constant source of confidence and motivation throughout this process. This study was funded by the 2010-11 American Meteorological Society Government/Industry Fellowship and by a National Science Foundation Graduate Research Fellowship, with computing support from the Department of Defense Center for Geosciences/Atmospheric Research at Colorado State University.

TABLE OF CONTENTS

1. INTRODUCTION AND MOTIVATION

As the world's fossil fuel reserves dwindle and the debate on their contribution to global climate change continues, renewable energy has been increasingly turned to as a reliable energy source. Biofuels are one such energy source. The use of biofuels for energy entails harnessing the power of plant matter and biomass to create ethanol, which can in turn be efficiently burned to generate power. This method of biomass usage originally arose from the advantageous burning of industrial byproducts, including paper mill waste and crop residue. However, as facilities for converting plant matter into clean ethanol have become more efficient, there has been a significant push toward growing crops specifically for conversion to energy: from 2000 to 2010, US production of ethanol from biomass increased from 1.6 billion gallons to 10.2 billion gallons (RFA, 2012).

The primary method of ethanol production currently employed in the US is the fermentation of corn (hereafter also referred to as maize) grain (RFA, 2012). As of 2012, 32% of the US maize crop is used for ethanol production (see Figure 1), a number that is expected to rise to 36% by 2018 (DOE, 2012). However, despite 14 x 10^9 gallons of ethanol being produced from this portion of the national maize crop (92.3 million acres [USDA-NASS, 2012]) in 2011, only 5% of the 2011 transportation energy demand was accounted for (Davis et al., 2011). The Advanced Energy Initiative (AEI) goal of 30% displacement of 2005 petroleum use with US ethanol in the US transportation sector by 2030 (Heaton et al., 2008) is thus impossible with maize alone, especially without interfering with maize grown for human and livestock consumption. Moreover, since maize is an annual crop it is also very energy-intensive during its spring and summertime growth due to its reliance on yearly tillage and planting, nitrogen fertilization, and pesticide application. Farrell et al. (2006) finds that using maize grain for conversion into ethanol is minimally cost effective and results in a net carbon balance that is only slightly positive.

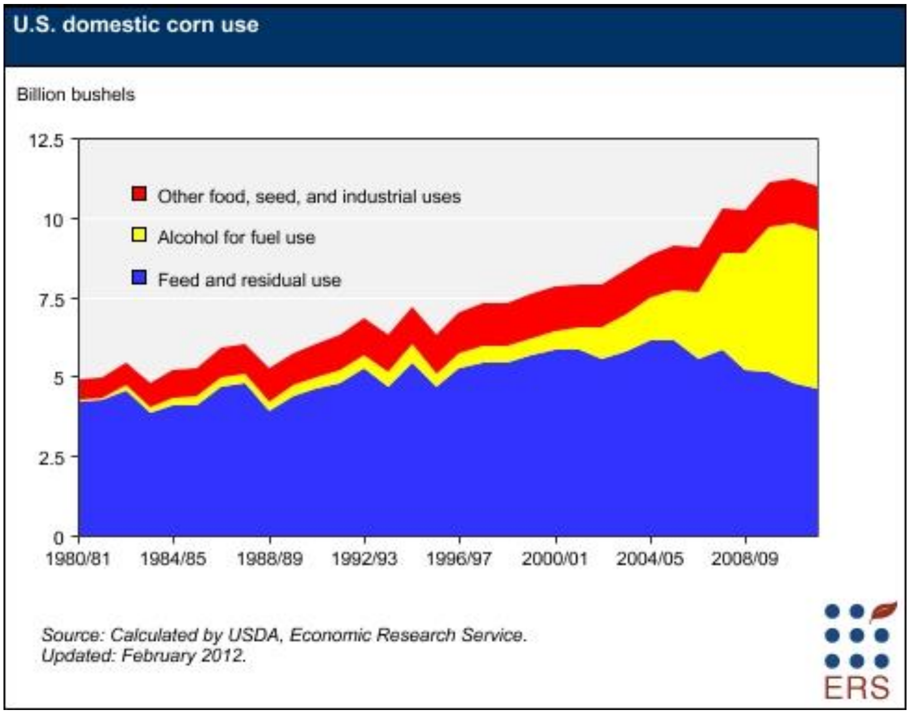

Figure 1: Historic corn crop usage in the United States, 1980-2012.

The growth and ethanol conversion of perennial (rather than annual) biofuel crops has been discovered to offer many solutions to this problem both in terms of energy output and economic impact. Two such perennial biofuel crops are *Miscanthus giganteus* (hereafter Miscanthus) and *Panicum virgatum*, more commonly known as switchgrass (Heaton et al., 2008). These grasses require only a single planting and then minimal fertilization and pest control after the first few years of growth, thereby alleviating much of the seasonal growing costs. Also, due to the size of Miscanthus specifically, which typically reaches 11 to 14 feet each year before harvest and grows much thicker than maize, was shown to have a 59% higher output of convertible biomass each year than maize in trials using a four year old stand of Miscanthus (Dohleman and Long, 2009). Before harvest, typically in October or November in the US, these perennial grasses return most of their vital nutrients to the soil, leaving just the carbohydrate shell stock in the shoots for harvesting and conversion, thus allowing Miscanthus to produce comparable amounts of biomass year after year. The ethanol produced from the conversion of plant stalks, stems, and leaves (e.g. from Miscanthus) is called cellulosic ethanol. This is in contrast with maize ethanol, which is ethanol converted from the sugar in the corn kernel alone.

While Miscanthus is still new to the United States, countries in Europe that planted Miscanthus as a biofuel crop as many as 30 years ago (e.g. Denmark) are still uniformly getting 90% of the yield attained 25 years before (Schill, 2007). Ultimately, Heaton et al. (2008) asserts that Miscanthus could provide 260% more ethanol per hectare than maize grain, thus making AEI's 30% petroleum displacement goal by 2030 attainable without impacting food production. The current majority practice of just using biofuel cropland for conversion into maize ethanol is much less area-efficient than using the same cropland for conversion into cellulosic ethanol, and helps to explain why this new method employing Miscanthus offers such a vast improvement in volume per area ethanol production from extant domestic cropland.

A widespread adoption of perennial grasses to supplant the percentage of US maize crops being grown for the purpose of biofuel production would lead to several not-insignificant changes to the land surface characteristics of areas undergoing this change. As shown in Figure 2, Miscanthus sprouts earlier and is typically harvested later than maize, resulting in a growing season 59% longer than maize (Dohleman et al., 2009). Such a change leads to a direct increase in year-round albedo, green vegetation fraction at the surface, and water usage.

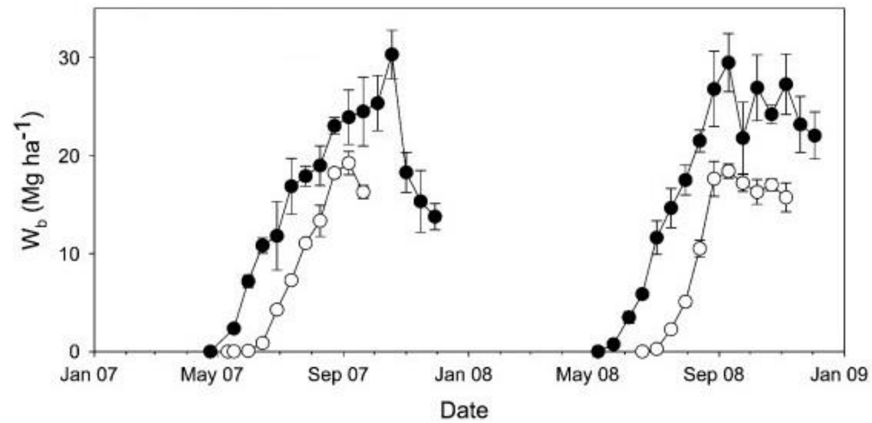

Figure 2: Accumulated aboveground dry biomass (W_b) of Miscanthus (black circles) and maize (white circles) over the 2007 and 2008 growing seasons. The x-intercept indicates the date of emergence. From Dohleman and Long, 2009.

Until recently, the majority of comparison studies of perennial vs. annual agriculture have focused on the biogeochemical effects of land use change, focusing on greenhouse gas emission differences and modifications to the carbon cycle. However, several recent comparison studies of the biogeophysical effects, or direct climate effects, of perennial vs. annual agriculture have been undertaken that seek to quantify the effect of such land use change on the surface radiation budget, hydrology, and near-surface temperature and humidity (Heaton et al., 2008; Georgescu et al., 2009; Skinner et al., 2010; Georgescu et al., 2011).

Using observations from instrumented flux towers over mature stands of Miscanthus and switchgrass, the preliminary consensus from these studies is that the early emergence and late senescence of green vegetation each year indeed leads to increased surface albedo, transpiration, and water usage, which can then affect the microclimate above the converted crops. Georgescu et al. (2011), the first to attempt an analysis of a modified atmospheric regime under a shift from maize to one of these perennial grasses, asserts that such a shift would increase average annual evapotranspiration, decrease the average annual near-surface temperature, and decrease column-averaged soil moisture. These direct climate effects of perennial agriculture are expected to be statistically significant at the local level and enough to locally offset the effects of projected surface warming due to increasing greenhouse gases over the next several decades (Georgescu et al., 2011). This research is detailed in Section 2.1.

The present research seeks to build upon this preliminary work by specifically quantifying the radiative and hydrologic effects of a shift to perennial agriculture at a representative grid point. When computationally parameterizing and resolving such a shift within a land surface model, changes in radiative forcing and water availability due to differences in the growing season and phenology of perennial vs. annual crops are indeed what will directly lead to subsequent atmospheric changes, and thus it is important that they are quantitatively understood. The research of Georgescu et al. (2011) predicts cooling of the near-surface atmosphere but neglects to discuss changes in the radiation budget. Beyond quantification of these changes under a hypothetical shift to perennial agriculture, another of the goals of the present research is to ascertain if this predicted cooling is primarily attributable to a decrease in net surface radiation or an increase in latent heat flux. The present research also hopes to determine if the increase in year-round water usage of perennial agriculture has a noticeable effect on local hydrology, especially if a significant increase in latent heat flux is observed. A more realistic parameterization of perennial agriculture than in past research will also be developed and its contributions to additional changes in the land surface modeling of perennials analyzed and compared.

2. BACKGROUND

2.1. Previous Research

Georgescu et al. (2011) alters certain default land surface parameters used by the Noah land surface model within the Weather Research and Forecasting Model (WRF) in order to ascertain whether or not a widespread shift from perennial to annual agriculture across the U.S. Corn Belt would have a meaningful direct climate impact on radiation budget and hydrology, and if so, to what extent. In all tiles in the U.S. Corn Belt within Noah, the monthly albedo and green vegetation fraction (GVF) files were shifted one month earlier in the spring and one month later in the fall to represent the longer growing season of perennial agriculture (see Figure 2). July and August parameters were held constant. WRF was then run in retrospective forecast mode from March through October of 1995. This was a coupled run of WRF, meaning that differences in surface radiation budget and moisture at each time step are capable of modifying the near surface atmosphere, which in turn is used as the new atmospheric forcing for the next time step (as opposed to continued use of retrospective observations and reanalysis). In addition to shifted albedo and GVF, a sensitivity run with just shifted GVF over this timeframe was performed, as was a sensitivity run with the addition of a rooting depth of 2 meters rather than 1 meter, which is more characteristic of annual vegetation.

It was found in all three runs that shifting said parameters decreased 2m temperature, increased 2m dewpoint, increased surface evapotranspiration, and decreased both net surface shortwave and longwave radiation. Exact area-average values for each of the three runs are shown in Table 1. Mentioned is that the surface cooling effect of a higher spring/fall albedo is of secondary importance to a higher spring/fall GVF, which indicates that increased evapotranspiration at the surface is the primary cooling mechanism in these simulations as opposed to decreased net surface radiation (due to a more reflective surface). Note that this projected cooling would be superimposed on any projected warming due to global climate change, not a complete reversal of the existing trend. Increased evapotranspiration is shown to lead to a lower sensible heat flux (higher latent heat flux) as well as an increase in cloudiness discovered in the coupled runs of WRF, which decreases downwelling shortwave radiation. It is unclear which of these mechanisms contributes to the bulk of the cooling. Additionally, summertime temperature, humidity, and radiative differences are much smaller because vegetation characteristics are not shifted during July and August, and it is mentioned that this approach "most probably omits additional features associated with summer season variability (e.g., albedo, canopy resistance)" (Georgescu et al., 2011).

Table 1: Mean April through October response of atmospheric and radiative variables between perennials and annuals, where Perennials-NoAlb represents the sensitivity test with just shifted GVF and Perennials-2m represents the sensitivity test with both shifted albedo and GVF as well as the addition of a deeper rooting depth of 2 meters for perennials within Noah. From Georgescu et al. (2011).

	2 m temp. [°C]: all land	2 m temp. [°C]: perturbed pixels	2 m dew-point temp: [°C]: all land	2 m dew-point temp [°C]: perturbed pixels	ET [mm day^{-1}]	Net surface SW [W m^{-2}]	Net surface LW [W m^{-2}]
Perennials—Annuals	−0.08	−0.51	0.02	0.16	0.1	−2.36	−0.65
Perennials-NoAlb—Annuals	−0.07	−0.45	0.02	0.18	0.1	−1.42	−0.23
Perennials-2m—Annuals	−0.16	−0.84	0.09	0.54	0.22	−3.63	−1.06

Where not specified, calculations are for perturbed pixels only. ET, evapotranspiration; SW, shortwave; LW, longwave

Also seen in Table 1 is that the addition of a deeper rooting depth acts to double 2m temperature and evapotranspiration as well as significantly decrease net radiation at the surface.

This is all broadly attributed to increased water availability in deeper soil layers, although soil moisture for each layer separately is never shown or discussed. Figure 3 shows the evolution of soil moisture in the top two layers together and the bottom two layers together. It is seen that the addition of a two meter rooting depth greatly separates this run from the others in terms of soil moisture (5% less deep layer soil moisture for perennials than for annuals). The increase in shallow soil moisture is attributed to an increase in precipitation due to the increase in evapotranspiration with a greater rooting depth.

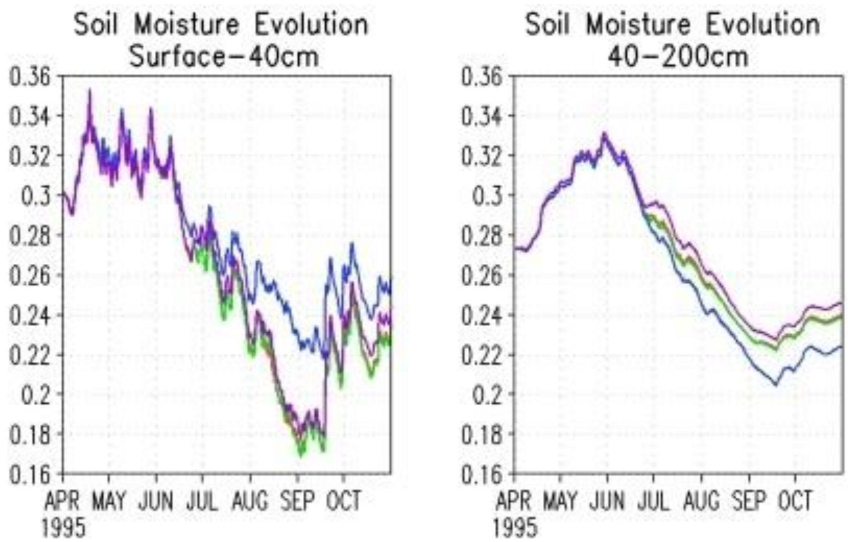

Figure 3: Top two layer (left) and bottom two layer (right) Noah soil moisture evolution, where purple line: Annuals; red line: Perennials; green line: Perennials minus albedo; blue line: Perennials plus 2m rooting depth.

A three-year uncoupled simulation is also conducted with a deeper rooting depth in order to ascertain if this difference in deep soil moisture content is transient or sustainable. It was found that deep-layer soil moisture levels off, but a sustained increase in evapotranspiration is still maintained (see Figure 4), indicating that even without the potential addition of increased precipitation at the surface, perennial vegetation with deeper roots and a longer growing season could indeed be sustainable.

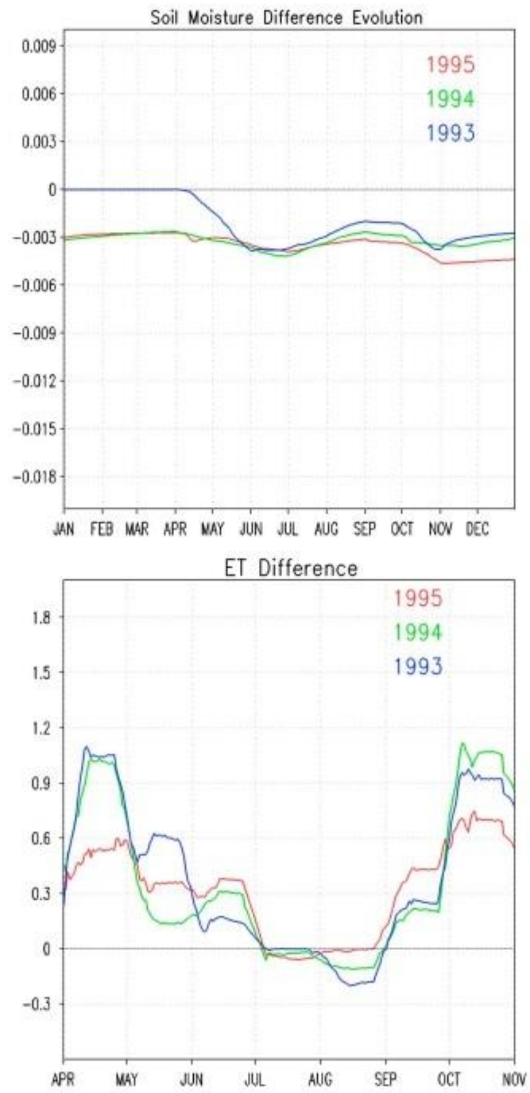

Figure 4: From Georgescu et al., 2011. Deep layer (40-200cm) soil moisture difference (top, volumetric fraction) and evapotranspiration difference (bottom, mm) simulated by Noah between Perennials with 2m rooting depth and Annuals.

2.2. Radiative Balance at the Earth's Surface

Sensible, ground, and latent heat fluxes at the Earth's surface directly link the surface thermal state to the overlying atmospheric boundary layer and thus the energy budget as whole. In order to determine how a broad scale shift in agricultural regime would affect surface characteristics, a thorough understanding of this radiative balance at the Earth's surface is necessary.

The Earth intercepts downward directed shortwave radiation from the sun during the daytime and longwave radiation from the surrounding atmosphere all the time proportional to the temperature of the atmosphere, which is constantly reemitting absorbed radiation. This energy input is countered by a compensating upward shortwave heat flux and longwave heat flux from the surface, the former again only during the day and the latter at all times proportional to the temperature of the surface. The difference between these downwelling and upwelling shortwave plus longwave radiative fluxes is called the net radiation, and can be expressed in its most basic form by Equation 1.

$$\textbf{(1)} \qquad SW\downarrow + LW\downarrow + SW\uparrow + LW\uparrow = Rnet$$

As stated, downward directed shortwave radiation is solely due to the sun, and is thus also called incident solar radiation. This quantity is affected by the angle of the Earth's surface in reference to the sun (i.e. time of day, seasons, and differences in the Earth's orbit around the sun over time) and by the surface albedo, α. The lighter or more reflective the surface material is, the higher the albedo will be. Thus the surface only absorbs $(1-\alpha)*SW\downarrow$, the rest returning back to the atmosphere as upwelling shortwave radiation in an amount directly proportional again to α, expressed as $\alpha*SW\uparrow$. Downward directed longwave radiation is emitted from the Earth's atmosphere at a rate directly proportional to the fourth power of the temperature of the radiating medium per the Stefan-Boltzmann law. The upward directed longwave radiation emitted from the Earth's surface is then dependent upon the surface emissivity (ε) which is related to the physical characteristics of the radiating media at the surface (for example, leaves have a greater emissivity than bare ground) as well as the instantaneous temperature at the surface, again per the Stefan-Boltzmann law. In other words, the net surface shortwave flux depends upon the sun angle and the surface albedo, while the next surface longwave flux depends upon the ability of the surface to emit radiation (emissivity) and the temperature of the surface. The result is the net radiation at the surface and is given by the simplified Equation 2, where T is the temperature at the surface and σ is the Stefan-Boltzmann constant. Remember that this is a simplified equation valid at the surface and does not take into account atmospheric composition, state, or interaction (e.g. cloudiness, greenhouse gasses, etc.).

$$\textbf{(2)} \qquad Rnet = (1-\alpha)SW\downarrow + \varepsilon(LW\downarrow - \sigma_s T_s^4)$$

This radiation budget is rarely perfectly balanced, and thus a surplus or deficit of radiative energy usually exists, typically during local summer for the former and local winter for the latter, although in many places closer to the equator there is a year-round surplus, just as there is a year-round deficit in many places close to the poles. As can be inferred, these seasonal and regional variations in net variations are inextricably tied to regional climate. But what exactly happens to this radiation deficit or surplus en route to affecting the overlying atmosphere?

Equation 3 shows depicts the partitioning, or reradiation and distribution, of net surface radiation due to the differences between upward and downward directed shortwave and longwave surface radiation in order to maintain the conservation of energy at the Earth's surface. The four terms into which the net surface radiation gets redistributed are a sensible heat flux (H), a latent heat flux (LE), a ground heat flux (G), and a near-surface, within-canopy storage term (ΔS). All of these fluxes are defined as being oriented upward in the present research, an important sign convention to remember (for example, ground heat flux at the surface is typically negative during the day, which means that there is actually a positive heat flux downward into the surface).

$$\textbf{(3)} \qquad Rnet = H + LE - G + \Delta S$$

H represents the heat conducted to the atmosphere from the Earth's surface with the result being a change in temperature. This heat is transported into the boundary layer and further upward through atmospheric turbulence. Higher winds, an unstable boundary layer, and greater friction at the surface all lead to more turbulence, which means greater turbulent transport upward of heat. H is typically positive during the day when the surface is warmer than the atmosphere above it and negative during the day when the surface radiatively cools (LW↑) without compensating solar insolation (SW↓)

While energy released into the Earth's atmosphere via LE is similarly transported into the atmosphere above, the energy released by this latent heat flux is due to a phase change of water, typically from liquid to vapor, which releases latent heat. Thus, it can be expected that over moister or more vegetated surfaces, a higher LE will be achieved during the day. At night, LE typically remains positive but is very small due to less turbulent transport at the surface under a stable nighttime boundary layer regime. The ratio between H and LE is commonly expressed as B, or the Bowen ratio, and is indicative of the general surface characteristics. For example, a typical daytime value of B over a desert can be over 10, while values over tropical rainforests are around 0.2.

G simply represents the heat from the surface being directly conducted to the soil layers beneath it, and will usually be negative during the day (positive, downward-directed) when the surface is radiatively warming and positive during the day (negative, downward-directed) during the night when the surface is radiatively cooling. ΔS corresponds to heat retained within the vegetation canopy, and is typically only non-negligible in deep forests and dense vegetation.

Figure 5 from the present research is an observational example of the diurnal cycle of upwelling and downwelling shortwave and longwave fluxes as well as the surface's response in partitioning a surplus in net radiation into sensible heat, latent heat, and ground heat fluxes. The observations are from an instrumented tower over an area of maize in central Illinois (Bondville) and are diurnally averaged over the month of August. It can be seen that SW↓ almost exactly corresponds to the sun's path above the sky and thus the incident angle of solar radiation upon the surface. Temporally coinciding with the SW↓ curve is the SW↑ response, indicating reflection of some of some solar radiation by the surface (albedo). An increase in LW↑ (emitted by the surface) can be seen shortly after the increase in SW↓, which is expected since it is directly tied to surface temperature, which has risen due to the sun heating the surface as day begins. Slightly less than LW↑ throughout the 24-hour period is LW↓, although a slight increase is seen later in the day as the atmosphere begins to warm due to surface warming and subsequent turbulent mixing upward. Recall that longwave radiation is proportional to the temperature of the radiating body, in the case of LW↓ the atmosphere.

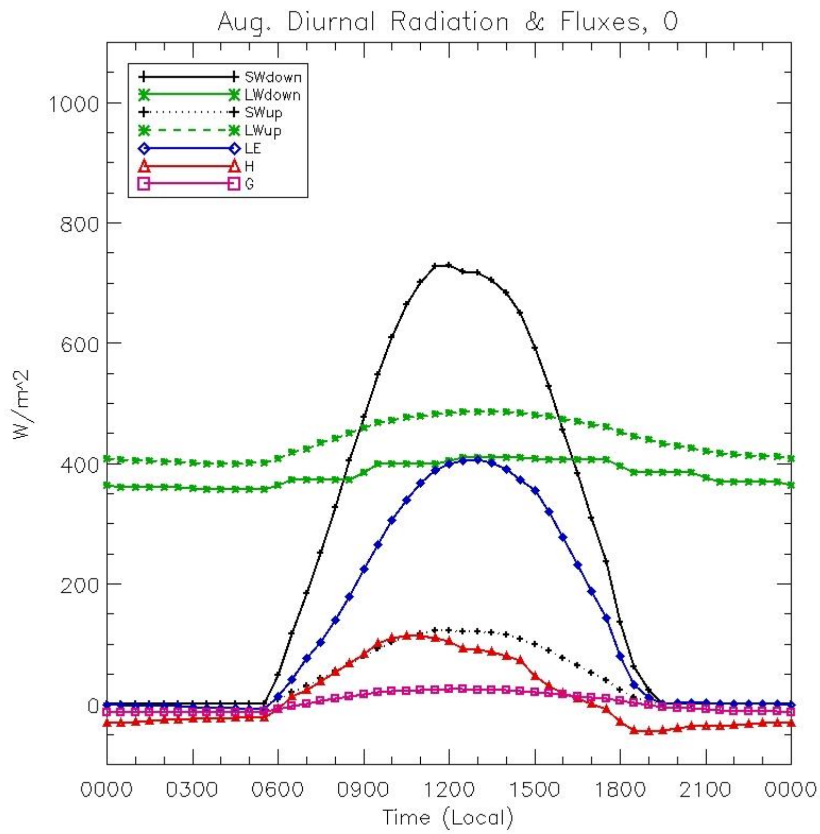

Figure 5: Diurnal average of August 2003 shortwave and longwave radiation as well as sensible (H), latent (LE), and ground (G) heat fluxes. Observations are every 30 minutes.

The net radiation surplus seen in Figure 5 over the site during the day leads to positive sensible (H) and latent (LE) heat fluxes, and a negative ground (G) heat flux, all contributing positively to net radiation per Equation 3. LE is over twice as large as H, resulting in a relatively low Bowen ratio, implying a moist surface with significant plant transpiration in this case.

LE is generally greater over areas with higher vegetation and moister soils but is limited when plants are stressed. Stressed plants have constricted or closed stomata, which are the small openings in leaves through which water, carbon dioxide, and oxygen are exchanged during photosynthesis. This stomatal constriction is a way for the plant to limit its water usage in an effort to survive until precipitation or irrigation remoistens the soil, and is called canopy resistance. Evapotranspiration (and subsequently LE) is lower for higher values of canopy stress. Thus, when evaluating the partitioning of Rnet into LE, soil moisture states must also be taken into account. For a more detailed overview of the equations and processes that govern evapotranspiration within the Noah land surface model see Appendix A.

2.3. LIS Architecture

The NASA/Goddard Space Flight Center's Land Information System (LIS [Kumar et al., 2006]) is a software framework that has the built-in architecture to run a variety of advanced land surface models (LSM) coupled with various sources of user-selected satellite/ground-based observational data to accurately characterize land surface states and fluxes. LIS is computationally efficient, extensible, and flexible. It has the capability to run a selection of LSMs, typically in a stand-alone manner, at a very high spatial resolution (from 1 degree down [~100km] to 1km) on points, regions, or the globe in real time (or faster) due to state-of-the-art, high-performance computing techniques including job partitioning for parallel processing on a Linux cluster as well as dynamic load-balancing and distributed data storage techniques (Tian et al., 2008).

LIS is built upon the Global Land Data Assimilation System (GLDAS [Rodell et al., 2004]) and the North American Land Data Assimilation System (NLDAS [Mitchell et al., 2004]). The goal of land surface modeling is to solve the governing equations of the soil-vegetation-snowpack system, thereby predicting the terrestrial water and energy processes. More recent LSMs even resolve certain biogeochemical processes, including a carbon budget (Sahoo et al., 2008). All the LSMs in LIS simulate energy and water variables (e.g. runoff, soil moisture), soil and skin temperature, and fluxes (e.g. sensible heat, partitioned evapotranspiration) at spatial resolutions of 25km (coarse) to 1km (fine) and at temporal resolutions of one hour or shorter (Kumar et al., 2006). The desired resolutions are selected by the user. The run domain can be as small as two grid cells by two grid cells, i.e. for point runs, single grid cell computations are done on a 2x2 model domain and then point output can be extracted from one of the four cells.

A schematic of the LIS land surface modeling process is shown in Figure 6. An LSM typically requires three distinct sets of input: initial conditions of the land surface, boundary conditions (which include both atmospheric [upper] and soil [lower] states and fluxes), and parameters, which can be functions of vegetation phenology, soil type, and other surface properties. LIS accepts a wide variety of such data (satellite products, global/regional reanalyses, station data, etc.), making interchangeability, extensibility, and comparison between parameters, datasets, and LSMs relatively easy for the user. This ability to easily transition between different LSMs and data/parameter sources without the necessary knowledge of underlying computer hardware or software is a major advantage of LIS's object-oriented framework. Kato et al. (2007) asserts that "the LSM itself is generally the most important factor governing output" (i.e. more so than the input or parameter data), and employing LIS for quick model comparison is helpful when attempting to answer a general question pertaining to the land-atmosphere interface with as little bias as possible. More information on the specific LSMs used in the present research is found in the following section.

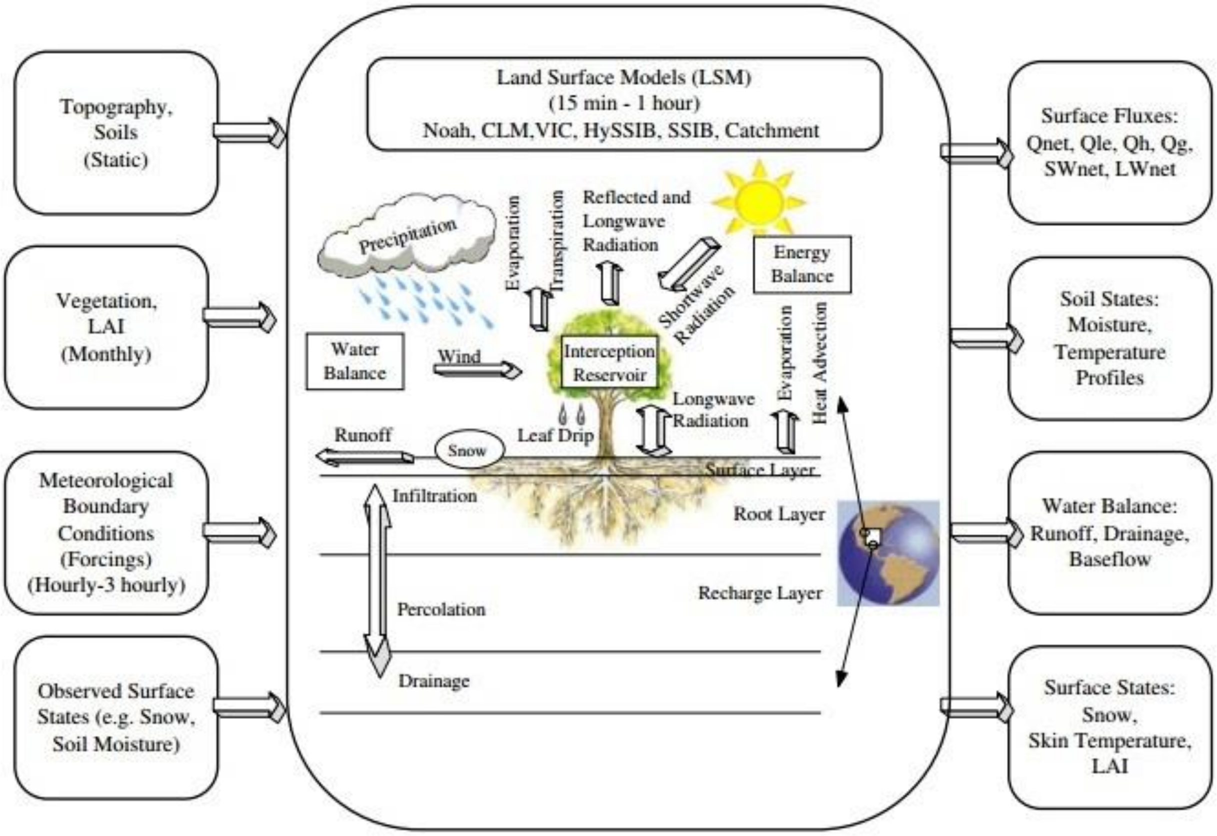

Figure 6: A schematic representation of land surface modeling in LIS. From Kumar et al., 2006.

LIS can be executed in two running modes: an uncoupled mode and a coupled mode (see Figure 7). In the uncoupled mode, meteorological, hydrological, and radiation data are used as unchangeable input for retrospective analyses of soil and surface radiative states. The coupled mode modifies near-surface atmospheric components of numerical weather prediction models as the Weather Research and Forecasting model (WRF) or the Goddard Cumulus Ensemble (GCE) (Peters-Lidard et al., 2007), and thus can be used for forecasting. The present research executes LIS in an uncoupled mode, while Georgescu et al. (2011) (previously detailed) executes WRF-Noah in coupled mode.

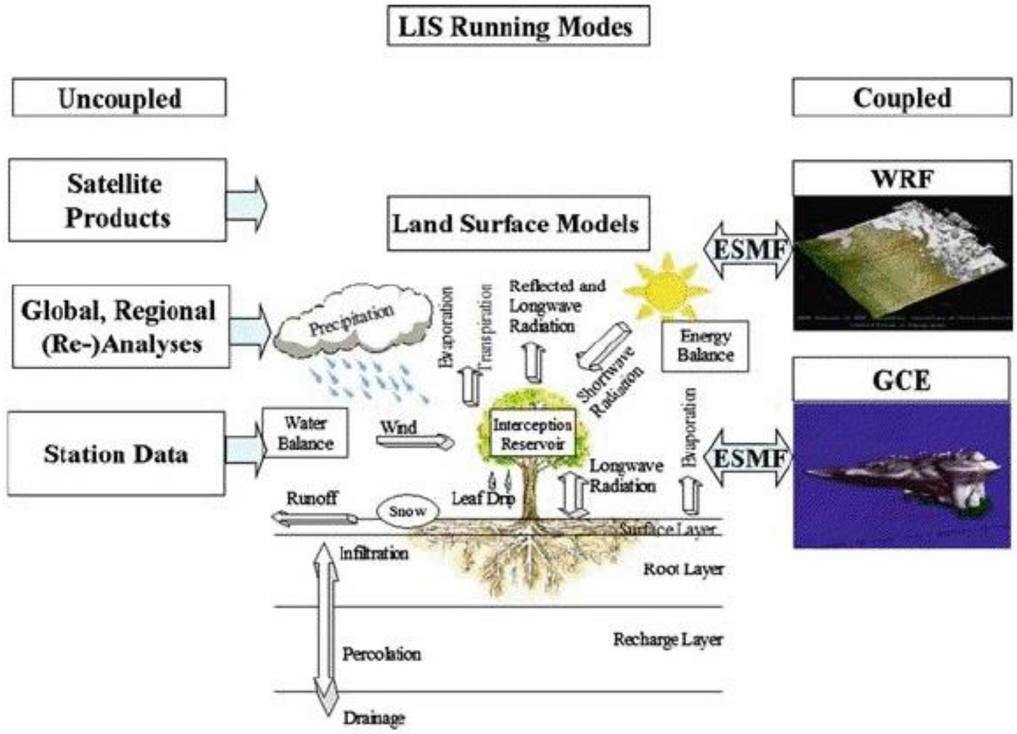

Figure 7: A schematic of the two LIS running modes: uncoupled and coupled. From Peters-Lidard et al., 2007.

The present research also utilizes Version 6.1 of LIS, which was released in 2011 and is the most recent version of LIS. Notable updates include the ability to use more recent versions of the Noah LSM (3.1 and 3.2) as well as support for North American Regional Reanalysis (NARR) atmospheric forcing data within NLDAS-2 GES-DISC (discussed in Section 2.5.1).

2.4. Land Surface Models

Georgescu et al. (2011) employs the Noah land surface model (LSM) to resolve the effects of a shift from annual agriculture to perennial agriculture across the US Corn Belt. The present research likewise seeks to use Noah in order to provide valid comparisons and improvements upon the existing research. However, in order to ensure that Noah is adequate at resolving such a shift in agriculture, Noah is first validated using actual observations from the US Corn Belt to assess performance. Additionally, the Community Land Model (CLM) is evaluated alongside Noah in order to analyze the comparative accuracy of Noah. CLM was chosen not only because of its inclusion in LIS but also because, like Noah, it is well-known and well-tested. Similarities and differences between the conventions of each LSM's input data, input parameters, and output data are shown in Table 2. Both Noah and CLM are also detailed in the following sections, with relevant discussions on updates from previous versions of each respective LSM. Previous validation studies for Noah and CLM are also discussed. Where possible, these validations are performed over the present research area of interest, the US Corn Belt, or over areas with similar land cover and climatologies, such as the US Great Plains.

Table 2: A comparison of required model inputs/parameters and available output for the Noah and CLM land surface models.

MODEL INPUTS/PARAMETERS	Noah 3.1	CLM 2.0
Near Surface Wind (m/s)	y	y
Rainfall Rate (kg/m2)	y	y
Convective Rainfall Rate (kg/m2)	y	y
Near Surface Air Temperature (K)	y	y
Near Surface Specific Humidity (kg/kg)	y	y
Surface Pressure (Pa)	y	y
Surface Incident Shortwave Radiation (W/m2)	y	y
Surface Incident Longwave Radiation (W/m2)	y	y
Leaf Area Index	n	y
Stem Area Index	n	y
Soil Color	n	y
Greeness Vegetation Fraction	y	n
Quarterly Snowfree Albedo	y	n
Maximum Albedo	y	n
Vegatation Classification	y	y
Elevation (m)	y	y
Canopy Height (m)	n	n

MODEL OUTPUTS	Noah 3.1	CLM 2.0
Net Shortwave Radiation (W/m2)	y	y
Net Longwave Radiation (W/m2)	y	y
Latent Heat Flux (W/m2)	y	y
Sensible Heat Flux (W/m2)	y	y
Total Evapotranspiration (kg/m2s)	y	y
Surface Runoff (kg/m2s)	y	y
Subsurface Runoff (kg/m2s)	y	y
Average Surface Temperature (K)	y	y
Surface Albedo	y	y
Snow Water Equivalent (kg/m2)	y	0-5 layers
Snow Depth (m)	y	y
Snow Cover	y	y
Average Layer Soil Moisture (kg/m2)	4 layers	10 layers
Average Layer Soil Temperature (K)	4 layers	10 layers
Total Canopy Water Storage (kg/m2)	y	y

2.4.1. Noah Land Surface Model

2.4.1.1. Noah 2.7.1

The Noah LSM originated from an LSM originally developed in the 1980s at Oregon State University and has been upgraded and extended by the National Centers for Environmental Prediction (NCEP) and various collaborators multiple times (Sahoo et al., 2008). Noah 2.7.1 is the predecessor of the current version of Noah employed by LIS version 6.1, Noah 3.1 (detailed in the following section), and has been validated through many model intercomparison studies, both coupled and uncoupled (Ek et al., 2003; Wood et al., 1998; Schlosser et al., 2000; Robock et al., 2003).

Noah has a vertical soil profile with a depth of 2-meters partitioned into 4 separate layers with delineations at 10cm, 40cm, 100cm, and 200cm below the surface (Chen et al., 1996). Above ground, there is one canopy layer and one snow layer. Prognostic variables include soil moisture and temperature within each soil layer, canopy water interception/storage, and ground snow volume. Total evaporation, as in CLM, is the sum of direct evaporation from the top layer of soil, canopy evaporation (from intercepted water), and plant transpiration. Surface temperature is determined through energy flux calculation using the surface energy balance equation. Noah uses a temporally-averaged value for incoming solar radiation (rather than a smooth function) with a 1 hour time step interpolated linearly every 15 minutes.

One of the key differences between Noah and CLM is that Noah employs a biome classification scheme to characterize land cover rather than defining discrete plant functional types. The biome dataset used by Noah was developed by the United States Geological Survey (USGS) and is comprised of 24 available biomes. Variations in plant cover and seasonal development are subsequently represented by regional changes in albedo and green vegetation fraction (GVF). A soil lookup table is used for static soil parameters such as wilting point and porosity, and a vegetation lookup table is used for vegetation characteristics such as rooting depth, minimum canopy resistance, and roughness length (Sahoo et al., 2008). Unlike CLM, LAI is also included in this lookup table as an assigned parameter.

Ek et al. (2003) details the use of Noah 2.7.1 in coupled mode using the NCEP Eta model with the Eta Data Assimilation System (EDAS). Various updates were made to previous versions of Noah in order to reduce existing biases. The bare soil evaporation correlation to soil moisture was made nonlinear as it was found that previous versions had evaporation diminishing too quickly as the soil dried, leading to unrepresentatively moist soils. Additionally the soil heat flux in previous versions was found to be too large due to a disproportionately large thermal conductivity in moist soils. This parameter was reduced in Noah 2.7.1. Also addressed was a warm bias in the Eta model, found to be the result of a canopy conductance that was too low, leading to under-predicted transpiration and thus more available energy for surface heating. This was ameliorated in Noah by increasing LAI upon input, which increased canopy conductance. All of these calculations and comparisons were made and validated over Champaign, Illinois.

Many offline simulations were also carried out that evaluated the performance of Noah, where land surface models were driven by atmospheric forcing with no corresponding feedback from the land surface back to the atmosphere. Wood et al. (1998) and Schlosser et al. (2000) evaluate an early version of Noah, the Oregon State University model (OSU), for the Red-Arkansas River basin and a boreal grassland at Valdai, Russia, respectively, during the Project for the Intercomparison of Land-Surface Parameterization Schemes (PILPS). Both concluded that despite a tendency toward slightly low net radiation, it was consistently one of the most accurate models at resolving the land-surface water balance, which suggests that the concomitant land-surface parameterizations at the time of the study were reasonable.

Robock et al. (2003) also details another offline simulation of Noah, this one a warm season evaluation of the original North American Land Data Assimilation System (NLDAS-1; see Section 2.5.1) coupled with four different LSMs (Noah, Mosaic, VIC, SAC) over the southern Great Plains, a region with extensive agricultural land use and very close in characteristics to the U.S. Corn Belt, albeit slightly warmer and drier. The NLDAS-1 domain extends over the contiguous United States at a 1/8° latitude-longitude resolution, and its baseline atmospheric forcing (precipitation and solar radiation) comes from NCEP's EDAS, with actual observations providing the precipitation data and satellite retrieval providing the solar radiation data. The NLDAS forcing dataset is discussed in greater detail later. Model output is validated at the majority of the Oklahoma Mesonet's 72 automated weather observation stations. Since the spatial variation of soil moisture has a small scale relative to hydrological processes and overall soil characteristics resolved by the model, spatial and temporal averaging was employed, and model output was only averaged when observational data from the same time and location was available. It was found that of the four models, Noah routinely exhibited the best performance. The Noah simulations were closest to observed turbulent and ground heat fluxes, near-surface soil temperature, and soil moisture, with the only noteworthy bias in these variables being Noah's tendency to reproduce higher-than-observed soil moisture values, a systematic bias of about 7% (m^3/m^3) that was reduced during the summer when the soil was much drier. The one area where other models outperformed Noah was midday skin (surface) temperature, which was usually higher in the model than observations. It is hypothesized that this might be due to an aerodynamic conductance that is too low in the model, as well as differences in actual soil texture and characteristics vs. the soil datasets in NLDAS used by the models.

2.4.1.2. Noah 3.0 and 3.1

In moving from Noah 2.7.1 to Noah 3.0 and quickly to Noah 3.1, several land parameterization schemes were updated or added on to. Noah 3.1 has the ability to use the land cover dataset derived by the Moderate Resolution Imaging Spectroradiometer (MODIS) for vegetation categories in place of the USGS dataset, for example. Various conventions for ice and snow are modified as well. The age of snowpack is recorded and taken into account when calculating albedo, slightly lessening albedo with time as snowpack becomes denser and dirtier (higher emissivity). Glacial ice is reparameterized to have a more realistic emissivity, thermal conductivity, and heat capacity values. A threshold for using latent heat of sublimation vs. vaporization is also included for snow-covered areas. Importantly, Noah 3.1 also has the capability to calculate surface background albedo, background emissivity, background roughness length, and LAI by scaling between climatological maximums and minimums of each quantity to correlate with real-time satellite-detected GVF. This allows for values of each quantity that are more in-tune with the year-to-year climate situation, especially during times of drought or flooding (UCAR, 2013a).

With these updates, improvements are observed when comparing Noah 3.1 and 3.0 output with observations at the Bondville flux tower site south of Champaign, Illinois (Bondville tower described in detail in Section 3.3.2). During the summer, sensible heat is less underestimated, although a slight daytime bias lower than observations still exists. Similarly, during the summer the overestimation of daytime latent heat flux (a known issue with Noah) is reduced to 60 W/m^2 from 80 W/m^2 (see Figure 8). Direct soil evaporation is slightly increased while plant transpiration is slightly decreased (on the order of a few W/m^2) throughout the year. Sublimation is also increased over snowpack during the winter. Overall, the average diurnal cycle (including skin temperature) is characterized as being improved. Noah 3.1 also has slightly higher soil moisture year round, which is more representative of observations (UCAR, 2013b).

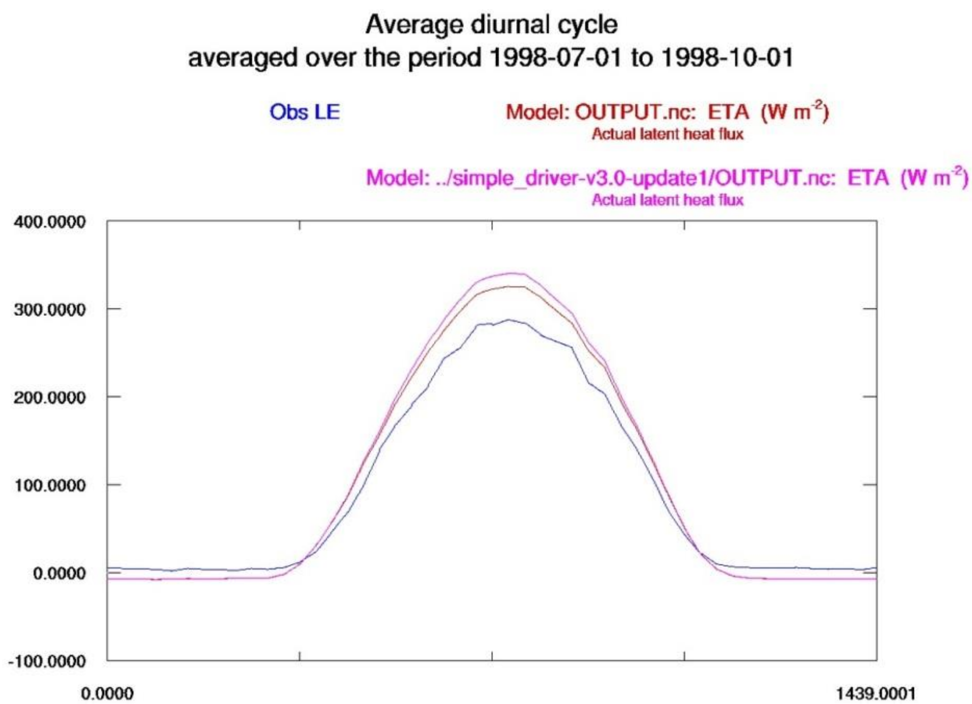

Figure 8: Average July through September diurnal cycle of latent heat flux at Bondville flux tower where x-axis is local minute of the day and y-axis is latent heat flux in W/m². Blue line represents observations; magenta line represents output from Noah 3.0 coupled with the NCEP Eta model; red line represents output from Noah 3.1 coupled with the NCEP Eta model. From UCAR, 2013b.

2.4.2. Community Land Model (CLM)

LIS version 6.1 utilizes the first version of the Community Land Model (CLM2.0, hereafter CLM2). CLM2 is a land surface model that simulates land surface energy, moisture, and momentum fluxes. CLM2 arose from modifications to the National Center for Atmospheric Research (NCAR) Land Surface Model (LSM2), which is used with the community climate model (CCM3.0) and the climate system model (CSM1) (Bonan, 1998) to validate performance.

CLM2, like LSM2, employs a prescribed land-cover dataset that gives the distribution and fractional abundance of vegetation (divided into tiles of various plant functional types [PFTs]), wetlands, urban areas, lakes, and glaciers. The PFT dataset is derived from 1-km satellite data from both the International Geosphere Biosphere Program Data and Information System (IGBP DISCover) and the University of Maryland (UMD) tree cover datasets. CLM2 allows for specific plant type, abundance, leaf area index, stem area index, and height to be input for each PFT of each grid cell of the model (see Figure 9) rather than giving an area of varied vegetation a single biome classification for each grid cell. (Bonan et al., 2002). The vegetated portion of each grid cell can be comprised of up to four PFTs, each one having its own characteristics and parameters that are subsequently averaged into a single value along with the characteristics and parameters of the other land cover type percentages (glacier, lake, wetland, urban).

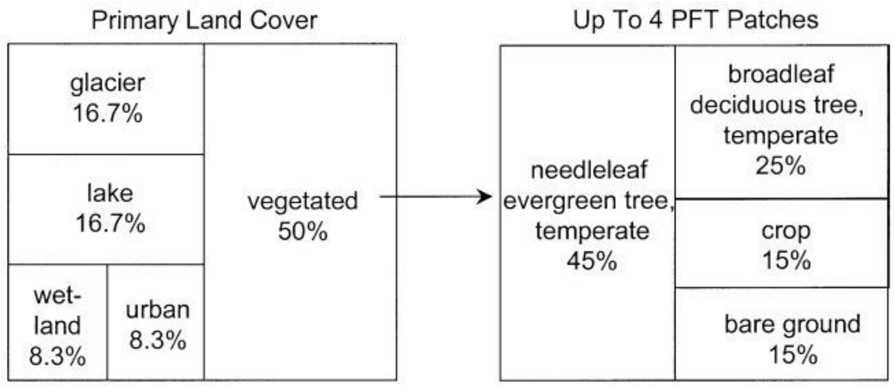

Figure 9: Each grid cell in CLM2 is divided into five primary land cover types, with the vegetated portion further divided into up to four types of plants. Bare ground is represented by a patch with no vegetation. From Bonan et al., 2002.

Monthly average datasets of prescribed leaf area index (LAI) are given for each 0.5° grid cell after being interpolated to daily values. This LAI dataset is also satellite-based, being derived from the 1-km Advanced Very High Resolution Radiometer (AVHRR) (Bonan et al., 2002). Contrarily, stem area index (SAI) and canopy height at a similar resolution are still merely prescribed using the same empirically-derived values as in LSM1.

CLM2 differs from LSM in its biogeophysical parameterizations (while still using the same surface datasets and representation schemes), one of the goals being to reduce known biases in the existing LSM while including a dynamic carbon cycle calculation. Some of the major differences include 10 layers for soil temperature and moisture (partitions at 1.8cm, 4.5cm, 9.1cm, 16.6cm, 28.9cm, 49.3cm, 82.9cm, 138.3cm, 229.6cm, and 342.3cm below the surface) rather than only 6 layers, a distinction for soil ice and water, snowpack of up to 5 layers rather than a one layer mass balance, and differences in the way sensible and latent heat are controlled. For example, CLM2 uses a lower roughness length for bare ground than LSM1, increasing the aerodynamic resistance to heat exchange between the ground and near-surface air. This more realistically inhibits evaporation and decreases the latent heat flux while representatively increasing net longwave loss (Bonan et al., 2002). Additionally, CLM2 invokes canopy interception of precipitation that is dependent upon LAI rather than being uniformly restricted to 20% of the precipitation as in LSM1, allowing increased precipitation interception in areas of high leaf cover, as in cropland in the summertime. This, coupled with the updated soil moisture parameterization of CLM2 that restricts plant photosynthesis and stomatal conductance (and thus transpiration) much earlier in the soil-drying process via a soil water factor for each soil type (see Figure 10), leads to higher canopy evaporation but lower transpiration and ground evaporation, contributing to an overall decrease in latent heat flux.

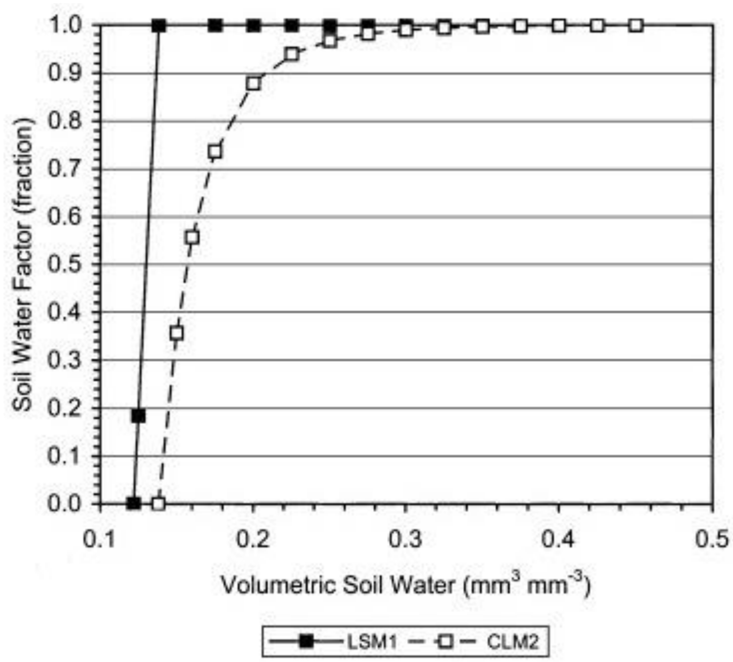

Figure 10: Dimensionless soil water factor vs. soil moisture content for loamy soil in LSM1 vs. CLM2. From Bonan et al., 2002.

Bonan et al. (2002) concludes that CLM2 does a good job at reducing or eliminating many known cold biases of LSM1. This realistic increase in surface air temperature is due to increased sensible heat and reduced latent heat fluxes. This reduction in latent heat flux is also presumed to lead to the observed decrease in annual precipitation in CLM2 vs. LSM1. Over the 12-year period of comparison between runs of both models, the Central United States averaged 85mm less precipitation in the CLM2 run (682mm vs. 597mm).

CLM2 is also found to do an adequate job reproducing both absolute values of soil moisture and soil moisture anomalies over Illinois. Guo and Dirmeyer (2006) evaluates 10-years of simulated soil moisture from eleven different land models (including Noah) against in situ observations from sites over grassland and agricultural regions over several different areas across the globe, including Illinois. In situ data over Illinois is from the Global Soil Moisture Data Bank (GSMDB) of Robock et al. (2000). Each model was run offline on a 1° by 1° grid from 1986-1995 using identical meteorological forcing and vegetation parameter datasets. CLM2 was found to be the best of the eleven land surface models at accurately representing soil moisture anomalies over Illinois (with a correlation of 0.8) and second-best at monthly mean columnar soil moisture (with a correlation of 0.9). Noah was also correlated within 0.02 of CLM2 for each of these variables. CLM2 was also routinely the best model at representing anomalies at all test sites (China, Mongolia, former Soviet Union, Illinois), producing significant temporal correlations between model estimates and observations at the 95% confidence level at 80% of the stations from the study period of 1986-1995.

2.5. Data and Parameters

2.5.1. Atmospheric Forcing Datasets

Each LSM run executed within LIS can use a number of atmospheric forcing datasets to drive retrospective simulations. Table 2b (Rodell et al., 2004) shows the required forcing fields and summary of the possible output fields of the Global Land Data Assimilation System (GLDAS), an example of one of such dataset. While the fields in this table are generally the input and output required of all LSMs and provided by such forcing datasets, important distinctions exist in the origin of model-provided forcing fields, spatial and temporal interpolation of variables, and additional observational forcings that may be provided from each of these datasets, and thus different forcing datasets are preferred over others in certain situations.

Table 3: GLDAS variables used to force LSMs and possible output fields (model-dependent). From Rodell et al., 2004.

TABLE 2. GLDAS forcing and output fields.

Required forcing fields	Summary of output fields
Precipitation	Soil moisture in each layer
Downward shortwave radiation	Snow depth, fractional coverage, and water equivalent
Downward longwave radiation	Plant canopy surface water storage
Near-surface air temperature	Soil temperature in each layer
Near-surface specific humidity	Average surface temperature
Near-surface *U* wind	Surface and subsurface runoff
Near-surface *V* wind	Bare soil, snow, and canopy surface water evaporation
Surface pressure	Canopy transpiration
	Latent, sensible, and ground heat flux
	Snow phase change heat flux
	Snowmelt
	Snowfall and rainfall
	Net surface shortwave and longwave radiation
	Aerodynamic conductance
	Canopy conductance
	Surface albedo

2.5.1.1. NLDAS-1

The original North American Land Data Assimilation System (NLDAS-1) retrospective and real-time forcing is a combination of observations and 40-km Eta Data Assimilation System (EDAS) model data. NLDAS-1 was developed in 1998 with the goal of providing land surface and flux data with as much reliance on observational data (rather than model-based forcing fields) as possible to constrain and force LSMs (Rodell et al., 2004). The contents of the NLDAS-1 forcing files are shown in Table 4, where all model-based fields are EDAS-derived (from Cosgrove et al., 2003). EDAS is one of NCEP's operational systems, a series of computer analyses and forecasts that covers the United States (25°N to 53°N; 125°W to 67°W). NLDAS-1 is based on 3-hourly EDAS data and 3-hourly and 6-hourly Eta forecasts when EDAS data are unavailable. These data are spatially interpolated onto NLDAS-1's grid at a resolution of 1/8° latitude-longitude, or roughly 11km by 14km, and temporally interpolated at an hourly time step (Cosgrove et al., 2003). When possible, observations of precipitation and instantaneous downward solar radiation are used in retrospective NLDAS-1 forcing so as to avoid any potential inherent model biases from EDAS. Precipitation observations come from hourly gauge data from the Doppler Radar and River Forecast Center and daily gauge data from the Climate Prediction Center. Radiation data are interpolated from the University of Maryland (UMD) 1/2° dataset derived from NOAA's Geostationary Operational Environmental Satellites (GOES) when sun angles are not too low. When sun angles are too low, modeled downward shortwave radiation values are instead used (Cosgrove et al., 2003). Surface pressure, incident longwave radiation, 2-meter air temperature, and humidity are adjusted to account for topographical differences between EDAS and NLDAS (Mitchell et al., 2003).

Table 4: NLDAS-1 model-based and observation-based forcing fields. Of the 15 hourly meteorological fields, 9 are primary forcing fields while 6 are secondary and may or may not be used depending upon the application. From Cosgrove et al., 2003.

Contents of NLDAS Forcing Files

Model Based	Observation Based
Primary Fields	
2 m temperature	GOES-based downward shortwave radiation
2 m specific humidity	stage 2/gauge-based precipitation
Surface pressure	
10 m U wind component	
10 m V wind component	
Downward longwave radiation	
Convective precipitation	
Secondary Fields	
Downward shortwave radiation	GOES-based skin temperature
Total precipitation	GOES-based photosynthetically active radiation
Convective available potential energy	stage 2 precipitation

NLDAS currently drives four LSMs over the United States: Noah, Mosaic, Variable Infiltration Capacity (VIC), and Sacramento (SAC) (Mo et al, 2011), all with a 1/8° horizontal resolution. Luo et al. (2003) validates NLDAS-1 across the southern Great Plains of the U.S. by comparing its forcing/constraint data to ground-based observations. First analyzed was how well the Oklahoma Mesonet (Brock et al., 1995) station observations match up with NLDAS model forcing data at time step zero. It was concluded that there is generally good agreement between NLDAS retrospective forcing and the observations at most of the stations, with small biases and root mean square differences (RMSD) overall. Variables with larger spatial and temporal scales (e.g. surface pressure, 2-meter temperature, humidity) agree well between NLDAS forcing and actual observations as expected, each with a correlation coefficient of 0.96 or higher. There was slightly more variation in downward longwave and shortwave radiation, but still with a correlation coefficient above 0.9. The largest bias was a systematic overestimation in downward shortwave radiation in both the EDAS and GOES fields (Cosgrove et al., 2003; Luo et al., 2003). Despite this, however, it is concluded after examining four different LSMs initiated with NLDAS data (including Noah) that these small differences in the atmospheric forcing data do not produce significant differences in modeled land surface conditions in this region, especially over longer time periods (i.e. weeks, months, years) (Cosgrove et al., 2003).

2.5.1.2. NLDAS-2

NLDAS-2 is a newer NLDAS forcing dataset that is concurrently available. The majority of the processes and parameter sources remain the same as in NLDAS-1, but there are a few significant differences. A big difference between NLDAS-1 and NLDAS-2 forcing data is the timeframe of available data: from mid-1996 through December 2007 for NLDAS-1 vs. January 1979 to present for NLDAS-2. Additionally, rather than using NCEP's 40-km EDAS as the surface radiation and atmospheric data source as does NLDAS-1, NLDAS-2 employs the 32-km resolution North American Regional Reanalysis (NARR) system at an hourly time step. Table 5 is a list of the parameters in the NLDAS-2 primary forcing dataset with units and time steps (from Xia et al, 2012). Hourly potential evaporation is now included in this dataset. NLDAS-2 also uses GOES data to bias-correct the NARR radiation information rather than using GOES data alone and EDAS when this information is unavailable or the sun angle is too low, as does NLDAS-1 (Xia et al., 2012).

Table 5: Parameters in the NLDAS-2 primary forcing dataset. From Rui, 2012.

PDS IDs	Full Name	Unit	Time
61	Precipitation hourly total	kg/m^2	Hourly backward-accumulated
157	180-0 mb above ground Convective Available Potential Energy	J/kg	Hourly instantaneous
153	Fraction of total precipitation that is convective	unitless	Hourly backward-accumulated
205	LW radiation flux downwards (surface)	W/m^2	Hourly instantaneous
204	SW radiation flux downwards (surface)	W/m^2	Hourly instantaneous
228	Potential evaporation	kg/m^2	Hourly backward-accumulated
1	Surface pressure	Pa	Hourly instantaneous
51	2-m above ground Specific humidity	kg/kg	Hourly instantaneous
11	2-m above ground Temperature	K	Hourly instantaneous
33	10-m above ground Zonal wind speed	m/s	Hourly instantaneous
34	10-m above ground Meridional wind speed	m/s	Hourly instantaneous

The NASA Goddard Earth Sciences Data and Information Services Center (GES DISC) maintains easily-accessible and gap-filled archives of all NLDAS data products including NLDAS-2 atmospheric forcing data.

2.5.1.3. GLDAS

The Global Land Data Assimilation System (GLDAS) has its roots in NLDAS. Developed about five years after NLDAS-1, it has the same goal of providing data to constrain modeled land surface states, both through observations and data assimilation techniques (Rodell et al., 2004), but for the entire globe. Satellite- and ground-based observations are used to generate accurate fields of land surface states and fluxes in near-real time. These data are then assimilated by the Global Data Assimilation System (GDAS) to subsequently produce operational, global analyses for four synoptic hours: 0000, 0600, 1200, and 1800 UTC, as well as 3-hour and 6-hour forecasts. GLDAS utilizes these analyses and derives finer temporal intervals of data at a time step as small as one hour, adjustable by the user. Spatial resolution is likewise user-selected with 1/4° being the finest grid spacing for Noah and 1° for all others. Leaf area index (LAI) for each grid cell is assigned using a static, 1-km resolution, global dataset of land cover class produced at UMD, which is based on AVHRR observations. Soil type is also classified using a lookup table. GLDAS is currently the dataset used to force four LSMs on a global scale: Noah, CLM, Mosaic, and VIC.

2.5.2. Representation of Vegetation Cover

As discussed in Section 2.4 there are two different land surface classification schemes utilized by Noah and CLM: Noah employs a 24-biome classification method of which each tile is subsequently characterized by satellite-detected albedo and green vegetation fraction (GVF), while CLM defines surface vegetation as one of five primary land cover types and then further divides each tile's vegetated portion into up to four heterogeneous patchwork of plant functional types (see Figure 9). In Noah, changes in land cover can be captured by changing the biome entirely or by modifying the overlaid albedo, GVF, or lookup table parameters. With CLM, land cover changes can also be represented by modifying the PFT composition for each grid cell.

3. METHODOLOGY

3.1. Overview

In an effort to validate and improve existing efforts to accurately ascertain the effects of a shift from annual to perennial agriculture, an experiment is constructed that mimics the setup of Georgescu et al. (2011) at a well-observed point in the US Corn Belt. This similar setup provides the groundwork to validate their findings as well as fill in existing research gaps, such as the determination of the principal source of model-predicted cooling at the surface as well as the contributions of decreased infiltration to higher model-predicted top-layer soil moisture under a perennial agriculture regime. Additional parameter changes are subsequently made to more accurately represent a surface shifted to perennial agriculture. Without the assurance of accuracy at a point resolved within an LSM, it is impossible to make specific conclusions about a broader domain shift, and thus the present research seeks to characterize the surface and its associated radiative/hydrologic processes as realistically as possible at a well-observed point.

A specific and likely perennial biofuel crop option is chosen, a timeframe and domain chosen, and parameters shifted representatively, as detailed in the following sections. Prior to executing LSM runs with shifted parameters, however, a model comparison study between Noah and CLM, two well-documented LSMs, is performed using actual observations from this domain in order to determine if Noah, the LSM employed by Georgescu et al. (2011), is an appropriate tool for this task. The NLDAS-2 GES-DISC 12.5-km dataset is likewise chosen and compared with Bondville observations to assure its validity for use as atmospheric and radiative forcing data for all retrospective runs. NLDAS-2 was chosen over GLDAS as the atmospheric/radiative forcing dataset due to its finer spatial resolution over the US.

3.2. Miscanthus vs. Switchgrass

Switchgrass (*Panicum virgatum*) was previously mentioned alongside Miscanthus (*Miscanthus giganteus*) as a perennial grass with great potential to replace maize as a viable and productive biofuel crop. Georgescu et al. (2011) mentions that their simulations can be used to represent both switchgrass and Miscanthus. In the present research, however, due to its greater desired degree of specificity in parameter modification between annual and perennial biofuel crops, only one of these perennial grasses must be chosen to focus on in particular.

Heaton et al. (2008) is the first to perform a side-by-side analysis of switchgrass vs. Miscanthus productivity. Stands of each perennial grass were established along the same latitudinal gradient in central Illinois and their performance and output analyzed for three years. It was discovered that on average Miscanthus was almost three times as productive as switchgrass in terms of harvestable biomass capable of being converted into ethanol, and nearly twice as productive as maize. As seen in Table 6, this results in an area of 11.8 million hectares of Miscanthus (9.3% of current US cropland) that would be need to achieve the existing US Advanced Energy Initiative goal of 30% displacement of 2005 transportation sector petroleum usage by 2030, i.e. 35 billion gallons of ethanol, compared to 33.7 million hectares of switchgrass or 18.7 million hectares of maize.

Table 6: Biomass per hectare, ethanol per hectare, and number of hectares of corn, switchgrass, and Miscanthus needed to attain the US Advanced Energy Initiative goal of 35 billion gallons of ethanol per year. From Heaton et al., 2008.

Feedstock	Harvestable biomass (Mg ha^{-1})	Ethanol (gal ha^{-1})*	Million hectares needed for 35 billion gallons of ethanol	Harvested US cropland (%) in 2006†
Corn grain†	10.2	1127	31.0	24.4
Corn stover‡	7.4	741	47.2	37.2
Corn total	17.6	1868	18.7	14.8
LIHD§	3.8	380	92.1	72.5
Switchgrass	10.4	1040	33.7	26.5
Miscanthus	29.6	2960	11.8	9.3

*DOE (2006).
†USDA-NASS.
‡Perlack *et al.* (2005).
§Tilman *et al.* (2006).
LIHD, Low-input high-diversity.

It is thus decided that the present research will focus on a shift from maize to Miscanthus, and will modify salient LSM parameters (e.g. albedo, green vegetation fraction, rooting depth, leaf area index) appropriately in accordance with empirical measurements of Miscanthus when possible.

3.3. Domain

3.3.1. US Corn Belt

To model a shift from maize to Miscanthus, a point within a broad area of existing maize and with ample meteorological and radiative observations must be chosen. The United States Department of Agriculture (USDA) defines individual counties in the US as either "major crop areas" or "minor crop areas" by each crop (e.g. corn, wheat, and soya) depending on their production and contribution to the national total. Figure 11 shows the USDA's agricultural map for corn [maize] crops in the United States (recall that 'maize' is a more specific term for corn, but when ‘corn’ is used in the present research it is used synonymously). The statistics in this map were compiled by the USDA’s National Agricultural Statistics Service and are valid from 2000 to 2004. Yellow numbers indicate the percent that each state contributed to the national corn production, with unnumbered states contributing less than 1% of the national total. Major corn crop areas account for 75% of the national production, while major and minor areas together account for 99%. The Corn Belt is defined as the extent of all counties designated as major crop areas.

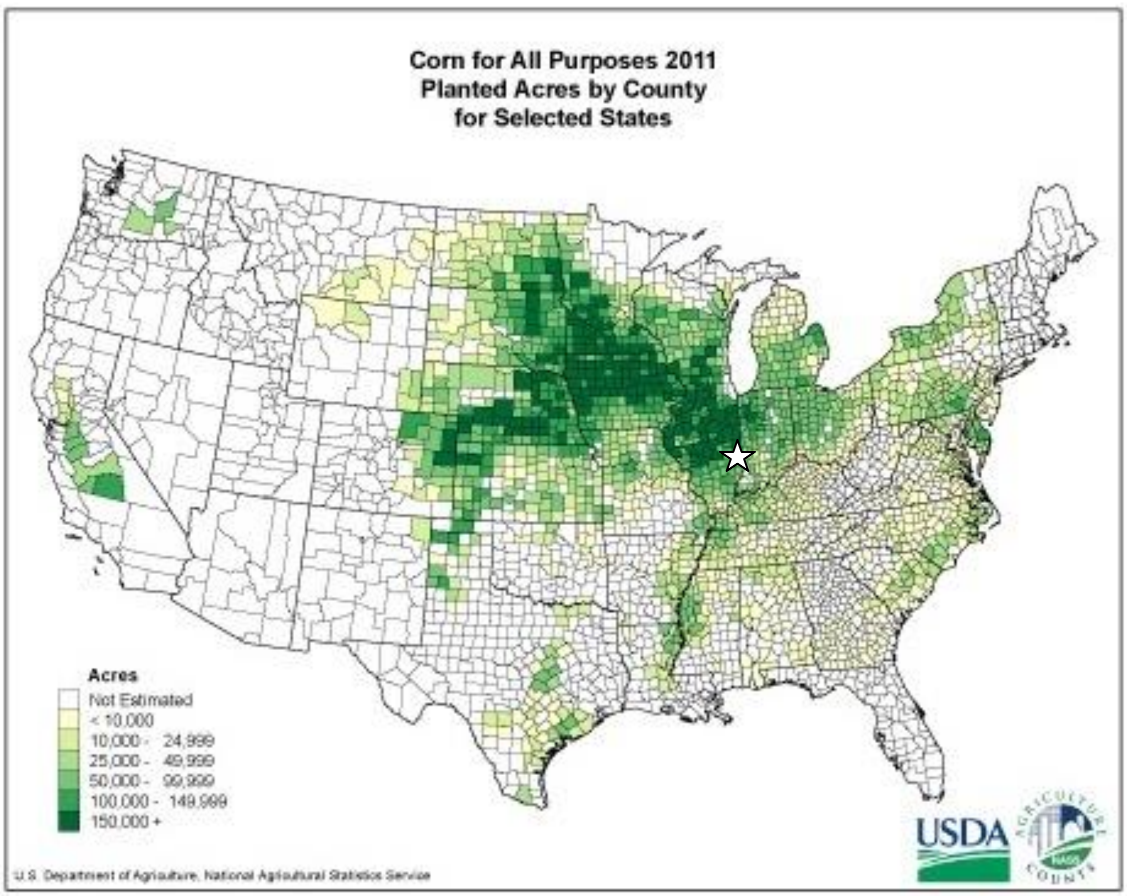

Figure 11: Corn crops in the US, 2000-2004. White star in East Central Illinois represents the location of the Bondville instrumented flux tower. Data is from the US Department of Agriculture.

3.3.2. Bondville Flux Tower

The white star in Figure 11 indicates the Bondville site, the grid point selected for the present research. The Bondville site (40.0062°N, 88.2904°W, elevation 216m) is located near Champaign, Illinois, and contains an instrumented flux tower maintained by the NOAA Atmospheric Turbulence and Diffusion Division, shown in Figure 12. Point observations of radiative fluxes over an extent maize crop at this location are used to validate forcing data and model performance.

Figure 12: A photo of the Bondville flux tower over a crop of maize. From AmeriFlux, 2013.

Average annual temperature at the Bondville site is 11.5°C (52.7°F) with an average annual precipitation of 58.2cm. Vegetation at the site alternates between maize during odd years and soy during even years, and as such is classified as non-irrigated (dryland) cropland/pasture in the USGS 24-class land cover dataset (see Figure 13). The soil at the site is moderately well-drained silt loam (Kato et al., 2007), and as such is classified as Silt Loam by the USDA State Soil Geographic database, or STATSGO.

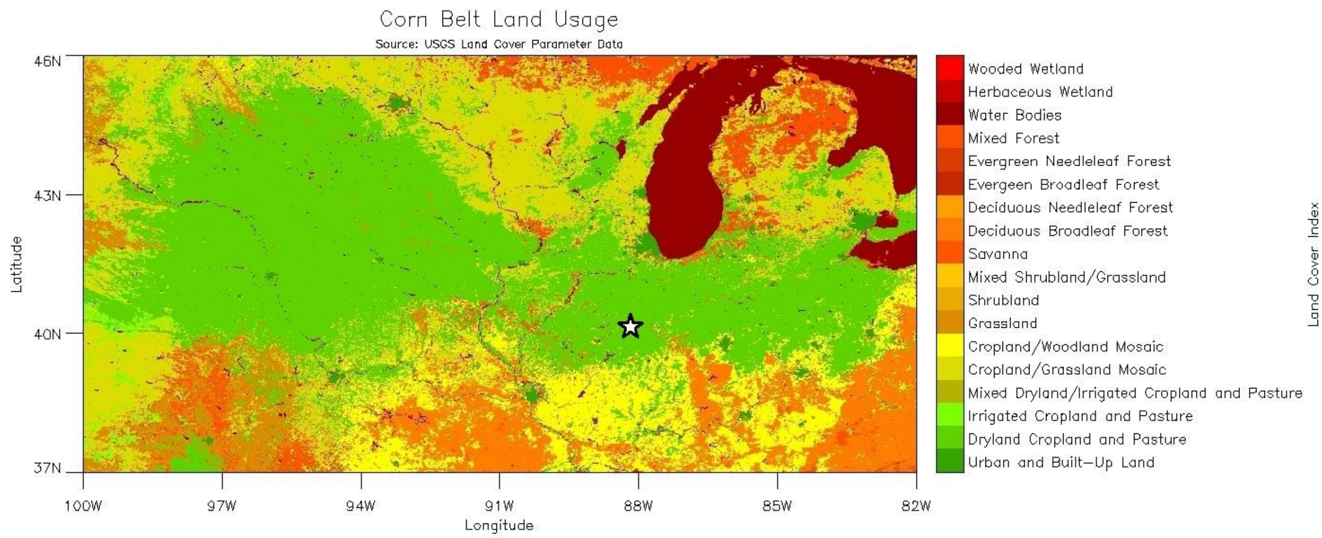

Figure 13: USGS land cover index over the US Corn Belt. Six classifications of various tundra/barren classifications not present over region are excluded from legend. Bondville tower site is indicated by the white star.

Tower observations include air temperature, humidity, wind speed and direction, pressure, precipitation, incoming and outgoing shortwave and longwave radiation, latent and sensible heat fluxes, and soil moisture. The raw data collected from this and other associated towers is compiled and formatted by the Oak Ridge National Laboratory in Oak Ridge, Tennessee and as a network is referred to as AmeriFlux data. Using AmeriFlux nomenclature, the data used in the present research is Level 2 data from the Bondville tower, meaning that raw observations from the tower have been checked for consistent units, naming conventions, and reporting intervals, and subsequently incorporated into the network-wide AmeriFlux database. Gaps or missing data are not interpolated by Level 2 convention, preserving the integrity of the dataset's completely observational nature. During the timeframe of the model validation/comparison using Bondville observations from March 2003 through October 2003, no gaps or missing data exist in the Bondville AmeriFlux dataset.

3.4. Timeframe

2003 was chosen as the retrospective analysis and modification period for this research. Since real-time NLDAS data begins in 1999 (Cosgrove et al., 2003), a year in the 21st century was necessary. Also as mentioned earlier maize and soy are grown in rotation in odd and even years respectively at the Bondville tower site, so an odd-numbered year was necessary for the point comparison. The six remaining eligible years were then scrutinized to discern which was characterized by an annual temperature and precipitation that were the closest to their long-term average, both across the entire Corn Belt domain and in central Illinois specifically. Figure 14 from the National Climatic Data Center (NCDC) show annual averages for each quantity by state. For Illinois specifically, the 1901-2000 statewide average annual temperature was 51.92°F and average annual rainfall was 37.82 inches. In 2003, the statewide average temperature was 51.6°F and annual rainfall was 38.32in. 2003 was thus chosen due to its being an appropriately average, odd-numbered, 21st century year. 2003 was also an El Niño Southern Oscillation (ENSO) neutral year, immediately succeeding a moderate El Niño event in 2002.

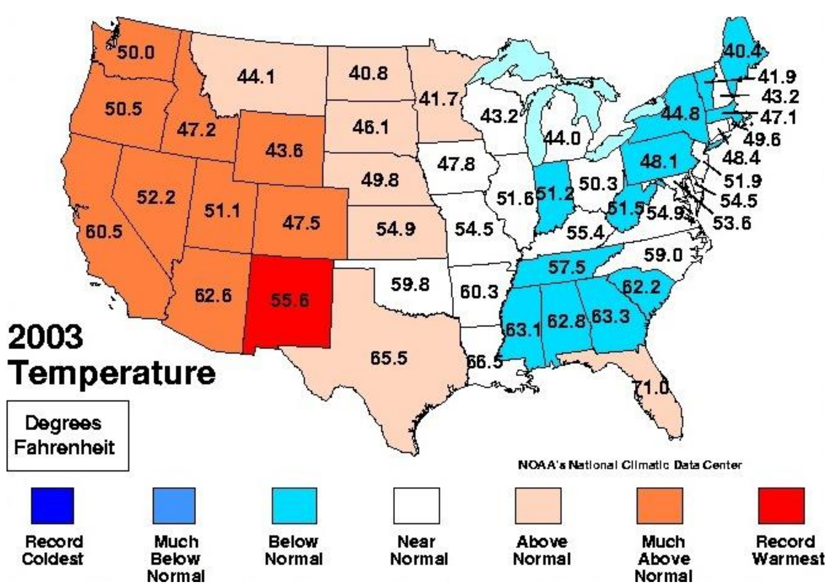

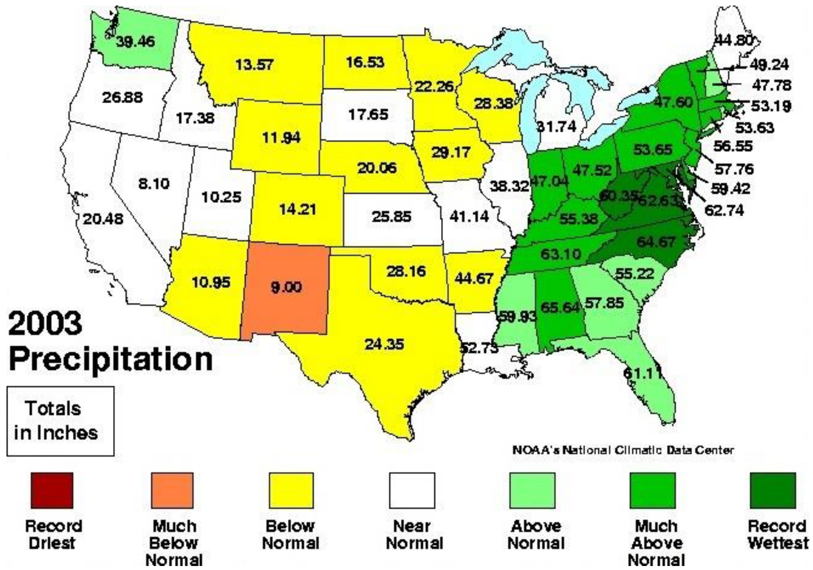

Figure 14: Average temperature and precipitation climate statistics for 2003 over the contiguous United States. Data from NCDC.

Although 2003 was average in terms of temperature and precipitation, a two week stretch of drought and mean temperatures well-above average occurred in mid-to-late August. Figure 15 shows the departure from average mean temperature during August 2003 in Champaign, Illinois, in the same county as the Bondville flux tower. From August 14 to August 25 there was no measurable precipitation, and only 0.06 inches total from August 14 to August 28 before 5.35 inches fell from August 29 to August 31, bringing the month to above climatological average precipitation (Peters, 2003). This month of extremes has soil moisture, evapotranspiration, and ultimately radiative implications to be considered during summertime analysis of a shift from annuals to perennials, discussed in Results.

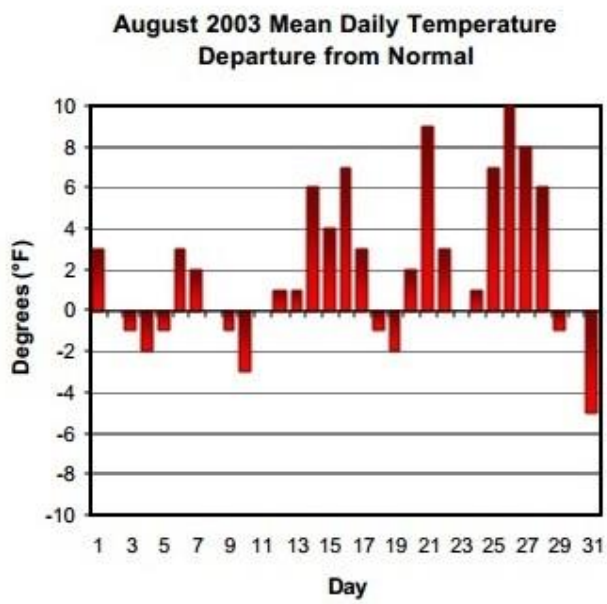

Figure 15: Departure from average mean daily temperature during August 2003 in Champaign, Illinois. From Peters, 2003.

3.5. Representing Miscanthus in Noah

The approach of Georgescu et al. (2011) in representing perennial biofuel grasses in place of maize simply shifts the default vegetation characteristics (albedo, GVF) represented by Noah one month earlier in the spring to depict earlier emergence and one month later in the fall to depict lagged senescence and harvesting. The same approach is used with albedo and GVF in the first experiment of the present research at Bondville in order to compare results. In the second experiment at Bondville, a deeper rooting depth is assigned in addition to shifted albedo/GVF. In the third experiment a higher maximum LAI is prescribed in addition to the previous changes. The details of each of these modifications are delineated in the following sections, and the experiments in which each shifted parameter dataset is used in the present research are shown in Table 9.

3.5.1. Surface Albedo

Snow-free surface albedo is a quantity used to represent how much shortwave radiation directed downward toward the Earth's surface from the Sun is reflected back upward and therefore not absorbed by the surface or by the vegetation on a cloudless day with no snow cover. Values range from 0 (zero radiation reflected) to 1 (all radiation reflected). The monthly 1-km resolution snow-free albedo dimensionless parameter files used by Noah in the present research are provided by the National Center for Environmental Prediction (NCEP) and are derived from satellite observations from the Moderate Resolution Imaging Spectroradiometer (MODIS). They are assumed to be valid on the 15th of each month; Noah then linearly interpolates between months to obtain daily values. Albedo is used within Noah to determine what percentage of downwelling shortwave radiation from the Sun gets absorbed by the Earth's surface/ vegetation and how much is reflected (per Equation 2).

Empirical measurements of typical albedo values over Miscanthus crops have yet to be performed. However, as mentioned, Miscanthus' being an annual crop will allow the surface to contribute to higher albedo quantities for a greater portion of the growing season. This is in contrast to maize which has a shorter growing season due to seed germination and earlier fall senescence.

Table 7 shows the actual snow-free albedo parameter values (along with GVF and leaf area index [LAI]) at the Bondville grid cell from March through October for maize and for Miscanthus. The parameter shift method employed by Georgescu et al. (2011) and the first phase of the present research can be seen in the spring values of albedo valid one month earlier than maize for Miscanthus in the spring and one month later than maize for Miscanthus in the fall, with summer values held constant. The discrepancies observed in LAI values are discussed in Section 3.5.4.

Table 7: Noah monthly land surface parameter values at Bondville for maize and for Miscanthus under the present research's parameter shift scheme.

	Albedo		GVF		LAI (Noah)	
	Maize	Miscanthus	Maize	Miscanthus	Maize	Miscanthus
MAR	0.104	0.112	0.074	0.168	1.87	2.26
APR	0.112	0.124	0.168	0.270	2.26	2.83
MAY	0.124	0.142	0.270	0.576	2.84	4.11
JUN	0.142	0.170	0.576	0.934	4.10	5.40
JUL	0.170	0.170	0.934	0.934	5.42	5.58
AUG	0.170	0.170	0.962	0.962	5.47	5.67
SEP	0.150	0.170	0.654	0.962	4.23	5.49
OCT	0.130	0.150	0.238	0.654	2.65	4.21

Figure 16 is a graphical representation of the daily values of albedo at Bondville for maize and Miscanthus for 2003, where the solid blue line represents Miscanthus and the dotted black line represents maize. In the winter it can be seen that snow cover makes the surface albedo much higher than monthly snow-free albedo values. However, in the spring and fall the shift is depicted quite clearly, with summertime values again held constant.

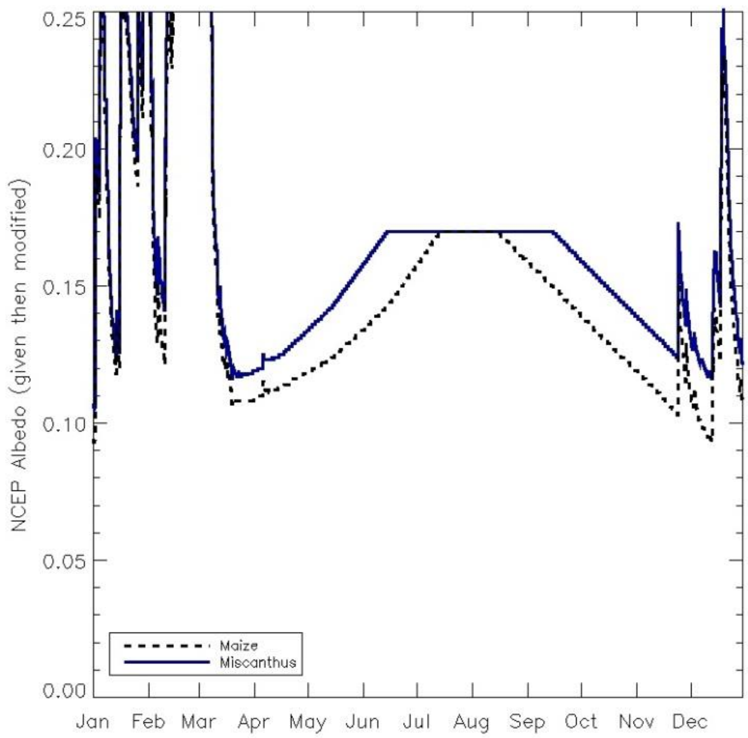

Figure 16: 2003 daily albedo parameter values at the Bondville grid cell for maize and for Miscanthus.

3.5.2. Green Vegetation Fraction

Green vegetation fraction (GVF) is physically defined as the model grid-cell fraction of midday downwelling solar (shortwave) radiation intercepted by a photosynthetically active canopy. Like albedo, the GVF dimensionless parameter data used by Noah in the present research are monthly 1-km files provided by NCEP and derived from MODIS satellite observations. This GVF parameter dataset is again assumed to be valid on the 15th of each month and subsequently linearly interpreted by Noah to obtain daily values. GVF is used within Noah to calculate several other important seasonal variables, including emissivity (used to determine how much longwave radiation the Earth's surface/vegetation reemits per Equation 2) and LAI (see Section 3.5.4).

Values of GVF for maize and for Miscanthus at Bondville are shown in Table 7. Figure 17 is a graphical representation of this shift, where the solid green line represents Miscanthus and the dotted black line represents maize. Like albedo, there are no empirical measurements of GVF over extant stands of Miscanthus at the time of the present research.

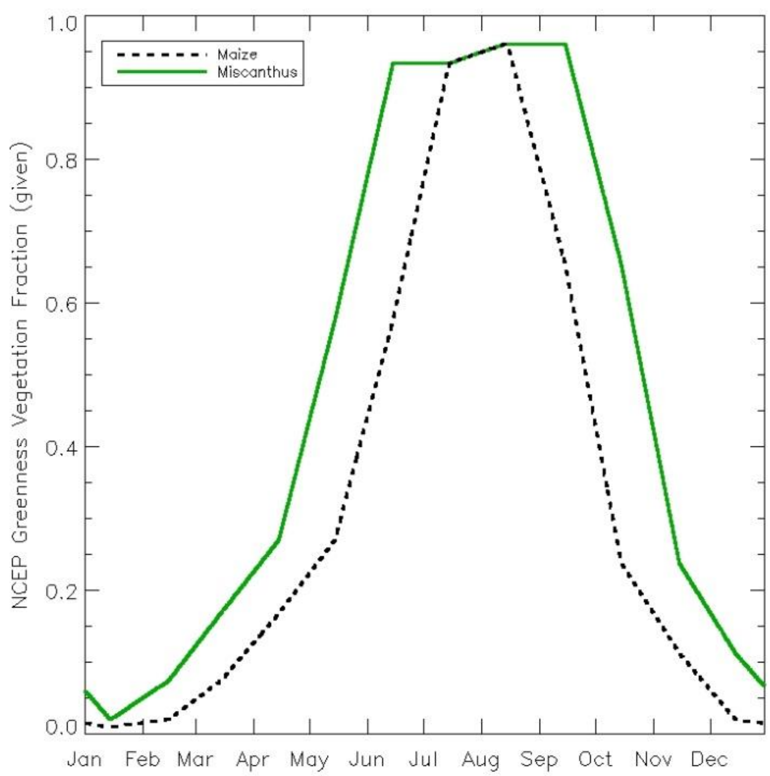

Figure 17: 2003 daily GVF parameter values at the Bondville grid cell for maize and for Miscanthus.

3.5.3. Rooting Depth

Georgescu et al. (2011) performs a single sensitivity experiment that extends the albedo/GVF shift to include a deeper Noah-assigned rooting depth for every land cover type across the central US, asserting that perennial crops tend to exhibit a much deeper rooting depth than annual crops. The second phase of the present research shifts the Noah-assigned rooting depth for dryland cropland/pasture from 40cm-100cm (third layer) to 100-200cm (fourth layer) specifically, as shown in Figure 18. These rooting depths are consistent with findings from previous agronomic research for maize and Miscanthus respectively (Kranz et al., 2008; Neukirchen et al., 1999), however Noah is slightly unrepresentative of actual crops in that it unrealistically draws all soil moisture used by the plants above solely from the soil layer defined to be the rooting zone rather than realistically pulling soil water from all layers where roots exist (and preferentially from the layer with the highest absolute soil moisture).

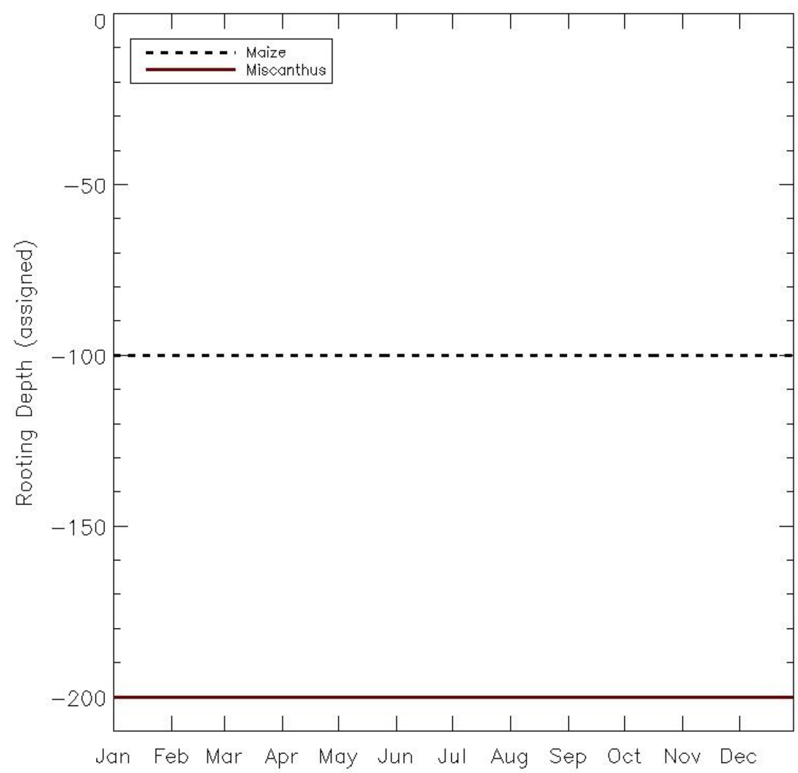

Figure 18: Noah-assigned rooting depth of maize and modified rooting depth of Miscanthus, in centimeters.

3.5.4. Leaf Area Index

Leaf area index (LAI) is defined as the ratio of total one-sided green leaf surface vegetation per unit ground surface (Chen and Black, 1992). It is a measure of the total vegetation biomass at the surface and also a factor that indicates the number of leaf surfaces available for evapotranspiration in a column extending from an area of ground under the canopy through the top of the canopy, maintaining the same dimensions. Daily LAI is calculated in Noah by scaling between a maximum and minimum LAI (assigned by lookup table based on USGS land cover type) in direct proportion with the scaling of daily GVF between a maximum and minimum prescribed GVF (based on climatology from the NCEP [MODIS] GVF dataset). This calculation is shown in Equation 4. Recall that daily values of GVF are linearly interpolated between prescribed values valid on the 15th of each month. Maximum LAI for USGS dryland cropland/pasture is 5.68 and minimum LAI is 1.56.

$$\textbf{(4)} \qquad LAI = \left(1 - \left(\frac{GVF - GVF_{min}}{GVF_{max} - GVF_{min}}\right)\right) \times LAI_{min} + \left(\frac{GVF - GVF_{min}}{GVF_{max} - GVF_{min}}\right) \times LAI_{max}$$

Table 7 shows LAI values for maize and for Miscanthus, depicted graphically by Figure 19. The small discrepancies between shifted monthly values are due to differences in the length of each month, and the higher summer LAI values for modeled Miscanthus are simply due to the fact that monthly parameter values are again valid on the 15th of each month and linearly interpreted to daily values, so the first 15 days of July and the last 15 days of August are still experiencing a slightly shifted GVF from the new June and September values.

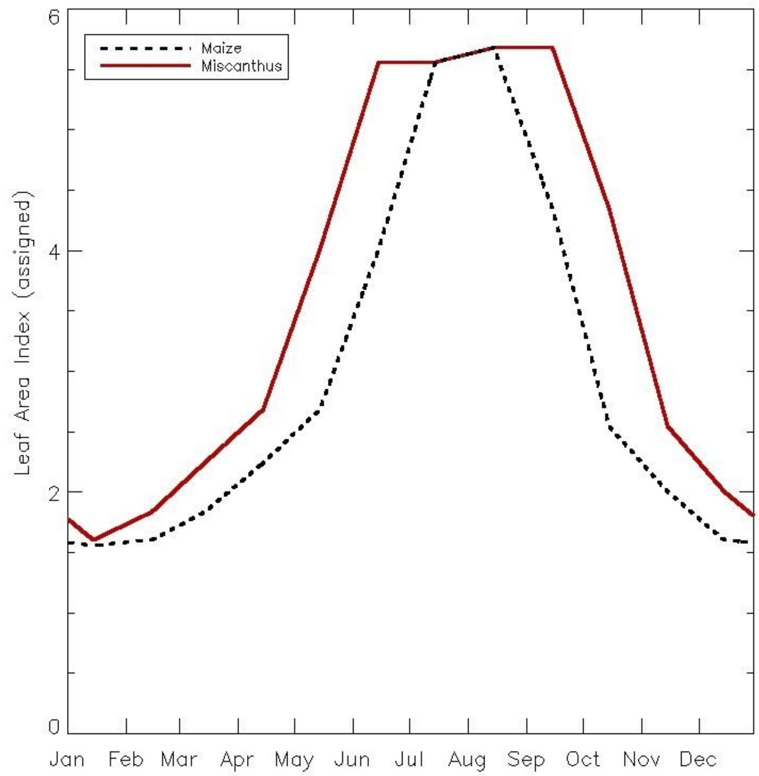

Figure 19: 2003 daily LAI parameter values at the Bondville grid cell for maize and for Miscanthus.

However, past empirical research has found Miscanthus to have a consistently higher LAI than both maize and switchgrass, a characteristic of which the atmospheric/radiative effects have not attempted to be resolved in any prior research, including Georgescu et al. (2011). While non-irrigated maize is found to achieve a maximum LAI of around 6.0 in the Central US, Heaton et al. (2008) empirically found mature Miscanthus in central Illinois to achieve LAI values greater than 10.0 during July and August (see Figure 20). To represent a realistically higher LAI in the third phase of the present research, the maximum LAI for dryland cropland/pasture is increased from 5.68 to 9.99 within Noah. Coupled with the effects of the previously shifted GVF in the Noah LAI calculation, the new monthly calculations of LAI are shown in Table 8 and graphically by Figure 21.

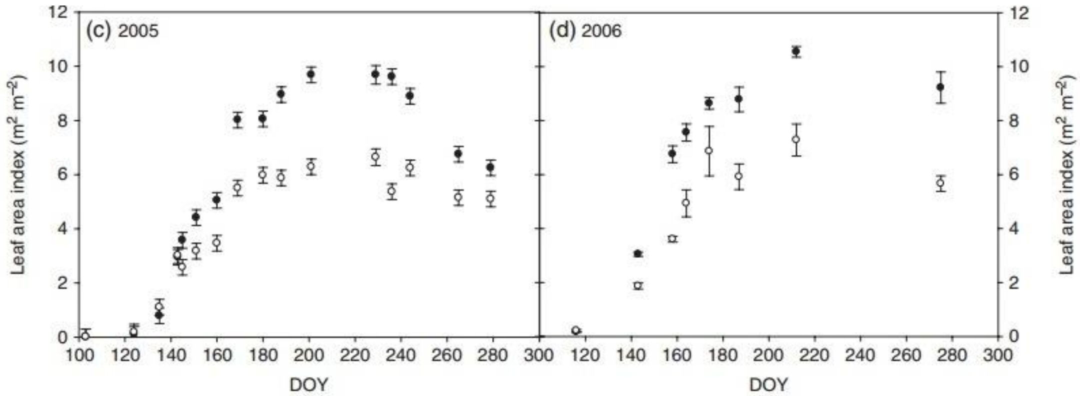

Figure 20: LAI development of Miscanthus (black circles) and switchgrass (white circles) in Central Illinois in 2005 and 2006. Values are least square means plus or minus one standard deviation. From Heaton et al., 2008.

Table 8: Noah monthly calculated LAI values at Bondville for maize, Miscanthus with shifted albedo/GVF and a maximum LAI of 5.68, and Miscanthus with shifted albedo/GVF and a maximum LAI of 9.99.

	LAI (Noah)		
	Maize	Miscanthus	New
MAR	1.87	2.26	3.00
APR	2.26	2.83	4.16
MAY	2.84	4.11	6.77
JUN	4.10	5.40	9.41
JUL	5.42	5.58	9.78
AUG	5.47	5.67	9.97
SEP	4.23	5.49	9.60
OCT	2.65	4.21	6.99

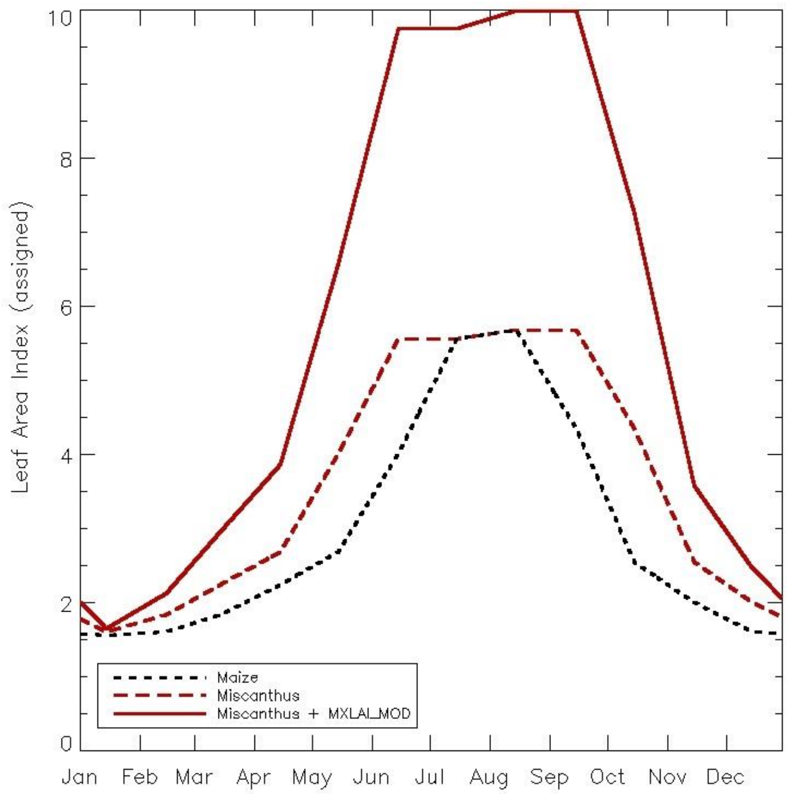

Figure 21: 2003 daily LAI parameter values at the Bondville grid cell for maize and for Miscanthus with a maximum LAI of 9.99 instead of 5.68.

3.6. Planned Analysis

With the selection of a crop (Miscanthus), observational flux tower, domain, timeframe, and parameterization scheme, the first step of the present research is to validate the NLDAS-2 GES-DISC atmospheric and radiative forcing dataset using Bondville AmeriFlux observations, with the standard set of skill scores (correlation, bias, and root mean square deviation) being used, as well as a time series of error calculation to find any existing instrument error. Following this validation, Noah and CLM will then be executed using both observational and NLDAS-2 data to assess their partitioning of the radiation budget and any biases that might exist. Noah will be compared against CLM to confirm that the use of Noah by Georgescu et al. (2011) is the most representative LSM option. This assessment will include correlation to observations and biases.

Following the validation of the datasets and LSM to be used, three different phases of shifted parameter point runs will be analyzed. A summary of these sensitivity experiments is shown in Table 9. The first phase will analyze the differences between an unmodified run of Noah (Maize) and a run with shifted albedo/GVF (Experiment A); the second will add a more realistic deeper rooting depth (Experiment B); the third will add a more realistic maximum LAI (Experiment C). The analysis of these sensitivity runs will include diurnal time series of the radiation budget partitioning to determine the average change in diurnal cycle that can be expected, as well as annual time series of LE, H, and soil moisture evolution and difference to determine season differences in radiative partitioning and hydrology. The isolation of these parameter shifts and timeframes will aid in arriving at physical explanations for any differences observed in Noah model output between Miscanthus and maize.

Table 9: A summary of all experiments performed in the present research. A ‘Y’ represent a temporally shifted or modified parameter.

Summary of all experiments performed

	GVF	Albedo	Rooting Depth	Max. LAI
Corn (unmodified)	-	-	-	-
Miscanthus: Experiment A	Y	Y	-	-
Miscanthus: Experiment B	Y	Y	Y	-
Miscanthus: Experiment C	Y	Y	Y	Y

4. RESULTS

4.1. Forcing Data Validation

NLDAS-2 12.5km forcing data compiled by NASA's Goddard Earth Science Data and Information Services Center (GES-DISC) is compared against observations taken at the Bondville, Illinois flux tower and processed by the AmeriFlux conventions described in Section 3.3.2. Data from every hour from March through October, 2003 is plotted against hourly observations for a total of 5880 time steps. Variables compared are near-surface temperature, relative humidity, surface pressure, downward shortwave radiation, and downward longwave radiation. All AmeriFlux observational data from the Bondville tower are valid "just above the canopy" (or ground during the winter), while all NLDAS-2 forcing data are valid at 2 meters with the exception of the downward radiative fluxes, which are valid directly at the surface. Any systematic errors can still be readily identified from this simple direct comparison.

Scatterplots of the results are shown in Figure 22, with observational values (Bondville AmeriFlux) along the x-axis and model forcing values (NLDAS-2 GES-DISC) along the y-axis. The correlation (R), bias, and root mean square difference for each variable are listed in Table 10. It is apparent that NLDAS-2 does an exceptional job at recreating the atmospheric and radiative forcing conditions at the Bondville tower, with all variables but downward shortwave radiation having a correlation of at least 0.98. Downward shortwave radiation, with a correlation of 0.947, is still adequately represented by forcing data, but is likely being slightly affected by local scattered cloud cover, as NLDAS is valid for the entire 12.5km by 12.5km grid box, while the observational measurements are of course point data. The slight negative bias in downward shortwave radiation corroborates this "passing cloud" theory. This discrepancy is negligible, however, especially given the high correlation between observations and forcing, and thus it is asserted that the NLDAS-2 forcing dataset is sufficiently accurate for the research domain.

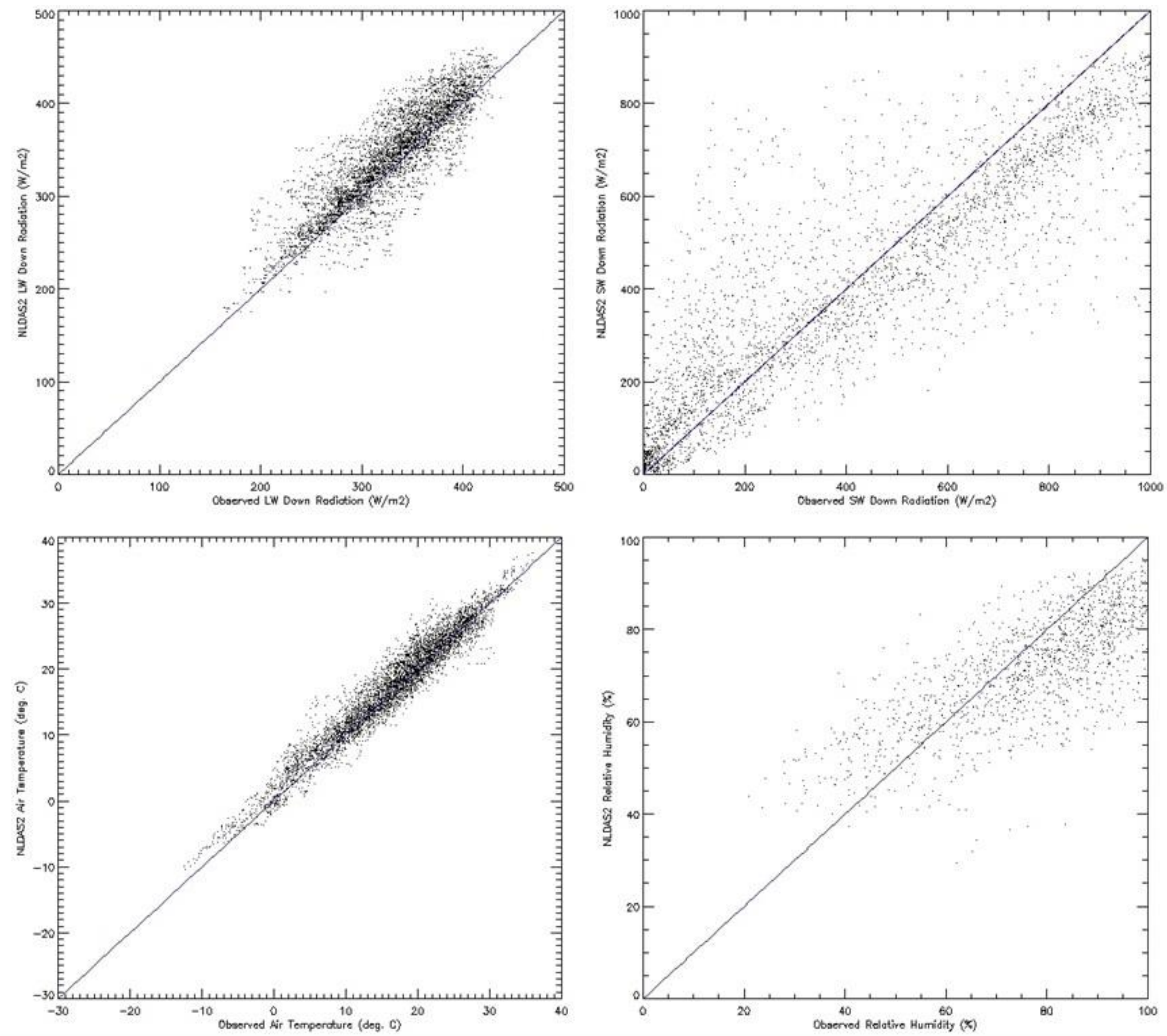

Figure 22: NLDAS-2 GES-DISC forcing data (y-axis) correlation with Bondville AmeriFlux observational data (x-axis). Data is hourly from March through October, 2003. Top left: LWdown; top right: SWdown; bottom left: 2-m temperature; bottom right: 2-m relative humidity.

Table 10: Skill scores of NLDAS-2 GES-DISC data correlated to Bondville AmeriFlux observations from March through October, 2003.

Variable	R	Bias	RMSD
Temperature (K)	0.986	+ 0.66	2.18
Rel. Humidity (%)	0.988	- 1.32	6.16
SW Down (W/m^2)	0.947	- 4.58	97.51
LW Down (W/m^2)	0.992	+ 10.21	28.49
Pressure (hPa)	1.000	+ 1.18	1.59

Hourly Timesteps: 5880

4.1.1. Bondville Time Series of Error

A time series of error calculation is performed for the Bondville AmeriFlux dataset in order to determine the margin of error that can be expected from the observational instrumentation used to measure radiative fluxes for each time step. Since the sum of all downward and upward shortwave and longwave radiation (net radiation at the surface) must by definition be equal to the sum of the sensible and latent heat fluxes minus the ground heat flux per Equation 2, discrepancies will indicate slight biases in instrumentation or data collection methodology, referred to as the closure error. Note that Equation 2 includes the effect of surface albedo (α), surface emissivity (ε), and the Stefan-Boltzmann constant (σ) within the Stefan Boltzmann law, which dictates that the energy radiated by a blackbody is proportional to the fourth power of its temperature.

$$\textbf{(2)} \qquad Rnet = (1-\alpha)SW\downarrow + \varepsilon(LW\downarrow - \sigma_s T_s^4)$$

The time series of error for March through October of 2003 at Bondville is shown in Figure 23. The average instrument error at the Bondville site was found to be 17.85 W/m^2, while the standard closure error for similar instrumentation is approximately 20 W/m^2. Thus, while the

Bondville error must be considered when analyzing future validation conclusions formulated from the same dataset, it is asserted that radiative flux observations from the Bondville tower are sufficient for use in the present research.

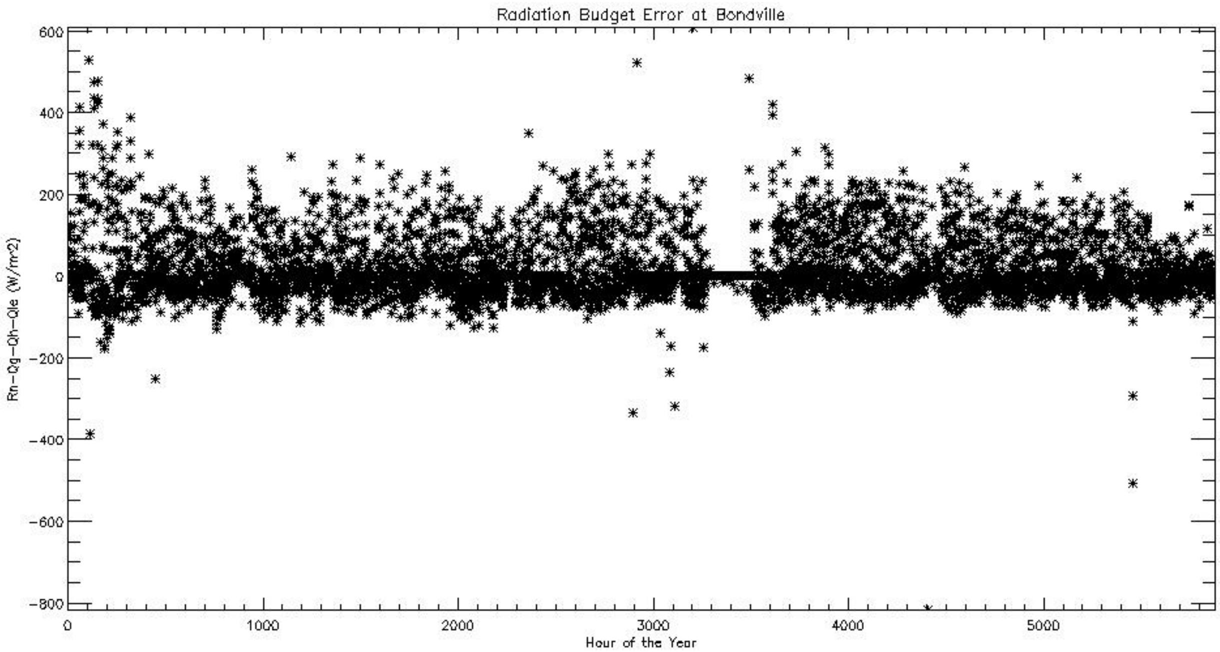

Figure 23: Time series of error in radiation budget from Bondville tower measurements from March through October, 2003. Data is hourly and y-axis equation is (Rn-Qg)-(Qh-Qle) (W/m²).

4.2. Land Surface Model Validation

As described in Section 3.3.2, the Bondville AmeriFlux tower is equipped to measure not only near-surface temperature, relative humidity, surface pressure, and downward shortwave and longwave radiation, but also upward shortwave and radiative fluxes, sensible and latent heat fluxes, and ground heat flux. Recall that net radiation is defined as the difference between the incoming and outgoing radiation, and is thus derived from observations by summing upward and downward longwave and shortwave radiation tower measurements per Equation 1. Each LSM upon receiving a net radiation value for each grid cell at each time step partitions this radiation into a sensible heat flux, latent heat flux, and ground heat flux at the surface per Equation 3. Despite each LSM receiving the same data for absorbed radiative energy, however, they can partition this energy very differently based on their respective inherent model physics. The ability of an LSM to accurately simulate the observed flux values at the same time step will be important in future simulations on a larger scale. Each LSM's radiation partitioning must therefore be analyzed in order to determine any biases that exist.

(1) $$SW\downarrow + LW\downarrow + SW\uparrow + LW\uparrow = Rnet$$

(3) $$Rnet = H + LE - G + \Delta S$$

With NLDAS-2 GES-DISC data having been confirmed as a valid forcing dataset that accurately represents observations from March through October of 2003, two separate runs are executed over a two by two grid containing the Bondville flux tower grid cell for Noah and CLM – the first runs using AmeriFlux observations as forcing data and the second runs using the NLDAS-2 GES-DISC dataset as forcing data. It is hoped that the radiative flux output from each LSM accurately portrays observed quantities from the same flux tower, indicating accurate partitioning and giving confidence in the models' ability to representatively simulate these processes on a larger domain.

To begin analysis of model performance in order to eventually determine which LSM performs better for the given domain and timeframe, both Noah3.1 and CLM2 are run on a 2x2 grid containing the Bondville flux tower from March 2003 through October 2003. Each of these runs is performed twice: once using Bondville AmeriFlux data as model forcing and once using NLDAS-2 data as model forcing. Due to earlier analysis of the integrity of the NLDAS-2 GES-

DISC forcing data set, it is expected that results from the two different forcing runs will be quite similar in both respective models.

Figure 24 shows a comparison of the correlation scores of each model run's predicted values of sensible heat flux, latent heat flux, and ground heat flux partitioned from the given net longwave/shortwave radiation. The correlation of the sum of the three fluxes is likewise calculated and plotted as derived net radiation. Both Noah and CLM when forced with AmeriFlux data have flux output correlations greater than 0.99, which is expected since in these cases both forcing and observational data are from the Bondville tower. The runs forced by NLDAS-2 data still perform quite well, however, with correlation values greater than 0.94. This gives confidence that Noah and CLM, even if not partitioning net radiation similarly, are still calculating the net radiation budget correctly (in that all fluxes must be equal to the net radiation from downwelling and upwelling shortwave and longwave radiation). It also confirms that neglecting the storage term (ΔS) in radiation calculations within maize crops is an accurate assumption.

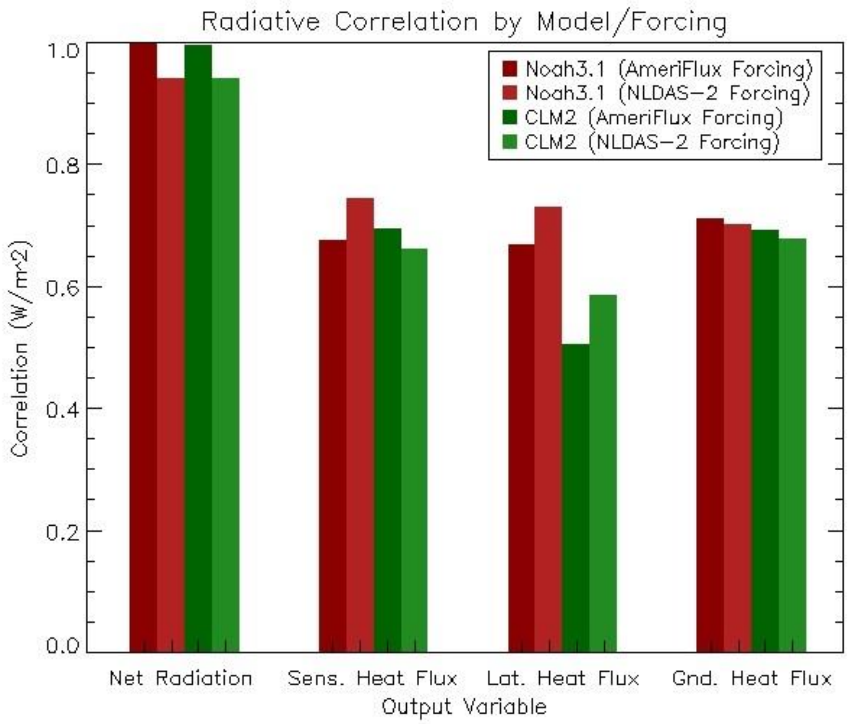

Figure 24: Radiative flux correlation scores of Noah3.1 and CLM2 forced separately by AmeriFlux data and by NLDAS-2.

Despite the fact that each LSM receives the same net radiation data and produces a retrospective net radiation calculation that matches up with observations, the partitioning of this radiative energy can and does vary fairly significantly from model to model due to each one's model physics and methods of processing input data. This is a well-documented land surface modeling problem, and understanding the known biases of each LSM can aid in more accurately interpreting later results. In this case, Figure 24 shows that Noah 3.1 at Bondville, when initialized with NLDAS-2 forcing data, is in all flux components better correlated with actual observations than CLM2. This is especially true for latent heat flux, which will be important to accurately resolve when attempting to model a lush, perennial grass such as Miscanthus. Sahoo et al. (2008) states that a radiative flux correlation value between 0.6 and 0.8 to observations of any particular LSM can be considered adequate performance, Thus Noah, with correlation values greater than 0.7 at Bondville for all flux quantities, is considered adequate for the present research. Interestingly, Noah forced by NLDAS-2 data actually resolves a more accurate sensible and latent heat flux than when forced by the actual tower observations.

Knowing that the NLDAS-2 dataset employed within Noah 3.1 to resolve radiative fluxes at Bondville performs well, the next step is to assess biases in radiative partitioning. Figures 25-27 show the seasonal mean diurnal cycles predicted by Noah and CLM at Bondville vs. AmeriFlux observations, with averages valid at every hour. Note that all fluxes are positive upward.

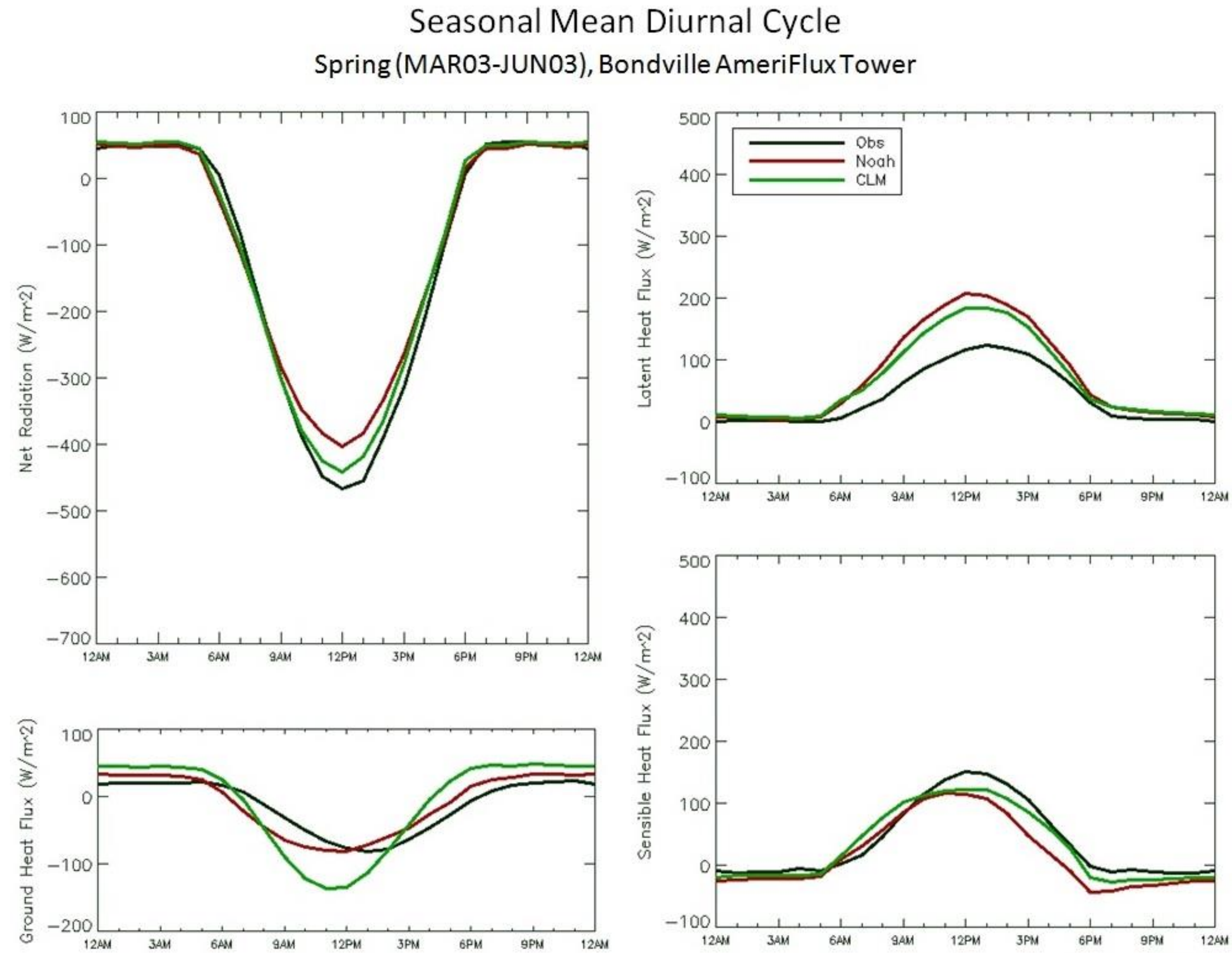

Figure 25: Mean predicted diurnal radiative flux cycle (observations vs. Noah vs. CLM) at Bondville, March-June 2003. Data are hourly. All fluxes are positive upward.

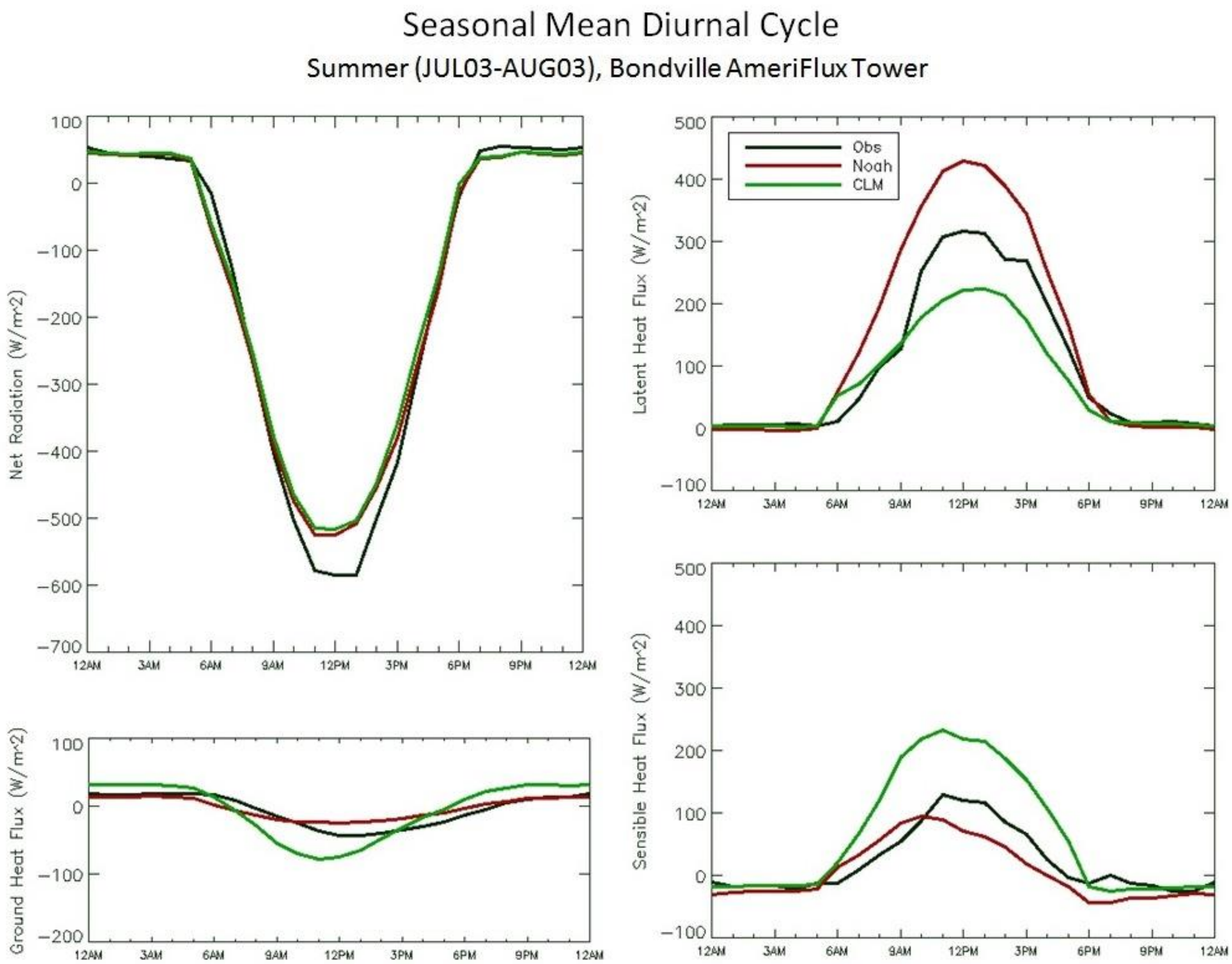

Figure 26: Mean predicted diurnal radiative flux cycle (observations vs. Noah vs. CLM) at Bondville, July-August 2003. Data are hourly. All fluxes are positive upward.

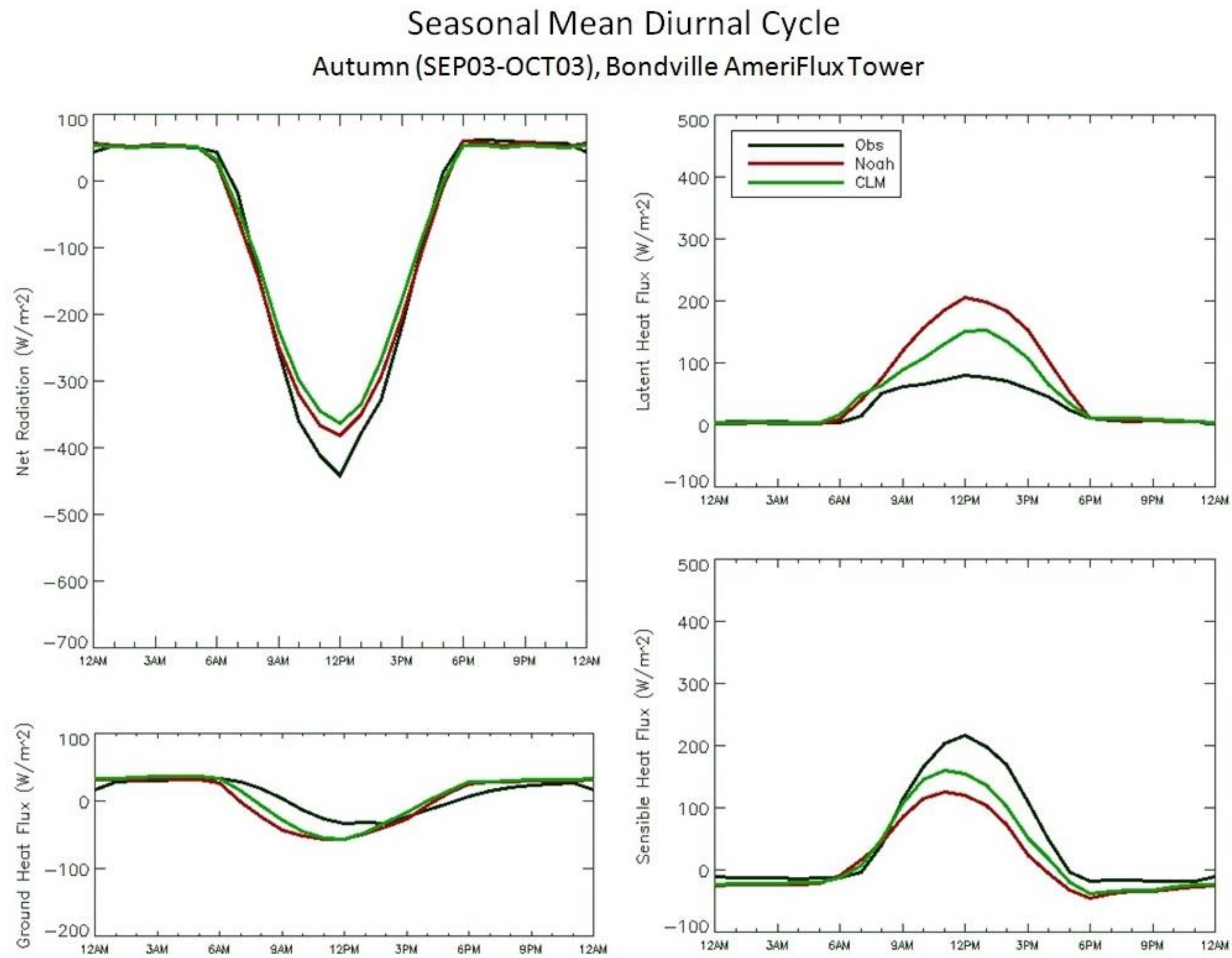

Figure 27: Mean predicted diurnal radiative flux cycle (observations vs. Noah vs. CLM) at Bondville, September-October 2003. Data are hourly. All fluxes are positive upward.

It is seen that Rnet is consistently slightly underestimated. Robock et al. (2003) also observes such a bias over the US Great Plains in Noah and suggests that it is likely attributable to a warmer surface temperature, which unrepresentatively increases upward longwave radiation thereby decreasing net radiation available for partitioning. LE is fairly consistently overestimated during the daytime during the spring and fall (by about 75%) by both Noah and CLM, although the absolute difference is not large. H is underestimated by the same magnitude in the fall, with a slighter underestimation in the spring.

The biggest difference in bias between the Noah and CLM comes during the daytime in the summer when H and LE are oppositely partitioned, with Noah systematically overestimating LE while underestimating H and vice versa for CLM. While the overestimations are of approximately the same absolute magnitude at solar zenith (~100 W/m^2), CLM overestimates H by a relative magnitude of approximately 60%, while Noah overestimates LE by a relative magnitude of approximately 35% at solar zenith. Similarly, CLM underestimates LE by a relative magnitude of 30% at solar zenith while Noah underestimates H by a maximum relative magnitude of 20%, while slightly overestimating H during the morning. CLM also exhibits the greater difference in G from observations, as seen in Figure 26. It is thus concluded that Noah exhibits a lower overall bias in the partitioning of the radiation budget than CLM at Bondville.

Noah and CLM are two well-documented LSMs that have consistently outperformed other existing LSMs at resolving a realistic surface radiation budget and hydrology in previous validation studies over areas with similar characteristics (vegetation, climate, geography) as the present area of interest (e.g. Schlosser et al., 2000; Robock et al., 2003; Guo and Dirmeyer, 2006; Kato et al., 2007; Sahoo et al., 2008). While both Noah and CLM have their own respective biases, it is concluded due to skill scores and comparison to observations from the Bondville tower when forced with NLDAS-2 GES-DISC data that Noah is the better of the two at this location. Since the present research seeks not absolute radiative flux values but instead differences in radiative flux partitioning between similar runs with shifted parameters, consistency suffices in place of absolute precision, a consistency that is validated by Noah's correlation skill scores. Comparison between Georgescu et al. (2011) (which likewise utilizes Noah) and further parameter modification to better represent the effects of a shift from maize to Miscanthus using Noah can thus proceed to be endeavored with confidence.

4.3. Shifted Parameter Point Runs

Four different runs of Noah are executed to represent different phases of a realistic shift to perennial agriculture from annual agriculture. The nomenclature of each of these runs and the parameters modified in each are detailed both in Table 9 and in each of the next three sections of results and comparisons between maize and Miscanthus modeled by the Noah LSM.

4.3.1. Shifted Albedo + GVF

Monthly prescribed albedo and green vegetation fraction (GVF) 1-km parameter files are shifted one month in each direction as described (see Table 7, Figure 16, and Figure 17) and Noah 3.1 is rerun for the year of 2003 over the Bondville grid cell.

4.3.1.1. Diurnal Time Series

The yearlong diurnal time series for the unmodified maize run (hereafter Maize) and for this new run (hereafter called Experiment A) are shown in Figure 28. The differences between the two runs are primarily during the daytime. Upwelling longwave radiation (hereafter LWup) has decreased by an average of 0.87 W/m^2 while upwelling shortwave radiation (hereafter SWup) has increased by an average of 2.29 W/m^2. The increase in SWup indicates the response to higher albedo at the surface, which is expected from the albedo modification method employed. The decrease in LWup implies a lower instantaneous surface temperature (due directly to decreased net shortwave radiation at the surface). Noah calculates emissivity in direct proportion with green vegetation fraction between a maximum and minimum emissivity for each vegetation type assigned by look-up table, and thus under a parameter shift scheme such as this one a higher year-round emissivity is calculated by the LSM. Thus, this decrease in LWup is an even more robust response given that a higher surface emissivity acts to increase LWup (see Equation 2). Together, these make for an available Rnet at the surface 1.42 W/m² less than Maize in Experiment A.

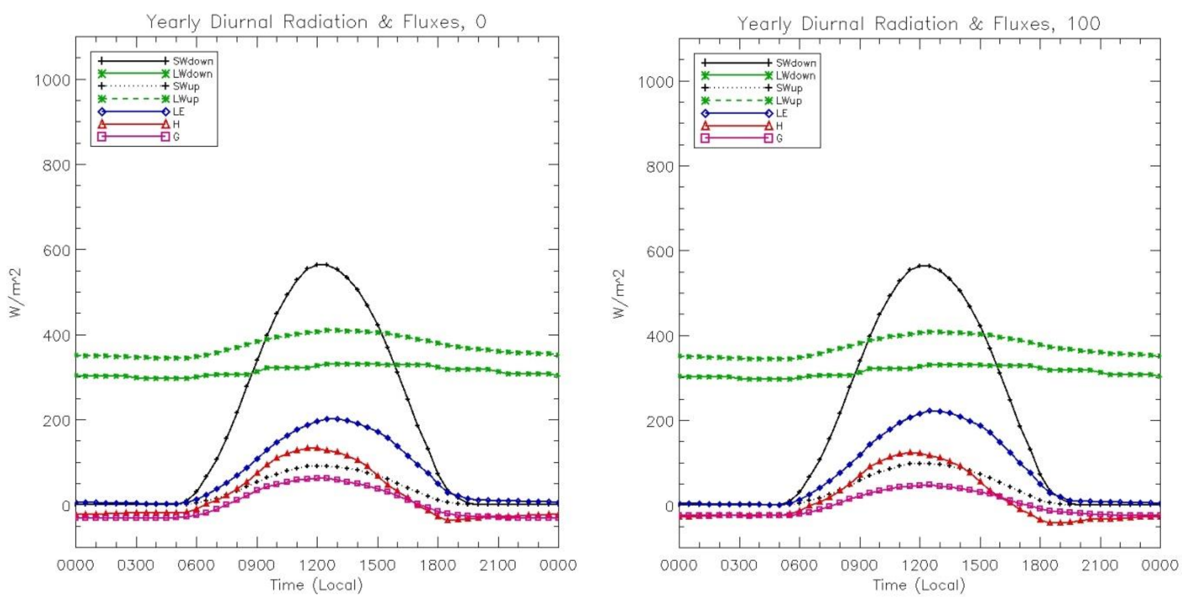

Figure 28: Yearlong diurnal averages of longwave and shortwave fluxes as well as latent, sensible, and ground heat fluxes for Maize (left) and Experiment A (right), referred to in the plots as 0 and 100 respectively. Observations are every 30 minutes. Overall from Maize to Experiment A LWup decreases by 0.87 W/m², SWup increases by 2.29 W/m², Rnet at the surface decreases by 1.42 W/m², LE increases by 4.99 W/m², and H decreases by 6.51 W/m².

Even greater than these differences are differences in the surface latent heat flux (hereafter LE) and the surface sensible heat flux (H), which increased by 4.99 W/m² and decreased by 6.51 W/m² respectively. Each of these differences in the radiation budget for this run and the two to follow are shown in Table 11. These averages include both nocturnal and diurnal measurements for the entire year over the Bondville grid cell. From just March through

October, the difference was -9.11 W/m² for H and +7.92 W/m² for LE. This increase in LE can be attributed to increased transpiration from the surface, which is greener and therefore exhibits greater evapotranspiration both earlier in the spring and later in the fall under the Experiment A parameter modification scheme. H has then decreased due simply to a higher partitioning of net radiation (hereafter Rnet) to LE, and also possibly due to greater shading of the surface with a higher LAI than Maize in the spring and fall. Recall that Noah assigns LAI based on the GVF percentage value between the bounds of an assigned minimum LAI and maximum LAI for each land cover type, and so will assign a higher LAI with the higher spring/fall GVF in Experiment A (see Table 7). Recall too that Rnet has decreased at the surface in Experiment A, so while a decrease in H would be expected, the observed increase in LE is therefore an even more robust response. Ground heat flux (hereafter G) has a much less robust annual response, with a decrease of only 0.32 W/m² from March through October.

Table 11: Yearlong difference in radiation budget partitioning between Experiment A and Maize, Experiment B and Maize, and Experiment C and Maize. Note that LE + H differences are almost identically equal to Rnet, which is expected. The rest of the difference is compensated by minute decreases in ground heat flux (G) approximately an order of magnitude smaller than LE and H.

Radiative Difference (Perennials - Annuals)

Field (W/m^2)	**Miscanthus Exp. A**	**Miscanthus Exp. B**	**Miscanthus Exp. C**
LE	4.99	10.09	12.16
H	-6.51	-10.88	-12.67
Rnet	-1.42	-0.74	-0.45
LWup	-0.87	-1.55	-1.84
SWup	2.29	2.29	2.29

Evaporative fraction is a metric that can be used to compare the partitioning of LE and H between these runs (Gentine et al., 2011). Evaporative fraction, which essentially gives a general idea of the evaporative efficiency of the surface at any time, is simply the instantaneous latent heat flux divided by instantaneous latent heat flux and sensible heat flux combined, or LE/(LE+H). Daytime values close to zero therefore mean that the majority of Rnet is being partitioned into H while values close to one mean that the majority is being partitioned into LE. Evaporative fraction is usually greater than one during the nighttime, when sensible heat flux becomes negative as the atmosphere becomes warmer than the surface due to continued longwave radiation of the Earth’s surface. Evaporative fraction is also tied to the Bowen ratio by

1/(1+B), where B=H/LE, with high values indicating a drier or more barren surface and lower values implying a moister or more-vegetated surface.

Table 12 shows the seasonal averages of evaporative fraction at Bondville for Maize and for Experiment A. While an increase in evaporative fraction during the spring and fall corroborate the March-October averages of LE and H previously found, a lower summer evaporative fraction in Experiment A indicates a higher plant evaporative stress during this time and a concomitant decrease in LE, increase in H, or both.

Table 12: Seasonal averages of evaporative fraction at Bondville, Maize vs. Experiment A.

Evaporative Fraction at Bondville, 2003

Noah	Maize	Miscanthus Exp. A	
MAR-JUN	0.701	0.816	↑
JUL-AUG	0.916	0.861	↓
SEP-OCT	0.697	0.870	↑

4.3.1.2. Annual Time Series

In order to further investigate the physical forcings that cause the observed differences in partitioning of the net radiation budget between Experiment A and Maize in Noah as well as the summertime increase in evaporative fraction, it is beneficial to look at the annual time series of LE and H as well as the evolution of soil moisture in each of Noah's four soil layers.

The time series of differences (Experiment A – Maize) from March through October values of LE and H calculated by Noah at the Bondville grid cell are shown in Figure 29. This March-October time frame is when the largest magnitude of difference can be observed between

LE and H. Two additional sensitivity runs are also plotted in Figure 29 that isolate the individual effects of albedo modification (hereafter Misc-alb) and GVF modification (hereafter Misc-gvf).

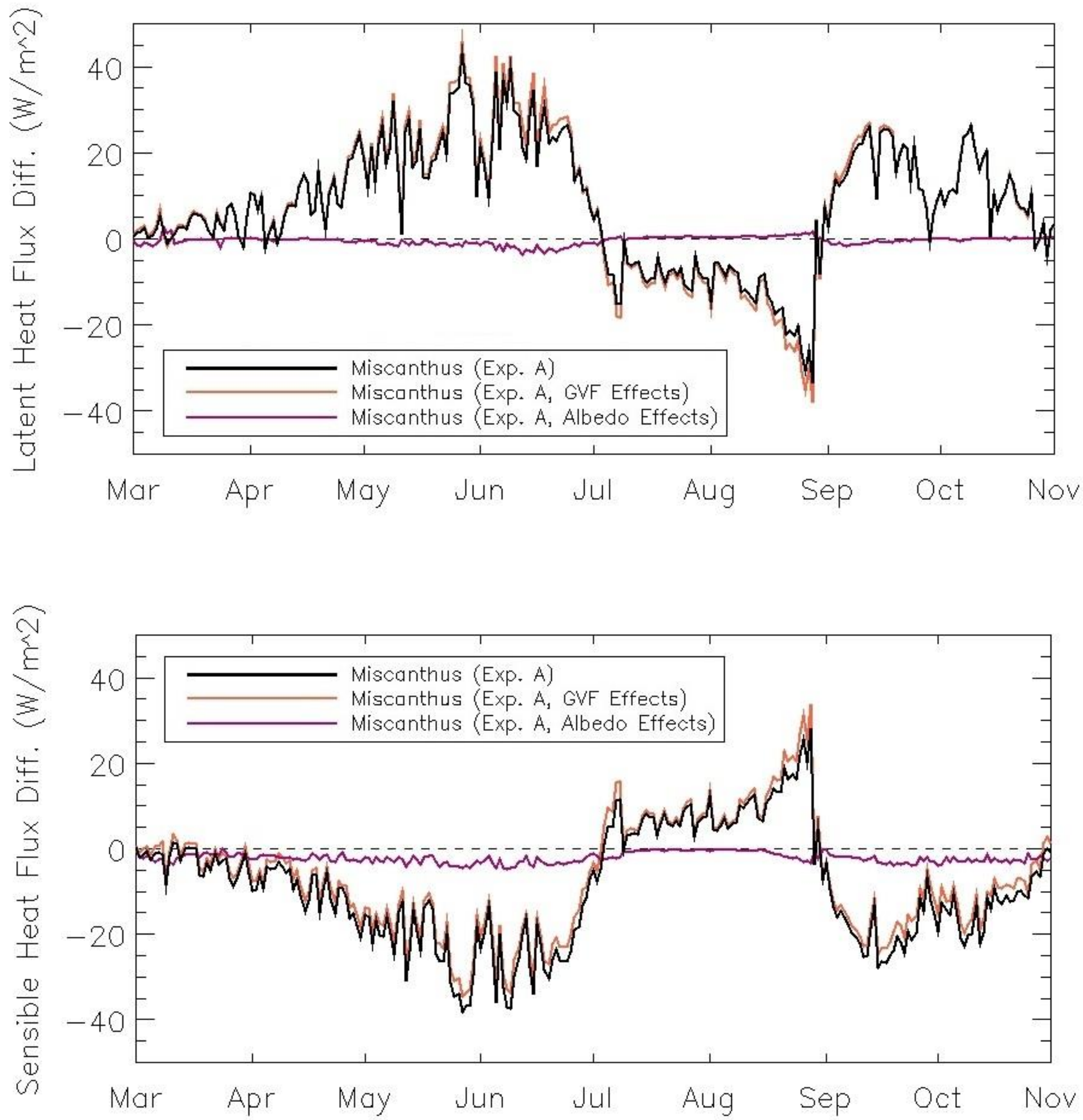

Figure 29: Annual time series of difference (diurnal flux averages valid every 24 hours) in LE (top) and H (bottom) between Experiment A and Maize, Misc-gvf and Maize, and Misc-alb and maize.

The primary feature noticed in these time series is the difference in LE and H partitioning between spring, summer, and fall. In the spring LE is much higher in Experiment A than in Maize, with some values in late May and early June close to or more than 40 W/m² higher than Maize. Meanwhile, H decreases between Experiment A and Maize at a similar magnitude. Then in mid-June a sharp decrease in LE difference and increase in H difference is seen. For all of July and August, LE is lower and H is higher in Experiment A than in Maize. In the fall this trend reverses once more, and LE is once again higher and H lower in Experiment A than in Maize. It is important to keep in mind the modified parameter files are valid on the 15th of each month and then integrated linearly on all other days between the previous and upcoming parameter values.

Another feature of these annual time series that can be seen is that the effect of shifted monthly albedo is roughly an order of magnitude smaller than the effect of shifted monthly GVF. This shift acts to decrease both LE and H in Experiment A by decreasing downwelling shortwave radiation received by the surface, thus decreasing the available Rnet subsequently partitioned into LE and H.

Overall with a greener and more reflective surface earlier in the spring and later in the fall, an increase in evapotranspiration and therefore LE accompanied by a decrease in H is expected at the surface, a hypothesis which is valid when averaged over the entire year as seen in the average diurnal time series of this run in Figure 28. However, it must be determined what is causing the opposite to occur during the summer months of June and July. In order to do so, it is helpful to examine the evolution of soil moisture in each of Noah's four soil layers. Recall that although the present Noah runs are uncoupled, meaning they do not interact with or modify the atmospheric and downwelling radiative forcings that initialize each successive time step, uncoupled runs still allow for both instantaneous changes in radiative fluxes as well as ongoing modification of existing soil moisture in each layer which carries over into each successive time step. In other words, in both coupled and uncoupled runs of Noah soil moisture is prognostic and not diagnostic.

Figure 30 shows the evolution of soil moisture and soil moisture difference (Experiment A - Maize) from March through October at Bondville for all four soil layers in Noah. Again both of the sensitivity experiments for modified albedo and GVF are shown alongside Experiment A. It can be seen that Experiment A leads to decreased soil moisture at each of the four layers, with the third layer (40-100cm) exhibiting the greatest decrease. Since Noah defines dryland cropland/pasture as having roots in this layer, this is expected. The response of the other layers to this increased water depletion in the third layer is infiltration from above and below, leading to their concomitant decrease in soil moisture. It can be seen that shifted albedo again has an order of magnitude lesser effect on this process than does shifted GVF and acts to increase soil moisture, since higher albedo leads to less Rnet and thus less radiation to partition to LE (and thus evapotranspiration) at the surface.

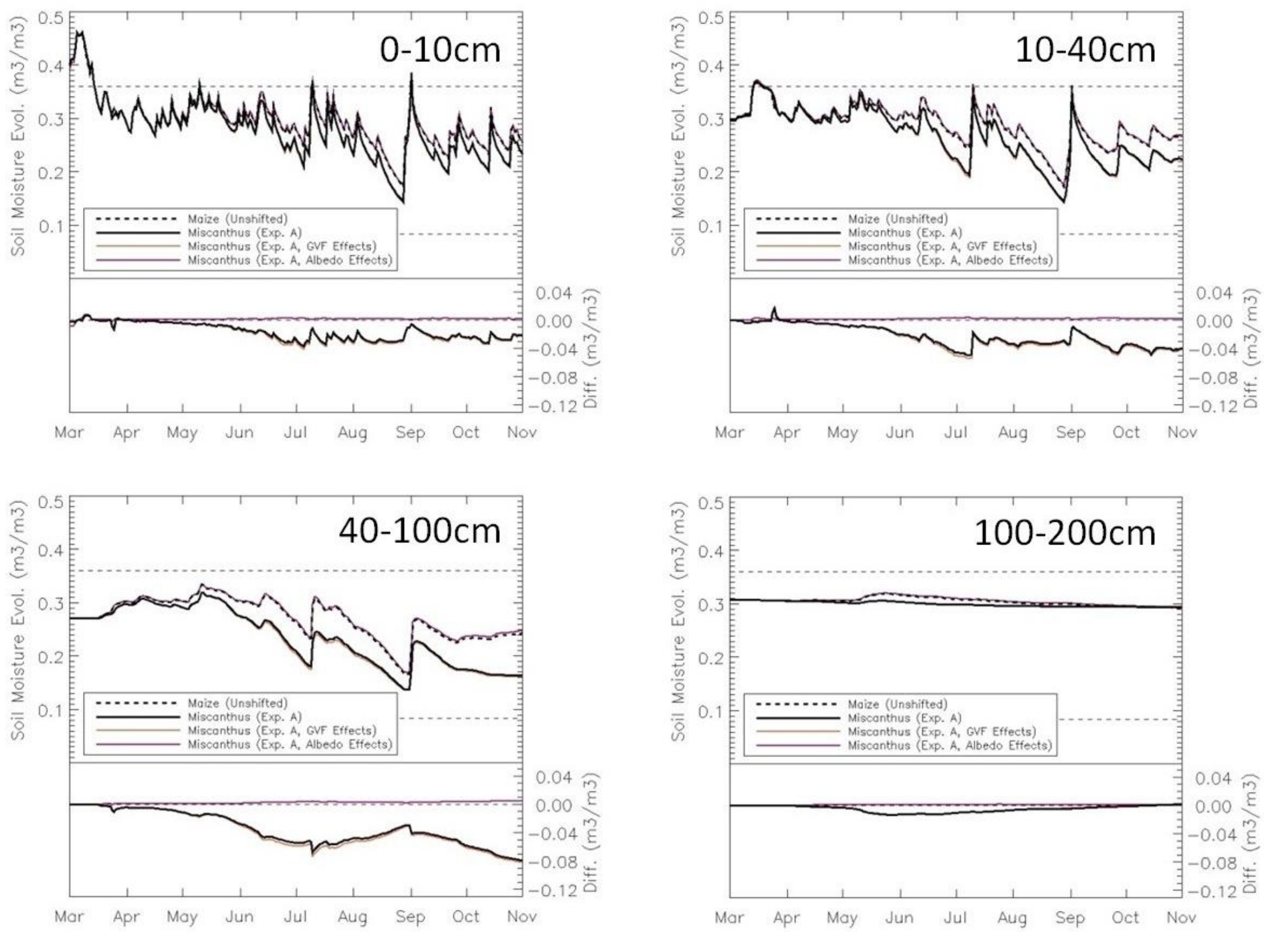

Figure 30: March through October Noah soil moisture evolution and run differences (Experiment A – Maize, Misc-gvf – Maize, Misc-alb – Maize) at Bondville. Thin black dotted lines in evolution plots (top panels) indicate the soil reference point (upper line) and wilting point (lower line).

A drastic change in soil moisture behavior is not seen during the summer months as it was for LE and H between Experiment A and Maize, but it is the direct cause of this difference in LE and H calculated by Noah between the two configurations. Appendix A discusses the canopy resistance term of the Noah LSM, which directly modulates how much evapotranspiration each vegetation (land cover) type is allowed to perform at any given time step. Noah's calculation of the canopy resistance term employs the Jarvis Scheme. The Jarvis Scheme is dependent upon a number of parameters and soil/atmospheric states, but the parameters relevant to the present research (unchanged atmospheric forcing, shifted parameters) are vegetation type, soil type, GVF, and soil moisture content. These in turn dictate several other assigned parameters: vegetation type determines minimum and maximum possible leaf area index (LAI) as well as the minimum canopy resistance, soil type determines the soil moisture content value at which a plant will become stressed (soil reference point [θ_{ref}]) as well as the value at which it will wilt (soil wilting point [θ_w]), and GVF is directly related to the LAI value that Noah assigns to each grid cell (alongside albedo and GVF) within the bounds of the minimum and maximum LAI previously assigned by vegetation type.

The Jarvis Scheme is unique in that it includes an LAI term in the denominator of the canopy resistance (hereafter Rc) calculation, which again is directly related to GVF. Because Experiment A prescribes a higher GVF for Bondville in the months leading up to summer, Noah assigns a higher LAI to Bondville as well. This acts to decrease Rc. With Rc subsequently in the denominator of the Noah calculation of evapotranspiration and potential evaporation in the numerator, evapotranspiration increases in Experiment A, the manifestation of which can be seen in the increased partitioning of Rnet to LE vs. H in the spring, and likewise in the increased water usage in Noah's third soil layer followed by infiltration from the other three layers.

With albedo and GVF held constant between Experiment A and Maize during July and August, it might be expected that their summertime difference returns to zero between the two runs. However, as previously mentioned, the key difference during the summer months is the lesser soil moisture content in Experiment A than in Maize. As discussed in Appendix A, while three of the metrics that accompany LAI in the denominator of the Rc calculation in the Jarvis

Scheme do not vary in an uncoupled retrospective run of Noah, the fourth, a dry soil stress metric (hereafter F4) is directly affected by soil moisture content (SMC). When SMC is at or above the reference SMC (θ_{ref}) assigned in Noah based on soil type, F4 does not have an effect on canopy resistance. However, when SMC is between θ_{ref} and the wilting point (θ_w, also assigned based on soil type) it acts to decrease F4, implying a drier soil. Since F4 is likewise in the denominator of the Rc calculation in the Jarvis Scheme, Rc increases for drier soils, therefore acting to limit overall evapotranspiration in Noah due to higher implied plant stress. Note that soil moisture content in the third layer is always between θ_{ref} and θ_w for Bondville's soil type, Silt Loam (0.36 m^3/m^3 and 0.084 m^3/m^3 respectively), in Experiment A.

The manifestation of this is precisely what can be seen in the annual time series of LE and H beginning in mid-June with a return to normal values of prescribed albedo and GVF. By July, Experiment A is resolved by Noah to have a lower LE and higher H than Maize, achieving differences of over 30 W/m^2 at the peak of the drought in August over Bondville. Interestingly, during this same drought the difference in root zone (third layer) soil moisture, while absolute soil moisture is still lower in Experiment A than in Maize, is actually decreasing. This gives confidence that the plant processes resolved in Noah are realistically representing the negative feedback of plants curbing their water usage (evapotranspiration via Rc via F4) with less available soil moisture, physically seen in the limiting/closing of leaf stomata in actual plants.

With a return to fall and once-again shifted albedo and GVF parameters, however, water usage from this layer again increases as does LE while H decreases in Experiment A. This implies that the resolved effects of an increased LAI (GVF) are outweighing the effects of a decreased F4 (SMC) in the denominator of the Rc calculation, leading to higher evapotranspiration than Maize once more. However, toward the end of October a return to a greater H and lesser LE in Experiment A can start to be seen again, indicating that drier soil might once again be outweighing the contributions of a higher GVF than in Maize as in summer. However, it must be considered that during this time of year a much lower absolute GVF than in the summertime is the case in both runs (see Table 7), which will have a significant impact on both LAI magnitude as well as potential evaporation (numerator of evapotranspiration in Noah). Further analysis of these metrics would provide a more specific answer to this.

Again, it is important to remember that the modified albedo and GVF parameter files (along with Noah-assigned LAI) are valid on the 15th of each month and then integrated linearly on all other days between the previous and upcoming mid-monthly parameter values. The decrease of LE difference starting in mid-June is a manifestation of this convention. This effect is not seen in mid-August to late September because of the mid-to-late August drought (see Section 3.4) that supersedes the effect of a once-again greater difference in albedo and GVF during the fall between Experiment A and Maize.

4.3.2. Shifted Albedo + GVF + Rooting Depth

Noah 3.1 is rerun for 2003 over Bondville with shifted monthly prescribed albedo and GVF as in Experiment A as well as a new rooting depth designation of 100-200cm instead of 40-100cm (layer 4 vs. layer 3 in Noah; see Figure 18) in order to better represent the deep root structure of a lush perennial grass such as Miscanthus.

4.3.2.1. Diurnal Time Series

The yearlong diurnal time series for Maize and for this new run with a greater rooting depth (hereafter called Experiment B) is shown in Figure 31. Again, the largest magnitude of difference comes during the daytime. Overall LWup decreases by 1.55 W/m² and SWup increases by 2.37 W/m², making for an Rnet decrease of 0.82 W/m². While SWup doesn't change with the addition of a deeper rooting depth, LWup, which is a function of surface temperature and emissivity, has decreased even further than in Experiment A, which implies that a greater amount of energy at the surface is going toward evapotranspiration rather than surface heating in Experiment B than in Maize. Recall that Noah calculates emissivity between an assigned maximum and minimum emissivity per vegetation type in direct proportion with green vegetation fraction and thus emissivity is higher for perennials than annuals. Because of this, a decrease in LWup is an even more robust response given that an increase in LWup would be expected of a surface with a higher emissivity.

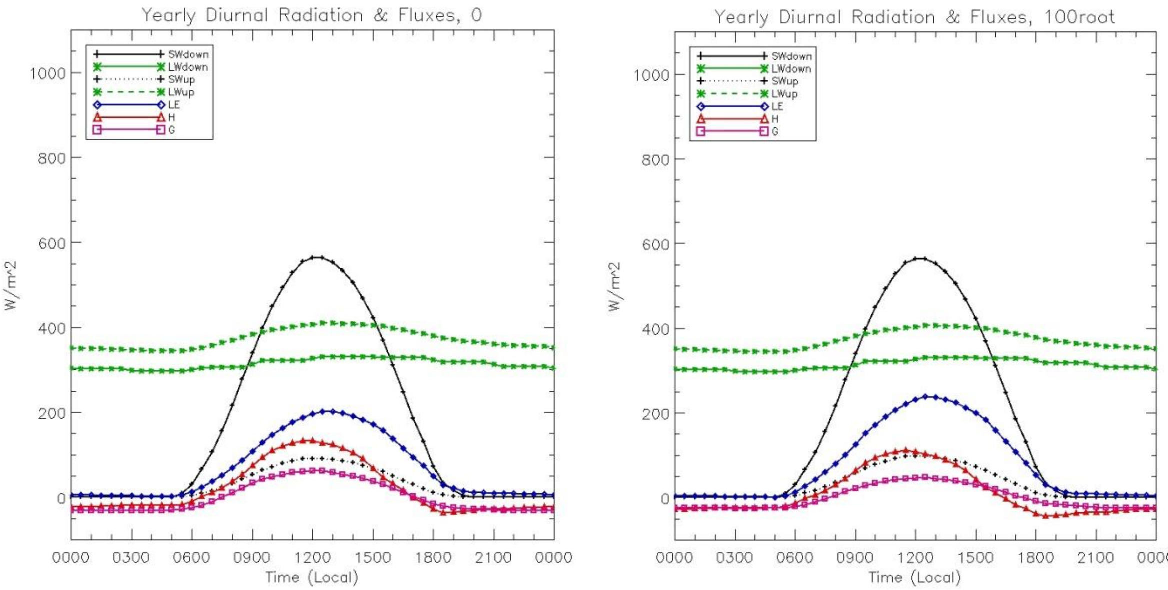

Figure 31: Yearlong diurnal averages of longwave and shortwave fluxes as well as latent, sensible, and ground heat fluxes for Maize (left) and Experiment B (right), referred to in the plots as 0 and 100root respectively. Observations are every 30 minutes. Overall from Maize to Experiment B LWup decreases by 1.55 W/m², SWup increases by 2.29 W/m² (no difference from Experiment A), Rnet at the surface decreases by 0.82 W/m², LE increases by 10.09 W/m², and H decreases by 10.88 W/m².

Greater than the differences in downwelling radiation again are the yearlong average changes in LE and H, which have increased by 10.09 W/m² and decreased by 10.88 W/m² respectively (see Table 11) For the same reason as for Experiment A, Experiment B exhibits this large increase in LE due to increased canopy evapotranspiration both in the spring and fall due to a greener surface; however, this difference is nearly twice the difference of Experiment A, so the deeper rooting depth is clearly creating a significant difference in Experiment B. The reasons for these differences are discussed in the following section detailing the annual time series of these flux values and of four-layer soil moisture.

4.3.2.2. Annual Time Series

Figure 32 shows the time series of difference (Experiment B – Maize) of LE and H from March through October 2003 plotted atop the previously discussed time series of difference (Experiment A – Maize). It can be seen that the inclusion of a deeper rooting depth in this run of Noah has generally increased LE and decreased H, especially during the summer. While the return to average or slightly negative difference values (from Maize) of both fluxes is seen during the first part of summer, a significant difference in Experiment B from Experiment A and from Maize is the high LE and low H values resolved by Noah during the drought over Bondville in mid-to-late August, with absolute differences from Experiment A over 80 W/m^2 at times.

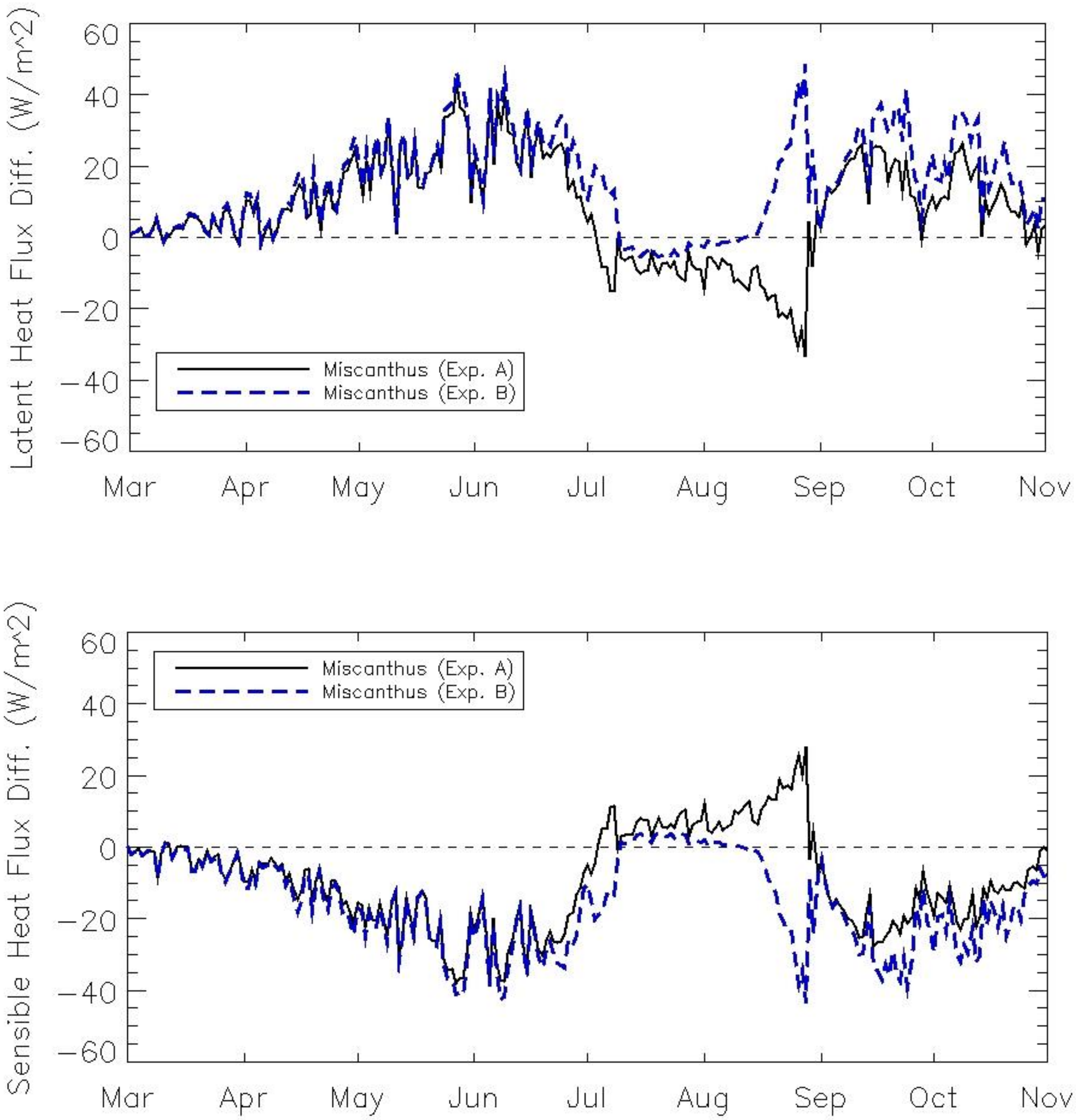

Figure 32: Annual time series of difference (diurnal flux averages valid every 24 hours) in LE (top) and H (bottom) between Experiment B and Maize (dashed blue) and between Experiment A and Maize (black).

The annual evolution and difference in soil moisture between Experiment B and Maize as well as between Experiment A and Maize is shown in Figure 33. It can readily be seen that absolute soil moisture in the top three layers has increased in Experiment B from Experiment A and decreased in the fourth layer. Absolute soil moisture in the top three layers is also higher (up to +0.03 to +0.05 m^3/m^3) in Experiment B than in Maize, although significantly lower (up to -0.11 m^3/m^3) in the fourth layer.

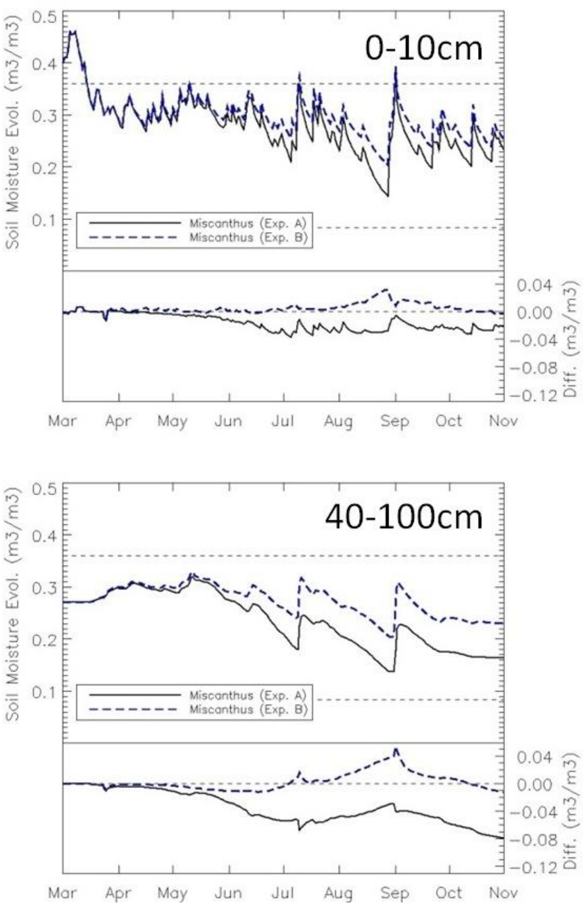

Figure 33: March through October Noah soil moisture evolution and run differences (Experiment B – Maize [dashed blue], Experiment A – Maize [black]) at Bondville.

It is obvious that a rooting depth now defined to be within the bottom soil layer in Noah has significantly altered the way the surface vegetation uses water. With higher soil moisture in the rooting zone (Noah's fourth rather than third layer), the vegetation above has a much lower canopy resistance and will transpire more freely than both Maize and Experiment A, utilizing more of the net available radiative energy at the surface for this process and resulting in the over 10 W/m^2 annual average increase in LE which has been partitioned away from H in almost identical proportion under this scenario. The model mechanics for this relate back to the soil stress metric in the denominator of the canopy resistance term per the Jarvis scheme, discussed in Appendix A. With higher soil moisture this term increases, thus decreasing canopy resistance. As in the previous run, soil moisture in the rooting zone (now the fourth layer) is within the reference soil moisture (0.36 m^3/ m^3) and wilting point (0.084 m^3/ m^3) for the duration of the run.

During the drought over Bondville in mid-to-late August these differences are especially noticeable, as the top three layers are significantly moister in Experiment B than in Experiment A since the water is being taken from the fourth layer instead of the third. Another result is that the decrease in rooting zone soil moisture at the end of October between Experiment B and Maize and between Experiment A and Maize is more significant in the former than the latter, approximately -0.11 m^3/ m^3 vs. -0.08 m^3/ m^3. This is directly due to the higher year-round rooting zone soil moisture content and thus lower year-round canopy resistance in Experiment B: Experiment A ends the season with a rooting zone (third layer) soil moisture content of 0.165 m^3/ m^3 while Experiment B ends the season with a rooting zone (fourth layer) soil moisture content of 0.185 m^3/ m^3. The two rapid increases in soil moisture in all four layers that can be seen in early July and again in late August are attributed to two separate heavy precipitation events over Bondville (see Section 3.4).

4.3.3. Shifted Albedo + GVF + Rooting Depth + Maximum LAI

Noah 3.1 is rerun for 2003 over Bondville for the final scenario of the present research – shifted monthly prescribed albedo and GVF and a rooting depth in the fourth layer as in Experiment B, plus the addition of a new maximum LAI of 9.99 for dryland cropland/pasture within Noah's vegetation parameter assignment table (by USGS land cover type; see Figure 13), up from 5.68. Since Noah assigns LAI between a defined minimum and maximum LAI based on GVF, the parameter effects of this change exist in all months in this run including July and August, which previously only experienced differences due to previously altered soil moisture values during the spring. This LAI parameter shift is discussed in Section 3.5.4 and is depicted well by Figure 21. This run with an increased maximum assignable LAI by Noah is hereafter referred to as Experiment C, as it now attempts to resolve the effects of Miscanthus vs. Maize with representative alterations of all four of these principal land surface parameters.

4.3.3.1. Diurnal Time Series

Figure 34 shows the yearlong diurnal average radiation budget over Bondville for Maize and for Experiment C. Once again the significant differences exist primarily during the daytime. Yearlong average LWup has decreased by 1.84 W/m^2 while SWup has continued to exhibit an increase of 2.29 W/m^2, the same as for each of the previous two Miscanthus runs with an identical albedo shift. This has made for an Rnet from Maize of -0.45 W/m^2, the smallest of any of the three runs. This implies an even cooler radiating surface than the other two runs, as the decreased LWup emission by the Earth's surface is approaching the shifted albedo effect of having a more reflective surface year-round.

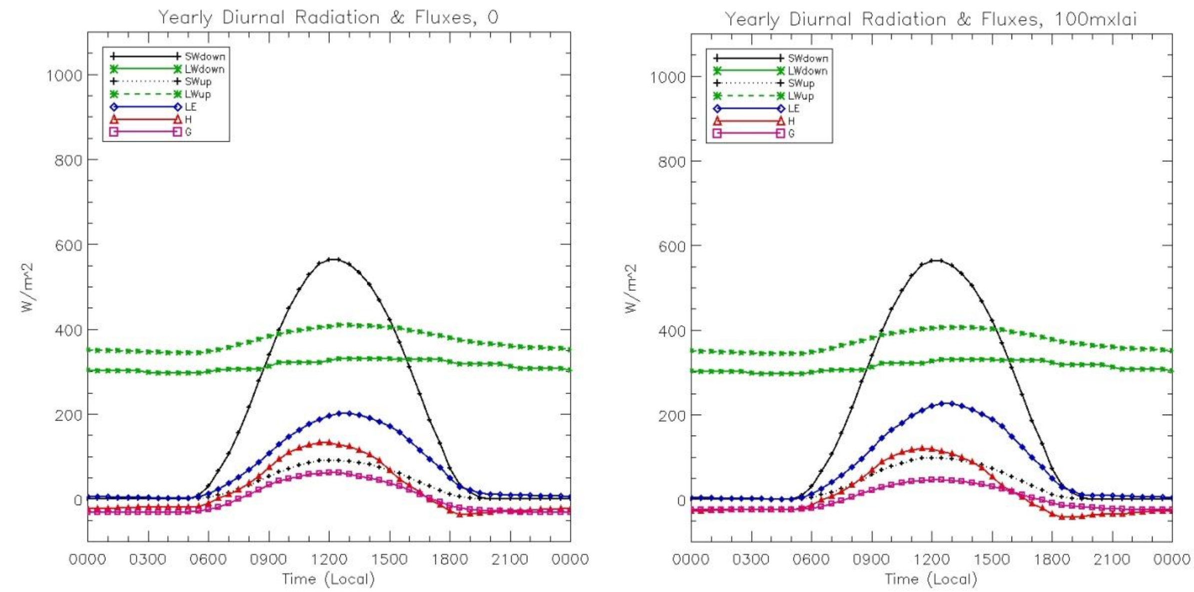

Figure 34: Yearlong diurnal averages of longwave and shortwave fluxes as well as latent, sensible, and ground heat fluxes for Maize and Experiment C, referred to in the plots as 0 and 100mxlai respectively. Observations are every 30 minutes. Overall from Maize to Experiment C LWup decreases by 1.84 W/m², SWup increases by 2.29 W/m², Rnet at the surface decreases by 0.45 W/m², LE increases by 12.16 W/m², and H decreases by 12.67 W/m². See Table 11 for a side-by-side comparison of these differences for all three runs of Miscanthus in Noah.

This decrease in LWup is related to an even greater partitioning of Rnet to surface evaporation (LE) rather than near-surface heating (H) in Experiment C vs. Maize (the comparison of which can again be seen in Table 11). The difference in LE and H between the two runs is now 12.16 W/m² for LE and -12.67 W/m² for H, higher than either of the previous two runs. Thus, an increased maximum LAI for dryland cropland/pasture in Noah is obviously leading to even more evapotranspiration at the surface and thus less surface sensible heating.

The seasonal averages of evaporative fraction at Bondville for Maize and for Experiment C along with the evaporative fraction values previously found for Experiment A are shown in

Table 13. It can now be seen that not only did evaporative fraction increase during the spring and fall, but also that summertime evaporative fraction is now greater for Experiment C than for Maize in Noah, which was not observed in Experiment A. This means that the surface is partitioning more net radiative energy to latent heat vs. sensible heat than in Maize or Experiment A. This in turn indicates that the surface vegetation is transpiring more freely and/or in greater quantity, conclusions that are corroborated by the annual time series of LE, H, and soil moisture in Experiment C in the following section. This is due to both a moister rooting zone (Noah fourth vs. third layer) as well a higher potential evaporation and LAI at the surface decreasing canopy resistance (Appendix A).

Table 13: Seasonal averages of evaporative fraction at Bondville, Maize vs. Experiment A above and Maize vs. Experiment C below.

Evaporative Fraction at Bondville, 2003

Noah	**Maize**	**Miscanthus Exp. A**	
MAR-JUN	0.701	0.816	↑
JUL-AUG	0.916	0.861	↓
SEP-OCT	0.697	0.870	↑

Noah	**Maize**	**Miscanthus Exp. C**	
MAR-JUN	0.701	0.850	↑
JUL-AUG	0.916	0.981	↑
SEP-OCT	0.697	0.976	↑

4.3.3.2. Annual Time Series

The annual time series of Experiment C minus Maize is shown in Figure 35, plotted alongside the previous two runs of Experiment A – Maize and Experiment B – Maize. The time series of difference of Experiment C closely follows that of Experiment B but is slightly greater at virtually all time steps for LE and commensurately less for H. Somewhat more significantly is that Experiment C has a higher LE and lower H than Maize for nearly all of summer too, which wasn't seen in the previous two Miscanthus runs. Because this run is the most realistic of the three in terms of model representation, this would imply that a switch to Miscanthus from Maize, while generating most of its direct atmospheric cooling effects (via greater partitioning of Rnet to LE than to H) during the spring and fall transition months, would not be conversely accompanied by atmospheric warming (higher H) during the summer months, but rather would hover around zero under summertime atmospheric conditions similar to those experienced in July and early August, 2003 (uncoupled in Noah). During drought conditions as experienced in mid-to-late August over Bondville, Miscanthus then retains its advantage of being more drought-resistant by drawing water from a deeper, moister soil layer. Of course, these conclusions are absolutely dependent upon available soil moisture in the fourth layer in Noah. If this layer becomes just as dry as the third layer does with Maize, especially with the increased water usage of Miscanthus, then these effects are negated because of an equally high canopy resistance. Plants represented by Noah are inherently only capable of drawing soil moisture from the rooting zone (rather than all layers through which roots pass), however, so this is an unrealistic scenario.

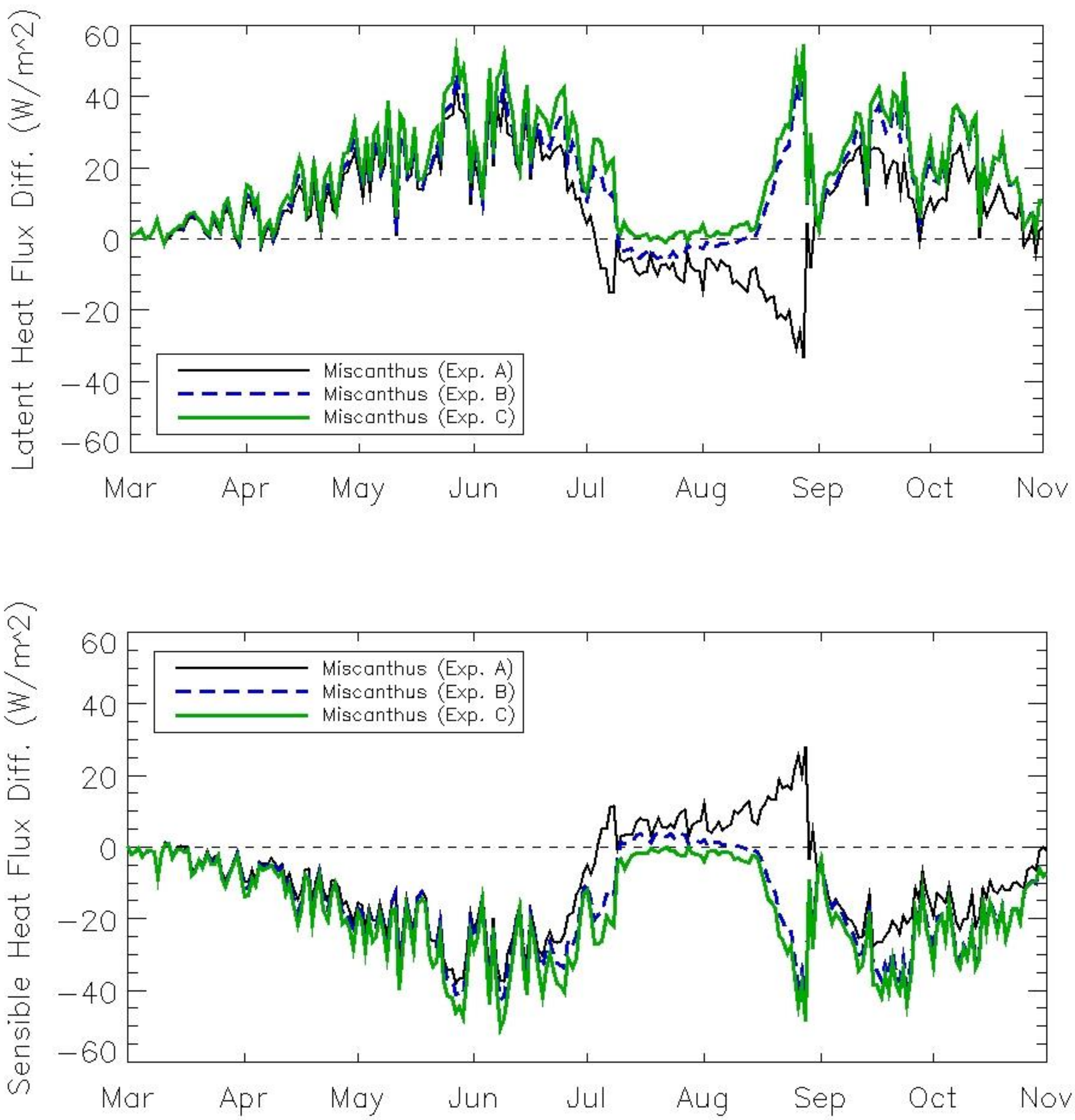

Figure 35: Annual time series of difference (diurnal flux averages valid every 24 hours) in LE (top) and H (bottom) between Experiment C and Maize (green), between Experiment B and Maize (dashed blue), and between Experiment A and Maize (black).

Figure 36 is once again a four-panel plot of soil moisture evolution and difference from Maize for each of Noah's four soil layers. The current run, Experiment C, is plotted in green above Experiment B (dashed blue) and Experiment A (black). Generally it can be seen that adding a new maximum LAI in Experiment C has decreased soil moisture content in all layers from Experiment B but has still resulted in top three layer soil moisture values 0.02 to 0.05 m^3/m^3 higher than Experiment A for most of summer and fall. The third and fourth layers again remain within the bounds of the silt loam soil moisture reference value (0.36 m^3/m^3) and wilting point (0.084 m^3/m^3).

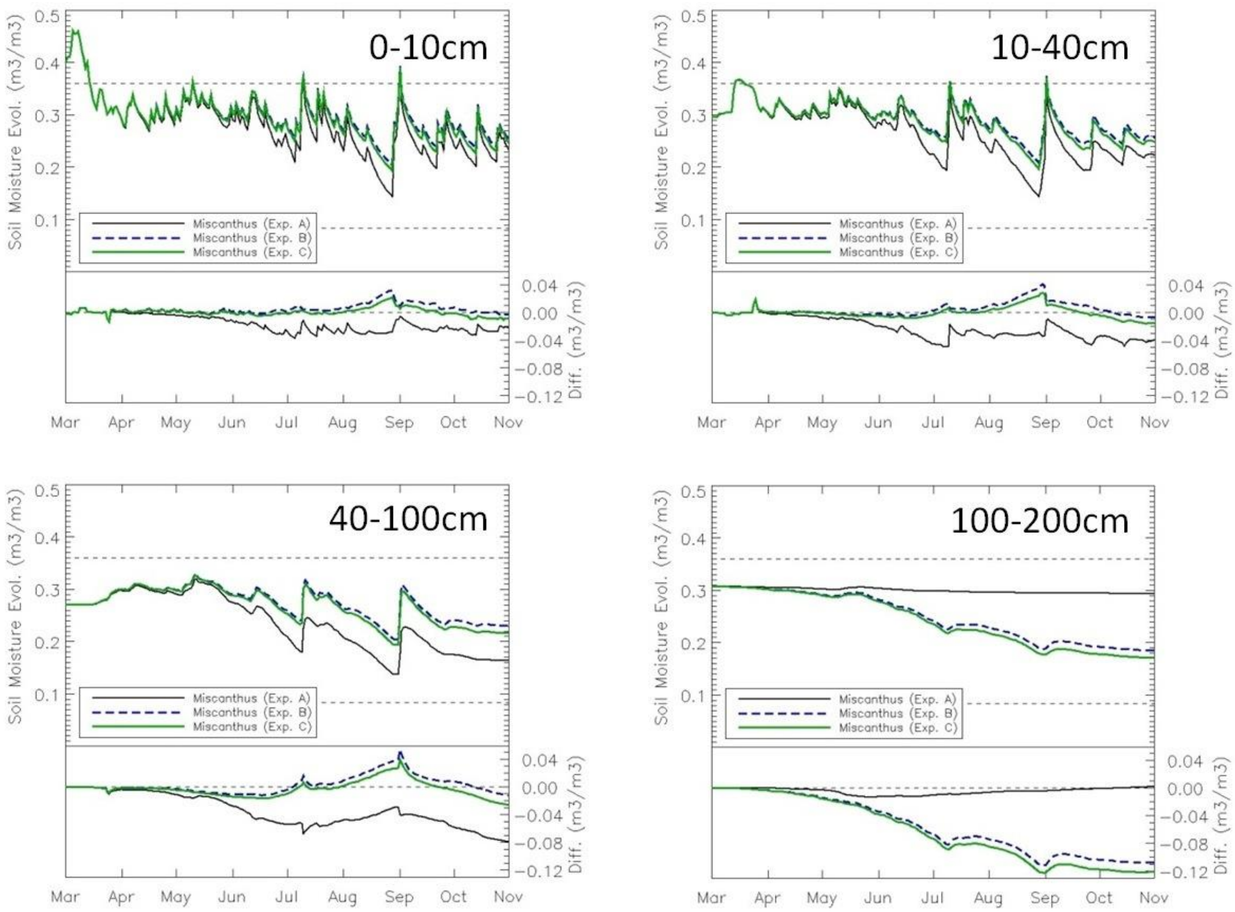

Figure 36: March through October Noah soil moisture evolution and run differences (Experiment C – Maize [green], Experiment B – Maize [dashed blue], Experiment A – Maize [black]) at Bondville.

The difference in fourth layer soil moisture can be attributed to a further-decreased canopy resistance from Maize and both of the previous two Miscanthus runs due to a higher calculated LAI, and the differences in the three layers above can subsequently be attributed to increased infiltration to lower layers. Recall from Appendix A that a higher LAI, because of its representation of lusher vegetation and thus greater potential water usage at the surface, will decrease canopy resistance due to its location in the denominator of the Rc calculation per the Jarvis Scheme within Noah. This lessened canopy resistance permits the land surface to utilize even more water for transpiration in Experiment C, thus further increasing LE and decreasing H at the surface.

With higher water usage from the rooting zone, a decrease is observed in Experiment C end-of-season soil moisture content of approximately 0.015 m^3/ m^3 from Experiment B, which did not include a higher maximum LAI more representative of Miscanthus. While this soil moisture decrease alone would act to increase canopy resistance in Noah because of its lessening of the dry soil stress metric (F4) in the Jarvis Scheme (Appendix A), a net increase in LE is still observed in the output. This indicates that in spite of Experiment C leading to drier soil, the presence of a greater amount of vegetation is still the dominant factor in our 2003 Miscanthus runs.

5. DISCUSSION

In modeling a shift from (annual) maize to (perennial) Miscanthus, it is important to understand all the factors contributing to any radiative/hydrologic changes resolved by the land surface model employed before attempting to ascertain the extent to which the near surface atmosphere would be modified. In running Noah in uncoupled mode for three different scenarios to analyze the direct effects of each necessary shift in land cover parameters, an in-depth analysis of the radiative and hydrologic effects can be completed.

Georgescu et al. (2011) in a coupled run of WRF with Noah concludes that a shift in albedo and GVF to represent perennial agriculture will decrease net surface radiation, decrease surface temperature, and increase precipitation, and also concludes that adding a deeper rooting depth will amplify these effects. The present research, by performing an uncoupled analysis of the effects of such parameter shifts, ascertains the precise contribution to these effects due solely to direct changes in radiation budget and hydrology. Additionally, a more realistic summertime model parameterization of Miscanthus is attempted by representatively increasing the maximum leaf area index assigned to dryland cropland/pasture by Noah. The results are summarized in the following sections.

5.1. Partitioning of the Radiation Budget

Table 11 summarizes the annual differences from maize of the three uncoupled runs of Miscanthus in LWup, SWup, Rnet, LE, and H. It can be seen that perennial agriculture will systematically decrease the net radiation at the surface by increasing SWup (higher year-round albedo), while LWup decreases. Since a higher annual GVF results in a higher annual emissivity and thus an expected increase in LWup per Equation 2, this modeled decrease in LWup is a more robust response and is directly due to a decreased soil top layer soil temperature. It is also seen that LE increases and H decreases at approximately the same magnitude, indicating that the energy required to perform increased evapotranspiration is being systematically partitioned away from energy that would otherwise go toward surface heating (rather than being attributable to decreased available energy at the surface because of higher SWup). This is likely the reason for the lower instantaneous skin temperature that results in a lower LWup, as discussed. This can graphically be seen in Figure 29, where shifted albedo's effect on the difference in daily H/LE is an order of magnitude smaller than the effects of shifted GVF.

The average annual increase in LE is 12.16 W/m² in the most physically realistic run of Miscanthus, Experiment C (discussed further in Section 5.3). During the daytime, when the majority of the surface evapotranspiration occurs, this increase is even greater. Table 14 shows average LE values at 9am, 12pm, and 3pm local time for August and for the entire year of 2003. It can be seen that daytime LE differences between Experiment C and Maize are well above the Bondville closure error of 17.85 W/m² discussed in Section 4.1.1. There is thus confidence that this modeled increase in LE for Miscanthus is statistically significant.

Table 14: Average August (top) and yearlong (bottom) daytime LE values for Maize and for each Miscanthus run.

Aug. Diurnal Cycle, LE (W/m^2)			
Local Hour	***0900***	***1200***	***1500***
Maize	225	399	355
Miscanthus, Exp. A	203	357	316
Miscanthus, Exp. B	238	427	382
Miscanthus, Exp. C	245	443	394

Yearly Diurnal Cycle, LE (W/m^2)			
Local Hour	***0900***	***1200***	***1500***
Maize	109	197	172
Miscanthus, Exp. A	119	216	188
Miscanthus, Exp. B	127	231	201
Miscanthus, Exp. C	130	239	206

Georgescu et al. (2011) finds an average decrease in temperature of 0.51 °C and 0.84 °C in their coupled runs of Experiment A and Experiment B, respectively. To determine whether this decrease is due principally to the higher LE confirmed by the present research or a lower SWdown because of more clouds/higher atmospheric water vapor content (higher atmospheric albedo) in a coupled run, the Miscanthus differences for both the uncoupled and coupled runs are compared in Table 15. Since an uncoupled run does not modify the atmospheric forcing for the next time step, a discrepancy in SWnet between the uncoupled and coupled scenarios will indicate that the atmosphere is indeed being modified and that increased cloud cover is contributing to the surface cooling.

Table 15: Differences in LWnet, SWnet, and Rnet between maize and Miscanthus runs. Uncoupled values are from present research; coupled values are from Georgescu et al. (2011).

Radiative Difference (Perennials - Annuals), Uncoupled vs. Coupled

Field (W/m²)	**Miscanthus Exp. A, Uncoupled**	**Miscanthus Exp. A, Coupled**	**Miscanthus Exp. B, Uncoupled**	**Miscanthus Exp. B, Coupled**	**Miscanthus Exp. C, Uncoupled**	**Miscanthus Exp. C, Coupled**
LWnet	+ 0.87	- 0.65	+ 1.55	- 1.06	+1.84	-
SWnet	- 2.29	- 2.36	- 2.29	- 3.63	- 2.29	-
Rnet	- 1.42	- 3.01	- 0.74	- 4.69	- 0.45	-

In Experiment A, SWnet is indeed nearly the same in both the uncoupled and coupled runs, so it is posited that the modeled difference is primarily due to increased partitioning of Rnet to LE rather than H. However, when adding the effects of a deeper rooting depth, the difference in soil moisture usage more than doubles as indicated by the increase in LE in the uncoupled run of Experiment B and the increase in evapotranspiration in the coupled run of Experiment B (see Table 1); this causes an average SWnet decrease that is 50% greater in the coupled run than in the uncoupled run, which points to increased cloud cover indeed acting to reflect additional downwelling solar radiation. A more detailed report of the radiative partitioning of the coupled Miscanthus run by Georgescu et al. would be helpful in determining the exact physical processes leading to this modeled surface cooling.

5.2. Changes in Soil Moisture Evolution

The most drastic difference observed in the partitioning of Rnet to LE/H occurs when setting the rooting depth to Noah’s fourth layer (100cm-200cm) rather than third layer (40cm-100cm). This systematically increased LE while decreasing H, and during the retrospective summer of 2003 allows Miscanthus to persist through the mid-to-late August drought with daily average LE at times nearly 50 W/m² higher than maize and 80 W/m² higher than Experiment A under identical atmospheric conditions. This was shown to be directly attributable to higher deep-layer soil moisture at Bondville, which directly increases LE in Noah by decreasing the canopy resistance (Appendix A). This drastic increase (decrease) in LE (H) can also be seen in the evaporative fraction (Table 13), which has not only increased for all three seasons but has switched from decreasing to increasing from annuals to perennials during the summer, thus resulting in a higher year-round evaporative fraction for Miscanthus. August average LE, H, and four layer soil moisture differences are shown for each Miscanthus run in Table 16. Note that soil moisture values are not the August decrease alone, but rather the average status of the soil moisture content achieved by August of 2003.

Table 16: August averaged differences of latent heat flux (LE), sensible heat flux (H), and Noah four-layer soil moisture for each Miscanthus run from maize. Note that changes in soil moisture are not the August change alone but rather the average soil moisture state by the time August arrives after already having been modified for the first part of the year.

August Avg. Differences (Miscanthus - Maize)	**Miscanthus (alb + gvf) .**	**Miscanthus (alb + gvf + root)**	**(alb + gvf + root + max_lai)**
Latent Heat Flux, W/m²	-13.64	10.67	14.96
Sensible Heat Flux, W/m²	10.95	-10.01	-13.60
Soil Moisture, 0-10cm (Layer 1), m³/m³	-0.027	0.017	0.009
Soil Moisture, 10-40cm (Layer 2), m³/m³	-0.032	0.022	0.014
Soil Moisture, 40-100cm (Layer 3), m³/m³	-0.041	0.024	0.015
Soil Moisture, 100-200cm (Layer 4), m³/m³	-0.005	-0.089	-0.100

In examining the effects of a deeper rooting depth, Georgescu et al. (2011) observes a modeled increase in top layer soil moisture of .02 m^3/m^3 by the end of October and posits that this is due to increased precipitation at the surface (because of increased evapotranspiration). Analysis of the uncoupled run Experiment B of the present research, however, shows almost no season-end difference in soil moisture from maize (while Experiment A resulted in a top layer soil moisture decrease of .03 m^3/m^3). During the August 2003 drought, however, an increase from maize of .02 m^3/m^3 is observed in Experiment B. The results of this uncoupled run demonstrate the manifestation of infiltration in Noah's soil moisture content calculation. With decreased evaporative stress during the drought because the roots are now resolved to be in a deeper, moister layer, the surface layers remain moister for Miscanthus than they do for maize. However, as a much higher deep layer soil moisture and thus lower canopy resistance continue to result in increased LE and water usage for the remainder of the year, infiltration from the upper layers to the lower layers increases and a trend toward decreased soil moisture from maize is seen at the end of October.

Surprisingly, Georgescu et al. (2011) concludes after a three-year uncoupled run of shifted albedo/GVF and a fourth layer rooting depth in Noah that despite this increase in soil moisture usage, such an incredible increase in LE is still sustainable and not transient. With the sharp downward trend in soil moisture content observed in the uncoupled runs of the present research toward the end of the year, this would imply that canopy resistance will continue to increase until soil moisture content reaches a new equilibrium for Miscanthus where the plants are optimally using water (in proportion with canopy resistance) to match available deep layer soil moisture. To confirm this, multiple years of analysis in a succession would need to be performed. This however would have the benefit of Miscanthus being more resistant to drought (times of extremely low top layer soil moisture) but much more efficient at evapotranspiration in times of plentiful or even excess water due to its higher year-round GVF, in the same way a water tower or reservoir stockpiles water in times of excess for use in times of scarce precipitation and drought.

The present research is also limited by two conventions. The first is a product of the experimental design in that surface changes are not permitted to modify the near-surface atmosphere, which is helpful in examining the radiative/hydrologic contribution to the cooling and moistening reported by Georgescu et al. (2011), but does not allow likely increases in atmospheric humidity and precipitation with higher LE to be realized. Increased precipitation would of course moisten the soil and decrease plant stress, and increased humidity would decrease the dry air stress metric in the denominator of Noah's canopy resistance per the Jarvis scheme. This would allow the surface vegetation to photosynthesize more freely. The second limitation of all studies with Noah is simply a product of Noah's inherent design in that vegetation is only permitted to draw water from the layer defined as its rooting zone. Maize and Miscanthus in reality draw water from every layer through which their roots passed both in proportion to the density of roots in each zone and preferentially from whichever layer has the highest available soil moisture content. If this rooting zone convention were resolved properly it is hypothesized that soil moisture stress would decrease, with the result being an increase in the likelihood of sustainability of water-intensive perennial agriculture such as Miscanthus.

5.3. Impacts of a More Realistic Maximum LAI

The final phase of the present research (Experiment C) resolved the addition of a new maximum LAI more representative of Miscanthus, a previously untried experiment. Modeled LE in Experiment C was the highest (H the lowest) of any of the runs. The total annual average of LE in this run was 2 W/m^2 higher than Experiment B, while the annual average during solar zenith was 8 W/m^2 higher and the August average during solar zenith was 16 W/m^2 higher at Bondville (see Table 16). Soil moisture usage was also the highest, with decreases of 0.01 m^3/m^3 in the top two layers and 0.02 m^3/m^3 in the bottom two layers (see Figure 36).

As seen in Figure 35, the greatest difference between perennials and annuals is still observed in the spring and fall under the present parameter shift scheme, when developmental differences between the two crops (perennials with earlier emergence and later senescence) are the greatest. However, the addition of a higher maximum LAI makes Experiment C the only run to resolve a higher LE and lower H than maize for the entire year, including summer. It is hypothesized that this tendency would be augmented with the addition of a more representative maximum albedo parameterization for Miscanthus, since lusher, denser vegetation will typically be characterized by a higher albedo. Inopportunely, no empirical observations of albedo for Miscanthus yet exist.

5.4. Conclusions

In modeling a local switch from maize to Miscanthus, it was found on average that the local latent heat flux increases with a nearly commensurate decrease in sensible heat flux. In Experiment C with shifted albedo, green vegetation fraction (GVF), rooting depth, and empirical maximum LAI, this increase in latent heat flux was the highest, at 12.16 W/m^2. An average increase in upwelling shortwave radiation of 2.29 W/m^2 (due to higher year-round albedo) and an average decrease in upwelling longwave radiation of 1.84 W/m^2 was also observed for Experiment C. Because Experiment C includes both shifted parameters as per current land surface modeling conventions as well as the first empirical LAI data from Miscanthus, it is asserted that this is the most realistic of the three runs performed in this study.

The largest differences in partitioning of the radiation budget occur during the daytime in all three runs (high downwelling shortwave radiation). GVF and rooting depth were found to be the parameters that, when representatively shifted, result in the greatest change in radiation budget partitioning. Additionally, the months of July and August displayed the greatest sensitivity to the specific method of representing a switch from maize to Miscanthus. For example, the addition of a deeper (more representative) rooting depth to an already-shifted albedo and GVF during a regional drought in the second half of August increases the net radiation being partitioned by Noah to the latent heat flux by nearly 80 W/m^2.

Several limitations include the inability of Noah to draw soil moisture from multiple layers, as well as the inability of Noah to representatively alter the within-canopy direct interception of downwelling shortwave radiation (i.e. to represent the denser vegetation of Miscanthus than maize). The former would amplify the effects discovered by this research (more available soil moisture would result in an even greater partitioning to latent heat flux (with modeled vegetation experiencing less stress) while the latter would act to decrease these effects on partitioning (less sunlight intercepted at lower layers than currently modeled, resulting in less evapotranspiration via photosynthesis and thus a lower average latent heat flux). In the selection of a land surface model, it was also found that Noah overestimates latent heat flux at solar zenith by an average of 35% at the grid cell of interest in 2003. Although this is a parameter shift comparison study and thus absolute values of latent heat flux are not of principal importance, a greater positive bias will result in a modeled increase in latent heat that may likewise be unrepresentatively high.

Finally, it is asserted that initial and ongoing water availability will likely play the greatest role in determining the sustainability of lush, dense Miscanthus in comparison with maize. With higher water usage throughout this modeled year of study, the average latent heat flux increases, but a 12% decrease in rooting zone soil moisture from maize is observed by the end of the growing season. If the rooting zone cannot replenish its soil moisture year to year, (e.g. through infiltration from below, decreased runoff in the winter months, etc.), then the rooting zone will eventually reach its wilting point value of volumetric soil moisture and all evapotranspiration will cease to occur at the surface, completely stopping any modeled partitioning of net surface radiation to the latent heat flux.

6. FUTURE WORK

With the groundwork laid for future experiments and very little existing research on the direct climate effects of a shift to a perennial agriculture regime, there are many intriguing and beneficial ways in which the present research could be expanded in the future. First and foremost, once empirical data of the maximum albedo and emissivity that can be expected from Miscanthus is obtained, an even more representative parameterization could be achieved and analyzed as was the addition of a new maximum LAI. The present research documents the effects of the current parameterization scheme on the radiation budget and hydrology at a well-documented grid point; subsequently rerunning Noah over the entire US Corn Belt with an identical parameterization scheme would give a better idea of the area-average radiative and hydrological response. Subtle differences would likely exist since NCEP albedo and GVF files have slight variations across tiles of the same USGS land cover type due to local differences in soil, climatology, hydrology, and even length of day. Additionally, instead of shifting every existing cropland tile in the US Corn Belt to exhibit a complete switch from annual to perennial agriculture (as in Georgescu et al., 2011), this domain shift could be more representative of a realistic scenario, such as shifting just 9.3% of the cropland tiles to perennial agriculture – a percentage that Heaton et al. (2008) states would be sufficient to offset the existing AEI goal of 30% displacement of the 2005 US transportation sector petroleum usage by 2030.

More research also needs to be undertaken that examines the hydrological sustainability of Miscanthus from year to year, especially with a more realistic parameterization scheme that accounts for the higher maximum LAI achieved by Miscanthus as well as the (likely) higher year-round albedo and emissivity. This crop's benefits of being a more efficient biofuel and directly contributing to the cooling and moistening of the local climate are completely irrelevant if its water demands are too high. In an uncoupled retrospective execution of Noah over multiple years, it is expected that a new equilibrium would be reached wherein the increase of LAI in the denominator of the Jarvis scheme is offset by a decrease in the dry soil metric F4 until canopy resistance attains a new sustainable level. If this equilibrium arrives at a soil moisture level too close to the defined cropland wilting point however, it could be asserted that the benefits and intense water usage of Miscanthus are not sustainable. And of course, a retrospective run using WRF coupled with Noah would be a more realistic way of resolving the shift to a new equilibrium since a modifiable near-surface atmosphere would likely undergo a moistening and cooling that could lead to increased precipitation and a much likelier conclusion of sustainability than in an offline run. Such an analysis has yet to be undertaken.

Miscanthus will be an appealing and successful biofuel crop across the United States if it can thus be proven beyond a doubt that beyond its efficient biofuel conversion and biogeochemical effects of processing more carbon dioxide year-round, it can also contribute to local surface cooling and is hydrologically sustainable by using deep soil moisture in the same way reservoirs stockpile water in times of excess precipitation for advantageous use in irrigation and times of drought. With any of these effects missing or proved statistically insignificant, it is unlikely that the benefits of Miscanthus will outweigh the status quo enough to be the impetus for a widespread change in US energy policy and biofuel crop production.

REFERENCES

AmeriFlux, cited 2013: General site information [for] Bondville. [Available online at http://ameriflux.ornl.gov/fullsiteinfo.php?sid=44].

Asner, G. P., J. M. O. Scurlock, and J. A. Hicke, 2003: Global synthesis of leaf area index observations: implications for ecological and remote sensing studies. *Global Ecol. & Biogeogr.,* **12,** 191-205.

Bonan, G. B., 1998: The land surface climatology of the NCAR land surface model coupled to the NCAR Community Climate Model. *J. Climate,* **11,** 1307-1326.

Bonan, G. B., S. Levis, L. Kergoat, K. W. Oleson, 2002: Landscapes as patches of plant functional types: An integrating concept for climate and ecosystem models. *Global Biogeochem. Cycles,* **16,** 10.1029/2000GB001360.

Bonan, G. B., K. W. Oleson, M. Vertenstein, S. Levis, X. Zeng, Y. Dai, R. E. Dickinson, and Z.-L. Yang, 2002: The land surface climatology of the Community Land Model coupled to the NCAR Community Climate Model. *J. Climate,* **15,** 3123-3149.

Brock, F. V., K. C. Crawford, R. L. Elliot, G. W. Cuperus, S. J. Stadler, H. Johnson, and M. D. Eillts, 1995: The Oklahoma Mesonet: A technical overview. *J. Atmos. Oceanic Technol.,* **12,** 5-19.

Chen, F., K. Mitchell, J. Schaake, Y. Xue, H. Pan, V. Koren, Y. Duan, M. Ek, and A. Betts, 1996: Modeling of land-surface evaporation by four schemes and comparison with FIFE observations. *J. Geophys. Res.,* **101,** 7251-7268.

Chen, J. M. and T. A. Black, 1992. Defining leaf area index for non-flat leaves. *Plant Cell Environ.,* **15,** 421-429.

Cosgrove, B. A., D. Lohmann, K. E. Mitchell, P. R. Houser, E. F. Wood, J. C. Schaake, A. Robock, C. Marshall, J. Sheffield, Q. Duan, R. W. Higgins, R. T. Pinker, J. D. Tarpley, and J. Meng, 2003: Real-time and retrospective forcing in the North American Land Data Assimilation System (NLDAS) project. *J. Geophys. Res.,***101,** 8842, doi:10.1029/2002JD003118.

Dickinson, R. E., K. W. Oleson, G. Bonan, F. Hoffman, P. Thornton, M. Vertenstein, Z.-L. Yang, and X. Zeng, 2005: The Community Land Model and its climate statistics as a component of the Community Climate System Model. J. Climate, 19, 2302-2324.

DOE, 2012: 2012 Annual Energy Outlook DOE/EIA 0383 (2012). US Department of Energy, Energy Information Administration, Office of Integrated Analysis and Forecasting, Washington, DC.

Dohleman, F. G. and S. P. Long, 2009: More productive than maize in the Midwest: how does Miscanthus do it? *Plant Physiol.,* **150,** 2104-2115.

Ek, M., K. Mitchell, L. Yin, P. Rogers, P. Grunmann, V. Koren, G. Gayno, and J. Tarpley, 2003: Implementation of Noah land-surface model advances in the NCEP operational mesoscale Eta model. *J. Geophys. Res.*, **108,** D22, 8851.

Farrell, A. E., R. J. Plevin, B. T. Turner, A. D. Jones, M. O'Hare, and D. M. Kammen, 2006: Ethanol can contribute to energy and environmental goals. *Science,* **311,** 506-508.

Gentine, P., D. Entekhabi, and J. Polcher, 2011: The Diurnal Behavior of Evaporative Fraction in the Soil-Vegetation-Atmospheric-Boundary Layer Continuum. *J. Hydrometeorol.,* **12,** 1-17.

Georgescu, M., D. B. Lobell, and C. B. Field, 2009: Potential impact of U.S. biofuels on regional climate. *Geophys. Res. Lett.,* **36,** L21806,

Georgescu, M., D. B. Lobell, and C. B. Field, 2011: Direct climate effects of perennial bioenergy crops in the United States. *Proc. Natl. Acad. Sci. USA,* **108,** 4307-4312.

Godfrey, C. M., D. J. Stensrud, and L. M. Leslie, 2007: A new latent heat flux parameterization for land surface models. Preprints, *87th Annual Meeting,* San Antonio, TX, Amer. Meteor. Soc., 6A.3. [Available online at https://ams.confex.com/ams/pdfpapers/118072.pdf]

Guo, Z. and P. A. Dirmeyer, 2006: Evaluation of the second global soil wetness project soil moisture simulations. *J. Geophys. Res.*, **111**, D22S02.

Gutter, K. T. and H. Hamer, 2012: Crop Production 2011 Summary. *USDA Nat. Agr. Stat. Serv.* ISSN: 1057-7823.

Hansen, M., R. DeFries, J.R.G. Townshend, and R. Sohlberg, 1998: UMD Global Land Cover Classification, 1 Kilometer, 1.0, Department of Geography, University of Maryland, College Park, Maryland. 1981-1994.

Heaton, E. A., F. G. Dohleman, and S. P. Long, 2008: Meeting US biofuel goals with less land: the potential of Miscanthus. *Glob. Change Biol.,* **14,** 2000-2014.

Kato, H., M. Rodell, Fr. Beyrich, H. Cleugh, E. van Gorsel, H. Liu, and T. P. Meyers, 2007: Sensitivity of Land Surface Simulations to Model Physics, Land Characteristics, and Forcings, and Four CEOP Sites. *J. Meteor. Soc. Jap.,* **85A,** 187-204.

Kranz, W. L., S. Irmak, S. J. van Donk, C. D. Yonts, D. L. Martin, 2008: Irrigation Management for Corn. Institude of Agriculture and Natural Resources, University of Nebraska-Lincoln, Lincoln, NE.

Kumar, S. V., C. D. Peters-Lidard, Y. Tian, P. R. Houser, J. Geiger, S. Olden, L. Lighty, J. L. Eastman, B. Doty, P. Dirmeyer, J. Adams, K. Mitchell, E. F. Wood, and J. Sheffield, 2006: LIS – An interoperable framework for high resolution land surface modeling. *Environ. Model. Softw.,* **21,** 1402-1415.

Lawrence, D. M., K. W. Oleson, M. G. Flanner, P. E. Thornton, S. C. Swenson, P. J. Lawrence, X. Zeng, Z.-L. Yang, S. Levis, K. Sakaguchi, G. B. Bonan, and A. G. Slater, 2011: Parameterization improvements and functional and structural advances in Version 4 of the Community Land Model. *J. Adv. Model. Earth Syst.*, **3,** doi:10.1029/2011MS000045.

Lawrence, P. J. and T.N. Chase, 2007: Representing a new MODIS consistent land surface in the Community Land Model (CLM3.0). *J. Geophys. Res.*, **112,** G01023.

Luo, L., A. Robock, K. E. Mitchell, P. R. Houser, E. F. Wood, J. C. Schaake, D. Lohmann, B. Cosgrove, F. Wen, J. Sheffield, Q. Duan, R. W. Higgins, R. T. Pinker, and J. D. Tarpley, 2003: Validation of the North American Land Data Assimilation System (NLDAS) retrospective forcing over the southern Great Plains. *J. Geophys. Res.*, **108,** D22, 8843.

Mitchell, K. E., D. Lohmann, P. R. Houser, E. F. Wood, J. C. Schaake, A. Robock, B. A. Cosgrove, J. Sheffield, Q. Duan, L. Luo, R. W. Higgins, R. T. Pinker, J. D. Tarpley, D. Lettenmaier, C. Marshall, J. Entin, M. Pan, W. Shi, V. Koren, J. Meng, B. Ramsay, and A. A. Bailey, 2004: The multi-institution North American Land Data Assimilation System (NLDAS): Utilizing multiple GCIP products and partners in a continental distributed hydrological modeling system. *J. Geophys. Res.*, **109,** D07S90, doi:10.1029/2003JD003823.

Neukirchen, D., M. Himken, J. Lammel, U. Czypionka-Krause, and H.-W. Olfs, 1999: Spatial and temporal distribution of the root system and root nutrient content of an established Miscanthus crop. *Eur. Agron. J.*, **11,** 301-309.

Oleson, K. W., G.-Y. Niu, Z. L. Yang, D. M. Lawrence, P. E. Thornton, P. J. Lawrence, R. Stockli, R. E. Dickinson, G. B. Bonan, S. Levis, A. Dai, and T. Qian, 2008: Improvements to the Community Land Model and their impact on the hydrological cycle. *J. Geophys. Res.*, **113,** G01021.

Peters, M., 2003: Local climatological data, Champaign-Urbana, IL – 118740, August 2003. [Available online at http://www.isws.illinois.edu/atmos/statecli/cuweather/2003/aug2003.pdf]

Peters-Lidard, C. D., P. R. Houser, Y. Tian, S. V. Kumar, J. Geiger, S. Olden, L. Lighty, B. Doty, P. Dirmeyer, J. Adams, K. Mitchell, E. F. Wood, and J. Sheffield, 2007: High-performance Earth system modeling with NASA/GSFC's Land Information System. *Innovations Syst. Softw. Eng.*, **3,** 157-165.

Qian, T., A. Dai, K. E. Trenberth, and K. W. Oleson, 2006: Simulation of global land surface conditions from 1948 to 2004: Part I: Forcing data and evaluations. *J. Hydrometeorol.*, **7,** 953-975.

Ramankutty, N., A. T. Evan, C. Monfreda, and J. A. Foley, 2008: Farming the planet: 1. Geographic distribution of global agricultural lands in the year 2000. *Glob. Biogeochem. Cyc.*, **22,** GB1003.

RFA, 2012: 2012 Ethanol Industry Outlook. Renewable Fuels Association, Washington, DC.

Robock, A., et al., 2003: Evaluation of the North American Land Data Assimilation System over the southern Great Plains during the warm season. *J. Geophys. Res.,* **108,** D22, 8846.

Robock, A., K. Y. Vinnikov, G. Srinivasan, J. K. Entin, S. E. Hollinger, N. A. Speranskaya, S. Liu, and A. Namkhai, 2000: The Global Soil Moisture Data Bank. *Bull. Am. Meteorol. Soc.,* **81,** 1281-1299.

Rodell, M., P. R. Houser, U. Jambor, J. Gottschalck, K. Mitchell, C.-J. Meng, K. Arsenault, B. Cosgrove, J. Radakovich, M. Bosilovich, J. K. Entin, J. P. Walker, D. Lohmann, and D. Toll, 2004: The Global Land Data Assimilation System. *Bull. Am. Meteorol. Soc.,* **85,** 381-394.

Rui, H., 2012: README Document for North America Land Data Assimilation System Phase 2 (NLDAS-2) Products. [Available online at http://hydro1.sci.gsfc.nasa.gov/data/s4pa/NLDAS/README.NLDAS2.pdf]

Sahoo, A. K., P. A. Dirmeyer, P. R. Houser, and M. Kafatos, 2008: A study of land surface processes using land surface models over the Little River Experimental Watershed, Georgia. *J. Geophys. Res.,* **113,** D20121.

Schill, S. R., 2007: Miscanthus versus switchgrass. *Ethanol Producer Magazine,* 3 October 2007.

Schlosser, C. A., A. G. Slater, A. Robock, A. J. Pitman, K. Y. Vinnikov, A. Henderson-Sellers, N. A. Speranskaya, K. Mitchell, et al., 2000: Simulations of a boreal grassland hydrology at Valdai, Russia: PILPS Phase 2(d). *Mon. Weather Rev.,* **128,** 301-321.

Skinner, R. H. and P. R. Adler, 2010: Carbon dioxide and water fluxes from switchgrass managed for bioenergy production. *Agric. Ecosys. Environ.,* **138,** 257-264.

STATSGO, 1994: State soil geographic (STATSGO) data base: data us information. Technical Report 1492. *U.S. Dept. Agric.*

Tian, Y., C. D. Peters-Lidard, S. V. Kumar, J. Geiger, P. R. Houser, J. L. Eastman, P. Dirmeyer, B. Doty, and J. Adams, 2008: High-performance land surface modeling with a Linux cluster. *Comput. Geosci.,* **2008,** 1492-1504.

UCAR, cited 2013a: Noah LSM version 3.1 … changes as compared to version 3.0. [Available online at http://www.ral.ucar.edu/research/land/technology/lsm/noahlsm-v3.1/CHANGES.]

UCAR, cited 2013b: Comparison -- Version 3.0-update1 with Version 3.1-prerelease. [Available online at http://www.ral.ucar.edu/research/land/technology/lsm/compare_3.1_3.0.html]

USDA-NASS, 2012: Corn National Statistics. United States Department of Agriculture, National Agricultural Statistics Service. [Available online at http://www.usda.nass.gov/]

Wood, E., et al., 1998: The Project for Intercomparison of Land-surface Parameterization Schemes (PILPS) Phase 2(c) Red-Arkansas River basin experiement. I: Experimental description and summary intercomparisons, *Global Planet. Change,* **19,** 115-136.

Xia, Y., K. Mitchell, M. Ek, J. Sheffield, B. Cosgrove, E. Wood, L. Luo, C. Alonge, H. Wei, J. Meng, B. Livneh, D. Lettenmaier, V. Koren, Q. Duan, K. Mo, Y. Fan, and D. Mocko, 2012: Continental-scale water and energy flux analysis and validation for the North American Land Data Assimilation System project phase 2 (NLDAS-2). *J. Geophys. Res.*, **117,** D03109, doi:10.1029/2011JD016048.

The data used in this study were acquired as part of the mission of NASA's Earth Science Division and archived and distributed by the Goddard Earth Sciences (GES) Data and Information Services Center (DISC).

APPENDIX A: CALCULATION OF EVAPOTRANSPIRATION IN NOAH

The amount of net radiative energy (Rnet) at the surface that Noah partitions into the latent heat flux (LE) vs. the sensible (H) or ground (G) heat flux is directly related to evapotranspiration (ET). Greater values of ET lead to greater partitioning of Rnet to LE. Of course, ET can only occur when water and/or vegetation exist at the surface. In order to determine the availability of water at the surface for ET, the Noah LSM's surface water budget is represented by Equation (**5**, where dS is net observable change in soil moisture content, P is precipitation, R is runoff, and E is evapotranspiration.

$$\textbf{(5)} \qquad P - R - E = dS$$

ET is a function of many parameters including existing soil moisture, vegetation and soil type, rooting depth, and green vegetation cover. Different LSMs resolve the interaction of all these factors slightly differently when calculating ET.

In Noah, ET is partitioned via Equation 6, where E is the total surface evapotranspiration, Edir is direct evaporation from the surface soil, Et is transpiration from the plant canopy, Ec is evaporation directly from the canopy (e.g. morning dew, canopy-intercepted rainfall), and Esnow is sublimation from snowpack. Et, transpiration from the plant canopy, is made possible by the uptake of soil moisture from each plant's roots. The amount of water that gets transported from soil through root to leaf to the atmosphere by Noah is referred to as the moisture flux, and is calculated by dividing the plant's potential evaporation (under optimal conditions) by canopy resistance (Equation 7).

$$\textbf{(6)} \qquad E = Edir + Et + Ec + Esnow$$

$$\textbf{(7)} \qquad Et = \frac{potential\ evaporation}{canopy\ resistance}$$

Canopy resistance is the most important factor contributing to canopy transpiration, and total LE is mostly determined by the canopy resistance (Godfrey et al., 2007). Any LE discrepancy seen in modified LSM run comparisons can therefore likely be traced back to the terms by which it is calculated. However, canopy resistance is not calculated similarly in all LSMs. In Noah, canopy resistance (Rc) is calculated via Equation 8, which is known as the Jarvis Scheme. In the Jarvis Scheme, Rc_min, the minimum canopy resistance, is assigned based on USGS vegetation type within Noah, LAI is the leaf area index, and F1 through F4 are metrics for plant stress. As described in Section 3.5.4, LAI is assigned by Noah in direct proportion with green vegetation fraction (GVF) within the bounds of a minimum and maximum LAI, both of which are assigned based on a lookup table by USGS-defined vegetation type. Each of the four canopy resistance metrics are bounded between 0 and 1 and represent the effects of solar radiation, vapor pressure deficit, air temperature, and soil moisture, respectively (Godfrey et al., 2007).

$$\textbf{(8)} \qquad Rc = \frac{Rc\_min}{LAI \times F1 \times F2 \times F3 \times F4}$$

It is within the Jarvis Scheme that the changed forcings associated with a parameter shift to represent perennial vs. annual agriculture in an uncoupled run of Noah act to modify instantaneous Rnet, H, and LE, and generate a difference in soil moisture that will persist time step to time step since soil moisture within Noah is prognostic and not diagnostic. A higher LAI, implying lusher vegetation at the surface and thus more rooting zone soil moisture usage, will act to decrease the canopy resistance term and thus increase ET simply due to there being more leaves available for transpiration with a sufficient moisture source.

The first three metrics for plant stress, F1, F2, and F3, are all dependent upon atmospheric and radiative forcings that do not vary in an uncoupled run of Noah with shifted parameters. This makes it simpler to isolate the contributions of altered soil moisture, represented in metric F4, to the canopy resistance. Equation 9 shows the general calculation of F4, where θ_i represents instantaneous soil moisture content, θ_w represents the soil moisture content at which the associated plants within Noah will begin to wilt, and θ_{ref} represents the reference soil moisture content at which the plants will begin to first feel stressed. The last two of these parameters are dependent upon on USGS soil type in Noah (see Section 3.3.2) which assigns representative values of θ_w and θ_{ref} based on an empirically-derived look-up table.

$$\textbf{(9)} \qquad F4 \sim \frac{\theta_i - \theta_w}{\theta_{ref} - \theta_w}$$

When instantaneous soil moisture is above both the wilting point and the stress reference point, the value of F4 is 1 (recall that these metrics are inherently bounded between 0 and 1), and will thus have no impact on limiting ET. However, when the instantaneous soil moisture lies between these two values F4 will be proportionally between 0 and 1. This smaller value in the denominator of Equation 8 will act to increase canopy resistance and thus decrease overall water usage, ET, and therefore LE, representing the physical process of stressed plants constricting their leaf stomata to conserve water while still being able to perform the vital process of photosynthesis. Of course, when soil moisture is below even the wilting point, F4 goes to 0, which will effectively maximize canopy resistance and shut down all ET and therefore any partitioning of Rnet to LE.